The role of the individual TOM subunits in the association of PINK1 with depolarized mitochondria

Dissertation

der Mathematisch-Naturwissenschaftlichen Fakultät

der Eberhard Karls Universität Tübingen

zur Erlangung des Grades eines

Doktors der Naturwissenschaften

(Dr. rer. nat.)

vorgelegt von

Klaudia Katarzyna Maruszczak

aus Piła, Polen

Tübingen

2022

The role of the individual TOM subunits in the association of PINK1 with depolarized mitochondria

Dissertation

der Mathematisch-Naturwissenschaftlichen Fakultät

der Eberhard Karls Universität Tübingen

zur Erlangung des Grades eines

Doktors der Naturwissenschaften

(Dr. rer. nat.)

vorgelegt von

Klaudia Katarzyna Maruszczak

aus Piła, Polen

Tübingen

2022

Gedruckt mit Genehmigung der Mathematisch-Naturwissenschaftlichen Fakultät der Eberhard Karls Universität Tübingen.

Tag der mündlichen Qualifikation:	24.05.2022
Dekan:	Prof. Dr. Thilo Stehle
1. Berichterstatter:	Prof. Dr. Doron Rapaport
2. Berichterstatterin:	apl. Prof. Dr. Tassula Proikas-Cezanne

Erklärung / Declaration: Ich erkläre, dass ich die zur Promotion eingereichte Arbeit mit dem Titel:

“The role of the individual TOM subunits in the association of PINK1 with depolarized mitochondria”

Selbständig verfasst, nur die angegebenen Quellen und Hilfsmittel benutzt und wörtlich oder inhaltlich übernommene Stellen als solche gekennzeichnet habe. Ich versichere an Eides statt, dass diese Angaben wahr sind und dass ich nichts verschwiegen habe. Mir ist bekannt, dass die falsche Abgabe einer Versicherung an Eides statt mit Freiheitsstrafe bis zu drei Jahren oder mit Geldstrafe bestraft wird.

I hereby declare that I have produced the work entitled: **“The role of the individual TOM subunits in the association of PINK1 with depolarized mitochondria”**, submitted for the award of a doctorate, on my own (without external help), have used only the sources and aids indicated and have marked passages included from other works, whether verbatim or in content, as such. I swear upon oath that these statements are true and that I have not concealed anything. I am aware that making a false declaration under oath is punishable by a term of imprisonment of up to three years or by a fine.

Tübingen, den

CONTENTS

1. LIST OF ABBREVIATIONS

BN-PAGE	Blue Native-PolyAcrylamide Gel Electrophoresis
DHFR	Dihydrofolate reductase
GFP	Green fluorescent protein
GST	Glutathione S-transferase
iMTS-Ls	internal MTS-like signals
KD	Knock down
KO	Knockout
MOM	Mitochondrial outer membrane
MTS	Mitochondrial targeting sequence
OMS	Outer mitochondrial membrane localization signal
PD	Parkinson's disease
PINK1	PTEN-induced putative kinase 1
SDS-PAGE	Sodium Dodecyl Sulfate–PolyAcrylamide Gel Electrophoresis
siRNA	Small interfering RNA
TcPINK1	*Tribolium castaneum* PINK1
TMD	Transmembrane domain
TOM	Translocase of the outer membrane
ΔΨm	Mitochondrial membrane potential

2. SUMMARY

Mitochondria are crucial for numerous cellular processes such as oxidative phosphorylation and β-oxidation of fatty acids. Therefore, they have to be monitored by specialized mechanisms to maintain cell homeostasis. One of the pathways of quality control of mitochondria is the PINK1-Parkin induced mitophagy. In depolarized mitochondria, PINK1 integrates in the mitochondrial outer membrane (MOM) where it phosphorylates various proteins including Parkin, which is then recruited to the mitochondrial surface. Parkin, an E3 ligase, conjugates ubiquitin onto phosphorylated substrates, which in turn are further phosphorylated by PINK1. This leads to the generation of substrates with long ubiquitin chains and triggers mitophagy. Mutations in PINK1 and Parkin abolish the induction of mitophagy and lead to the development of Parkinson's disease demonstrating the importance of the quality control of the organelle.

While the PINK1-Parkin pathway has been well described, not much is known about the initial events of PINK1 integration into the MOM. PINK1 is the first player to be triggered in the pathway leading to the removal of malfunctional mitochondria. Thus, the aim of my work was to understand how PINK1 import pathway is regulated at the level of the TOM complex in depolarized mitochondria.

To address this aim, I established and validated an assay for the analysis of the formation of PINK1-TOM complex. Subsequently, I studied the interactions between PINK1 and the TOM70 and TOM20 receptors with peptide scan assay and *in vitro* pull downs. I could show that TOM70 binds directly various sections in the N-terminal region of PINK1. I also showed that the MTS of PINK1 is dispensable for this interaction. Next, I performed a series of *in vitro* import assays of radiolabeled PINK1 combined with isolated depolarized mitochondria depleted for TOM70, TOM20 or both TOM70/TOM20. TOM70 KD significantly affected PINK1 association with the MOM upon CCCP treatment, while TOM20 had a marginal role for PINK1 import. However, double depletion of both receptors showed that TOM70 and TOM20 might have exchangable roles in PINK1 recognition. Furthermore, I found that TOM7 KD impaired the import of the TOM complex clients probably due to its negative effect on the stability of the complex. PINK1 import into depolarized mitochondria isolated from TOM7 KD cells was moderately affected. However, double depletion of both TOM70,

the major recognition factor for PINK1 in the MOM, and TOM7, the TOM complex stabilization factor, had a synthetic effect on PINK1 membrane integration. Next, I studied the effect of TOM40 pore blockage on PINK1 MOM association. When TOM40 lumen was clogged with excess amounts of mitochondrial precursor protein and the membrane potential was dissipated, PINK1 membrane association was dramatically affected. Finally, I wanted to check whether PINK1 could trigger the mitophagy cascade when stalled within the TOM40 pore. Hence, I blocked the TOM40 barrel with recombinant amounts of TcPINK1 and imported radiolabeled hPINK1 as well as TOM40 molecules. The membrane integration of both proteins was reduced, suggesting that PINK1 resides in the TOM40 lumen of depolarized mitochondria and thus, hinders the import of other TOM clients.

Collectively, my results provide a new insight into PINK1 association with the TOM complex upon mitochondrial membrane potential dissipation, suggesting the indispensable role of the TOM complex in the proper positioning of PINK1 to initiate the mitophagy cascade.

3. ZUSAMMENFASSUNG

Mitochondrien sind entscheidend für zahlreiche zelluläre Prozesse wie die oxidative Phosphorylierung und die β-Oxidation von Fettsäuren. Daher müssen sie durch spezielle Mechanismen überwacht werden, um die Zellhomöostase aufrechtzuerhalten. Einer der Wege der Qualitätskontrolle von Mitochondrien ist die PINK1-Parkin-induzierte Mitophagie. In depolarisierten Mitochondrien integriert sich PINK1 in die äußere Mitochondrienmembran (MOM), wo es verschiedene Proteine und auch Parkin, eine E3-Ligase, phosphoryliert, das dann an die Mitochondrienoberfläche rekrutiert wird. Parkin, konjugiert Ubiquitin an phosphorylierte Substrate, die ihrerseits von PINK1 weiter phosphoryliert werden. Dies führt zur Bildung von Substraten mit langen Ubiquitin-Ketten und löst die Mitophagie aus. Mutationen in PINK1 und Parkin heben die Induktion der Mitophagie auf und führen zur Entwicklung der Parkinson-Krankheit, was zeigt, wie wichtig die Qualitätskontrolle der Organelle ist.

Während der PINK1-Parkin-Weg gut beschrieben ist, ist über die ersten Ereignisse der PINK1-Integration in die MOM nicht viel bekannt. PINK1 ist der erste Akteur, der in dem Weg, der zur Beseitigung von nicht funktionsfähigen Mitochondrien führt, ausgelöst wird. Ziel meiner Arbeit war es daher, zu verstehen, wie der PINK1-Importweg auf der Ebene des TOM-Komplexes in depolarisierten Mitochondrien reguliert wird.

Um dieses Ziel zu erreichen, habe ich einen Test zur Analyse der Bildung des PINK1-TOM-Komplexes entwickelt und validiert. Anschließend untersuchte ich die Wechselwirkungen zwischen PINK1 und den TOM70- und TOM20-Rezeptoren mittels Peptid-Scan-Assay und *in vitro* Pull-Downs. Ich konnte zeigen, dass TOM70 direkt an verschiedene Abschnitte im N-terminalen Bereich von PINK1 bindet. Ich konnte auch zeigen, dass die MTS von PINK1 für diese Interaktion entbehrlich ist. Als Nächstes führte ich eine Reihe von *In-vitro*-Importtests mit radioaktiv markiertem PINK1 in Kombination mit isolierten depolarisierten Mitochondrien durch, die für TOM70, TOM20 oder beide TOM70/TOM20 abgereichert waren. TOM70 KD beeinflusste signifikant die Assoziation von PINK1 mit dem MOM nach CCCP-Behandlung, während TOM20 eine marginale Rolle für den PINK1-Import spielte. Die doppelte Deletion beider Rezeptoren zeigte jedoch, dass TOM70 und TOM20 bei der

Erkennung von PINK1 eine austauschbare Rolle spielen könnten. Darüber hinaus stellte ich fest, dass TOM7 KD den Import der TOM-Komplex-Kunden beeinträchtigte, wahrscheinlich aufgrund seiner negativen Auswirkungen auf die Stabilität des Komplexes. Der PINK1-Import in depolarisierte Mitochondrien, die aus TOM7-KD-Zellen isoliert wurden, war mäßig beeinträchtigt. Die doppelte Deletion sowohl von TOM70, dem wichtigsten Erkennungsfaktor für PINK1 in der MOM, als auch von TOM7, dem TOM-Komplex-Stabilisierungsfaktor, hatte jedoch eine synthetische Wirkung auf die PINK1-Membranintegration. Als Nächstes untersuchte ich die Wirkung der TOM40-Porenblockade auf die PINK1-MOM-Assoziation. Wenn das TOM40-Lumen mit überschüssigen Mengen an mitochondrialem Vorläuferprotein verstopft war und das Membranpotential abgeleitet wurde, war die PINK1-Membranassoziation dramatisch beeinträchtigt. Schließlich wollte ich prüfen, ob PINK1 die Mitophagie-Kaskade auslösen kann, wenn es in der TOM40-Pore blockiert ist. Daher blockierte ich das TOM40-*Barrel* mit rekombinanten Mengen von TcPINK1 und importierte radioaktiv markierte hPINK1- sowie TOM40-Moleküle. Die Membranintegration beider Proteine war reduziert, was darauf hindeutet, dass sich PINK1 im TOM40-Lumen depolarisierter Mitochondrien aufhält und somit den Import anderer TOM Interaktoren behindert.

Insgesamt bieten meine Ergebnisse einen neuen Einblick in die Assoziation von PINK1 mit dem TOM-Komplex beim Abbau des mitochondrialen Membranpotenzials und deuten auf die unverzichtbare Rolle des TOM-Komplexes bei der richtigen Positionierung von PINK1 zur Einleitung der Mitophagie-Kaskade hin.

4. LIST OF PUBLICATIONS CONTAINED IN THIS THESIS

1. Bus, C., Zizmare, L., Feldkaemper, M., Geisler, S., Zarani, M., Schaedler, A., Klose, F., Admard, J., Mageean, C. J., Arena, G., Fallier-Becker, P., Ugun-Klusek, A., **Maruszczak, K. K.**, Kapolou, K., Schmid, B., Rapaport, D., Ueffing, M., Casadei, N., Krüger, R., . . . Fitzgerald, J. C. (2020). Human Dopaminergic Neurons Lacking PINK1 Exhibit Disrupted Dopamine Metabolism Related to Vitamin B6 Co-Factors. *iScience*, *23*(12), 101797. https://doi.org/10.1016/j.isci.2020.101797

2. **Maruszczak, K. K.**, Jung, M., Rasool, S., Trempe, J. F., & Rapaport, D. (2022). The role of the individual TOM subunits in the association of PINK1 with depolarized mitochondria. *Journal of Molecular Medicine*, *100*(5), 747–762. https://doi.org/10.1007/s00109-022-02191-6

5. PERSONAL CONTRIBUTION TO THE PUBLICATIONS CONTAINED IN THIS THESIS

1. Bus, C., Zizmare, L., Feldkaemper, M., Geisler, S., Zarani, M., Schaedler, A., Klose, F., Admard, J., Mageean, C. J., Arena, G., Fallier-Becker, P., Ugun-Klusek, A., **Maruszczak, K. K.**, Kapolou, K., Schmid, B., Rapaport, D., Ueffing, M., Casadei, N., Krüger, R., . . . Fitzgerald, J. C. (2020). Human Dopaminergic Neurons Lacking PINK1 Exhibit Disrupted Dopamine Metabolism Related to Vitamin B6 Co-Factors. *iScience*, *23*(12), 101797. https://doi.org/10.1016/j.isci.2020.101797

I performed *in vitro* import assays with radiolabeled pSu9-DHFR and Fis1 into mitochondria isolated from either control or PINK1 KO hDANs. I analyzed the import reactions by SDS-PAGE and autoradiography and quantified the relevant bands.

2. **Maruszczak, K. K.**, Jung, M., Rasool, S., Trempe, J. F., & Rapaport, D. (2022). The role of the individual TOM subunits in the association of PINK1 with depolarized mitochondria. *Journal of Molecular Medicine*, *100*(5), 747–762. https://doi.org/10.1007/s00109-022-02191-6

To be able to study the biogenesis of PINK1 in depolarized mitochondria, I first established the protocol for PINK1 analysis via BN-PAGE (Figures 1 and S1). To identify the receptors responsible for PINK1 recognition by the TOM complex, I performed peptide scan assays and *in vitro* pull-downs with radiolabeled PINK1-FL, PINK1(1-120)-eGFP, PINK1(35-120)-eGFP and purified cytosolic domains of TOM70 and TOM20 (Figure S2). To validate the importance of both receptors, I carried out a series of *in vitro* imports assays with radiolabeled PINK1 and polarized and depolarized mitochondria isolated from TOM70 KD HeLa cells, TOM20 KD U2OS cells and TOM70/TOM20 KD HeLa cells (Figures 2, 3, and 4). To investigate the importance of TOM7 and both TOM7 and TOM70, I performed an *in vitro* import of radiolabeled PINK1 into depolarized mitochondria isolated from either TOM7 KD U2OS cells (Figure 5) or TOM7/TOM70 KD HeLa cells (Figure 6). To understand the relevance of the TOM40 pore to the association of PINK1 with the MOM upon CCCP treatment, I blocked the import pore with purified chemical amounts of pSu9-DHFR and reimported radiolabeled PINK1 as well as various control proteins (Figure 7). To study the localization of PINK1 at the MOM upon dissipation of ΔΨm, I blocked the TOM40 lumen with excess amounts of purified TcPINK1 and imported radiolabeled versions

of hPINK1 and a control protein (Figure 8). I prepared all the figures, wrote the first draft of the manuscript, and participated in the writing of the final version.

6. INTRODUCTION

6.1 MITOCHONDRIAL BIOGENESIS AND QUALITY CONTROL

Mitochondria are versatile organelles that form tubular networks inside eukaryotic cells. They are highly dynamic structures undergoing fission and fusion processes in order to adjust to existing conditions and to maintain the cells in a healthy state (Youle & van der Bliek, 2012). Two membranes confine mitochondria, the outer and inner membrane, which define within the organelles two different aqueous compartments: the intermembrane space (IMS) and the matrix, both providing different environmental conditions for numerous mitochondrial processes. The cristae structures, the tubular inner membrane invaginations, harbor enzymes that are crucial for oxidative phosphorylation and ATP synthesis (Friedman & Nunnari, 2014). Various metabolic pathways, such as the Krebs cycle and the β-oxidation of fatty acids also take place in mitochondria (Chenette, 2011 & Houten *et al.,* 2016). In addition, these organelles are crucial for supplying the cells with various metabolites *i.e.* amino acids and steroids and are the major site for iron-sulfur clusters synthesis (Osellame *et al.,* 2012).

Mitochondria contain around 1500 various proteins in mammals and 1000 different proteins in yeast (Nunnari & Suomalainen, 2012). Among them, the vast majority are encoded by nuclear DNA and synthesized in the cytosol and only 13 proteins (in human) are encoded by the mitochondrial genome. These latter ones are subunits of the respiratory chain complexes as well as the F_1F_0-ATPase synthase. Hence, the vast majority of the mitochondrial proteins have to be imported from the cytosol to mitochondria via specialized import pathways. Various targeting and sorting signals exist to direct precursor proteins to specific locations within the mitochondria (Figure 1) (Wiedemann & Pfanner, 2017). The presequence pathway, also termed the classical pathway, comprises the import of proteins with presequence, which is located at their N-terminus and functions as the mitochondrial targeting sequence (MTS) (Schulz *et al.,* 2015). These protein precursors are imported via the translocase of the outer membrane (TOM) and subsequently via the translocase of the inner membrane (TIM23). Protein translocation into matrix is driven by the presequence translocase-associated motor (PAM) and subsequent cleavage of the presequence is carried out by the mitochondrial processing peptidase (MPP).

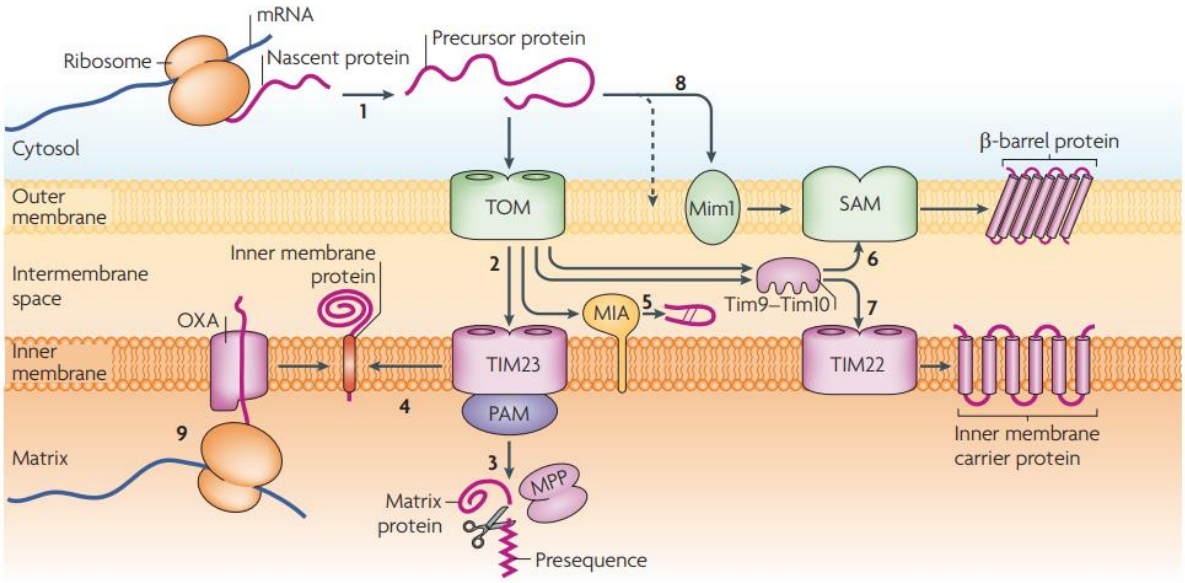

Figure 1. Biogenesis of mitochondrial proteins. Majority of mitochondrial proteins are encoded in the nucleus and synthesized on cytosolic ribosomes (1). Hence, they have to be translocated into mitochondria. Depending into which mitochondrial compartment the protein will be imported, different pathways exist: (2,3) presequence pathway, (2,4) assembly of inner membrane proteins via lateral release from the TIM23 complex, (5) mitochondrial import and assembly (MIA) machinery of the intermembrane space, (6) sorting and assembly machinery (SAM) of the β-barrel proteins, (7) carrier pathway involving TIM22 complex, (8) MOM-integration via Mim1 (*S. cerevisiae*), (9) proteins that are synthesized in matrix are exported into the mitochondrial inner membrane by the oxidase assembly (OXA) machinery. For the full description, refer to the chapter 6.1 Mitochondrial biogenesis and quality control. Adapted from "Mitochondrial protein import: from proteomics to functional mechanisms" by O. Schmidt, N. Pfanner and C. Meisinger, 2010, *Nature Reviews Molecular Cell Biology*, *11*(9), 655–667. https://doi.org/10.1038/nrm2959

However, the TOM complex is also capable of importing proteins containing non-cleavable signal sequences. One of those is the carrier pathway that is crucial for translocating multispan proteins of the inner membrane (Kurz *et al.,* 1999). The latter ones are imported by the TOM complex and the small TIM chaperones of the intermembrane space and afterwards inserted into the inner membrane through the carrier translocase of the inner membrane (TIM22). Another protein import route is called the β-barrel pathway (Becker *et al.,* 2008). The TOM complex serves as an initial gate for the precursors of β-barrel proteins that should integrate into the mitochondrial outer membrane (MOM). Subsequently, the small TIM chaperones help to stabilize the β-barrel proteins before their integration into the MOM, which is

facilitated by the sorting and assembly machinery (SAM) known also as topogenesis of outer membrane β-barrel proteins (TOB) complex.

Additional group of proteins are those that are destined to the mitochondrial IMS. A common feature of a large portion of these proteins is the presence of characteristic cysteine motifs (Stojanovski *et al.,* 2012). These proteins are imported through the TOM complex and afterwards via the mitochondrial import and assembly (MIA) machinery of the intermembrane space. The next pathway applies to various outer membrane proteins that have α-helical transmembrane segments. These proteins utilize the mitochondrial import (MIM) complex of the outer membrane (Horvath *et al.,* 2015) in *S. cerevisiae* and other fungal species, however its mammalian homologue remains to be discovered.

Being very crucial for cell homeostasis, mitochondria have to be continuously monitored by different quality control proteins and mechanisms. The mitochondrial unfolded protein stress response pathway (UPRmt) was characterized with the use of *Caenorhabditis elegans* (Haynes *et al.,* 2010). ATFS1, a transcription factor, is continuously translocated in healthy organelles into the mitochondrial matrix, where it undergoes degradation. Upon mitochondrial depolarization, the import efficiency of ATFS1 decreases and this leads to enhanced import into the nucleus where it boosts the transcription of mitochondrial chaperones and proteases. This in turn leads to remodeling of metabolism resulting in less dependency on respiration. Similar mechanism was suggested to occur in mammals where ATF5 is a transcription factor regulating the UPRmt pathway (Fiorese *et al.,* 2016).

Another quality control process deals with the destiny of the mitochondrial protein OPA1. In healthy cells, OPA1 is actively processed by the i-AAA protease YME1L resulting in the generation of long transmembrane anchored and short soluble isoforms that are necessary for mitochondrial fusion (Song *et al.,* 2007). Upon membrane potential attenuation, the long OPA1 isoforms are processed by the metalloprotease OMA1 and that leads to mitochondrial fusion inhibition and therefore shifting of the morphology balance towards mitochondrial fission. Such alterations may result in mitophagy induction and/or cell death.

A different quality control pathway relies on the kinase PINK1 and the E3 Ub ligase Parkin (Vincow *et al.,* 2013). In healthy mitochondria, PINK1 is imported into the

organelle where the protease PARL cleaves it within the transmembrane domain. Such altered PINK1 is subsequently translocated into the cytosol and degraded by the proteasome. Upon mitochondrial depolarization, PINK1 is accumulated in the MOM where it phosphorylates ubiquitin conjugated to various MOM proteins. In addition, PINK1 phosphorylates Parkin, which in turn ligates another ubiquitin molecule to the previously phosphorylated ubiquitin. This process leads to the formation of long ubiquitin chains and generation of positive feedback that result in mitophagy. Mutations in PINK1 and Parkin have been associated with the occurrence of familial Parkinson's disease (PD). This observation indicates how crucial their function is. PINK1 recognition by the TOM complex and its import into mitochondria remain elusive. Therefore, it is relevant to elucidate these mechanisms specially since such insights would help to better understand the PD pathological mechanism.

6.2 PINK1 DOMAIN STRUCTURE AND FUNCTION

PINK1 is a Ser/Thr mitochondrial kinase consisting of 581 amino acids and its molecular weight is 64 kDa. PINK1 stands for a PTEN-induced putative kinase 1 since it was originally found to be upregulated by PTEN (the tumor suppressor gene) in cancer cells (Unoki & Nakamura, 2001). The protein is built from a mitochondrial targeting sequence, transmembrane domain, kinase domain and the C-terminal tail (Figure 2).

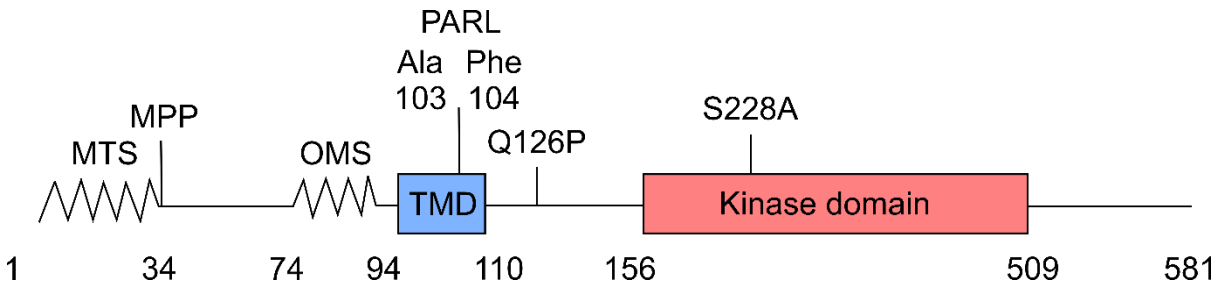

Figure 2. Schematic representation of PINK1 domain structure. PINK1 is built of N-terminally localized mitochondrial targeting sequence (MTS), outer mitochondrial membrane localization signal (OMS), transmembrane domain (TMD), kinase domain and C-terminal extension. Predicted MPP and PARL cleavage sites are annotated. Two mutations used in the study are shown: Q126P and S228A.

6.2.1 MITOCHONDRIAL TARGETING SEQUENCE OF PINK1

The general feature of the MTS is the capability to form an amphipathic helix with one hydrophobic face and one positively charged face (Sekine & Youle, 2018). Upon aligning of the PINK1 orthologue sequences, it was found that the human PINK1 MTS might stretch up to 100 amino acids (Sim *et al.,* 2012). Hence, it was suggested that PINK1 could be cleaved more than once by MPP, however the exact cutting sites remain unknown (Greene *et al.,* 2012). By knocking down various mitochondrial proteases using different small interfering RNAs, two of them *i.e.* MPP comprising of the MPPα and MPPβ subunits and, to a lesser extent, ClpP (matrix ATP-dependent protease), were identified to be involved in the processing of PINK1 (Greene *et al.,* 2012). Comparison of known MPP cleavage site motifs found in different mitochondrial proteins suggested that the conserved arginine residue is the one that is recognized by MPP (Sim *et al.,* 2012). Accordingly, two potential cleavage sites were mapped to the 8-18 and 67-77 residues of human PINK1 (Sim *et al.,* 2012). Both amino acid stretches were found to contain a conserved arginine and hydrophobic amino acids, which are necessary for the MPP processing. However, the aforementioned predictions were never experimentally confirmed. Different studies focused on determining the minimum sequence length of the MTS in order to be targeted to mitochondria. Muqit et al. (2006) showed that fusing the first 34 amino acids of human PINK1 with enhanced green fluorescent protein (eGFP) resulted in mitochondrial targeting of the fusion protein. Another research revealed that the first 93 residues are enough to translocate enhanced cyan fluorescent protein (eCFP) into mitochondria (Silvestri *et al.,* 2005).

6.2.2 THE TRANSMEMBRANE DOMAIN OF PINK1

Two different classes of transmembrane proteins can be distinguished: those containing one or more α-helical transmembrane domains or those composed of β-strands forming β-barrels (Sharpe *et al.,* 2010).

The putative transmembrane domain of human PINK1 is built of a single α-helix containing 21 amino acids and encompassing residues 91-111 (Sim *et al.,* 2012). The transmembrane domain of PINK1 serves as a “stop transfer” signal for the protein translocation and arrests it in the TIM23 complex. PINK1 undergoes a cleavage

carried out by the PARL protease (which is described in details below) while being captured within the inner membrane. This cleavage results in the formation of the 52 kDa mature form of the protein (Yamano *et al.,* 2016).

6.2.3 THE KINASE DOMAIN OF PINK1

The kinase domain of PINK1 encompasses amino acid residues 156-509 and exhibits a high degree of homology to the Ser/Thr kinase of the Ca^{2+}/calmodulin-dependent kinase family (Zhou *et al.,* 2008). The kinase activity was confirmed by utilizing recombinant PINK1 and its enzymatically inactive mutants *i.e.* K219A, D362A or D384A. The mutated residues play a central role in orienting ATP within the enzyme and transferring a phosphate group onto the acceptor residues of the substrates (Okatsu *et al.,* 2012). Apart from phosphorylating other proteins, PINK1 undergoes autophosphorylation (Yamano *et al.,* 2016). Phos-tag gel analysis revealed that upon loss of mitochondrial inner membrane potential, PINK1 exhibits a mobility shift, which is the result of its phosphorylation (Okatsu *et al.,* 2012). Following the latter discovery, Okatsu et al. (2012) found two residues, Ser228 and Ser402, that are relevant for the PINK1 autophosphorylation, and therefore for its activation. Besides protein phosphorylation and autophosphorylation, PINK1 can also undergo trans-phosphorylation. Co-expressing PINK1 wild type and its kinase mutant (G409V), which is not autophosphorylated when expressed on its own, led to the activation of the kinase domain of the G409V mutant indicating the trans-phosphorylation event (Okatsu *et al.,* 2012). Furthermore, mutating both residues Ser228 and Ser402 to Ala confirmed the specificity of the autophosphorylation sites, since the mutants did not display any mobility shift upon phos-tag gel analysis (Okatsu *et al.,* 2012).

6.2.4 THE C-TERMINUS REGION OF PINK1

The C-terminus of protein kinases often comprises various functional motifs responsible for the regulation of the kinase activity (Nolen *et al.,* 2001). In order to investigate the functions of the C-terminal region of PINK1, Sim et al. (2012) performed a sequence alignment search for protein domains similar to the carboxyl terminus of PINK1. However, the aforementioned analysis failed to identify any similarities between the C-terminal region of PINK1 and other proteins, hence it was concluded that the C-terminus of PINK1 has a unique function. A secondary structure prediction

suggested that the carboxyl terminus comprises three α-helices and three disordered loops (Sim *et al.,* 2012). Recent structural studies of PINK1 orthologs from *Pediculus humanus corporis* (lice) and *Tribolium castaneum* (beetle) showed that the protein C-terminus is built of helical bundle that piles on top of the C-lobe, overall called a C-terminal extension (CTE) (Rasool *et al.,* 2021). The evolutionary conservation of these structural elements might indicate that the C-terminus of PINK1 has some importance for its structure and function (Sim *et al.,* 2012). Indeed, PINK1 structure resolved by Rasool et al. (2021) shows that the N-terminal helix (NT) binds to the C-terminal extension, which was proposed to play a role in stabilizing PINK1 on the TOM complex. Along this line, NT-CTE interaction was speculated to facilitate the contacts of PINK1 with helical TOM core subunits.

6.3 PINK1 IMPORT PATHWAY AND PROCESSING IN HEALTHY MITOCHONDRIA

PINK1 is encoded by nuclear DNA, synthesized on the cytosolic ribosomes and subsequently imported into mitochondria via a classical pathway utilizing TOM complex at the outer mitochondrial membrane (Sekine & Youle, 2018). PINK1 possesses the MTS at its N-terminus that is recognized by the TOM20 receptor cooperating with TOM22 (Valente *et al.,* 2004). Such precursors are afterwards translocated via the translocation pore (TOM40) and handed over onto the TIM23 complex of the inner mitochondrial membrane (Neupert & Herrmann, 2007). Positively charged MTS translocation into the matrix is dependent on the membrane potential (ΔΨm) across the inner membrane. The MTS of PINK1 was suggested to be cleaved off by MPP in the matrix of mitochondria (Greene *et al.,* 2012). It was shown that upon PINK1 overexpression, a lower molecular weight band at 52 kDa was detected apart from the full-length protein of around 64 kDa (Muqit *et al.,* 2006). A different study revealed that when the mitochondrial import was hindered by the addition of an uncoupler, the lower molecular band corresponding to 52 kDa disappeared. Hence, it was concluded that the other form of PINK1 was generated by the import-associated activity of an unknown protease (Silvestri *et al.,* 2005). This protease was later identified by a genetic study that used *Drosophila melanogaster* to be a Rhomboid-7 protease. Presenilin-associated rhomboid-like/PINK1/PGAM5-associated protease (PARL) is its mammalian homologue (Whitworth *et al.,* 2008). Indeed, the knockout

(KO) of PARL in mouse embryonic fibroblasts induced the formation of 60 kDa PINK1, which could be the MTS-cleaved form of the protein.

PARL resides in the mitochondrial inner membrane and belongs to the family of rhomboid proteases (Jin *et al.,* 2010). This rhomboid protease is capable of catalyzing the cleavage within the transmembrane domains that have been arrested in the TIM23 complex. The cleavage by rhomboid proteases depends on several features (Ha et *al.,* 2013). One of them is the presence of helix-destabilizing amino acids such as proline or glycine that create a kink in the helical structure. The second requirement is the recognition of specific and among vertebrates conserved residues surrounding the cleavage site *inter alia* alanine, glycine, cysteine and serine at the P1 position (before the cleavage site). Edman degradation assay showed that PINK1 is cleaved by PARL between Ala103 and Phe104 (Deas *et al.,* 2011).

6.4 N-END RULE-DEPENDENT DEGRADATION OF PINK1

The 52 kDa PINK1 variant was found to be localized to the cytosol. This form is considered as unstable as compared to the full-length protein since its accumulation was only detected upon addition of the proteasomal inhibitor MG132 (Narendra *et al.,* 2010). The mechanism of PINK1 retro-translocation into the cytosol and subsequent degradation by the proteasome was explained by the N-end rule proteasome pathway (Yamano & Youle, 2013). After being cleaved by PARL, PINK1 with the newly generated N-terminus (Phe104) is retro-translocated back into the cytosol.

It was found that several amino acids at the amino terminus of proteins may promote ubiquitination and are called degrons (Tasaki *et al.,* 2005). Degrons can be divided into basic ones or bulky hydrophobic, type 1 or type 2, respectively. The phenylalanine at the N-terminus of the cleaved PINK1 falls into the category of type-2 N-degrons (Tasaki *et al.,* 2012). Therefore, after PINK1 retro-translocation into the cytosol, its altered N-terminus is recognized by the E3 ubiquitin ligating enzymes *i.e.* UBR1, UBR2 and UBR4 and subsequently undergoes proteasomal degradation (Yamano & Youle, 2013).

6.5 PINK1-PARKIN INDUCED MITOPHAGY

Upon depolarization of mitochondria, PINK1 accumulates at the MOM (the mechanism is discussed later in this chapter). Activated PINK1 phosphorylates proteins, which as a part of their turnover, were previously ubiquitinated by the E3 ligases Mul1 and March5 that reside on the MOM (Yoo *et al.,* 2015, Rojansky *et al.,* 2016). Subsequently, Parkin is translocated to the MOM where it is activated by binding to phosphoubiquitin (Ordureau *et al.,* 2014). Furthermore, Parkin is an E3 ligase possessing ubiquitin-like domain that is phosphorylated at Ser65 residue by PINK1. This phosphorylation leads to Parkin stabilization in an active state (Kondapalli *et al.,* 2012). Subsequently, Parkin ubiquitinates different mitochondrial proteins that are localized at the MOM, forming poly-ubiquitin chains that are in turn phosphorylated by PINK1 (Sarraf *et al.,* 2013). The latter process results in a positive feedback amplification cycle, which eventually leads to mitochondrial autophagy termed mitophagy.

Abundant ubiquitination triggers p97 and the proteasome to be recruited to mitochondria where proteins such as Mfn1 and Mfn2, that play a role in mitochondrial fusion, undergo proteasomal degradation (Tanaka *et al.,* 2010). It is believed that fast poly-ubiquitination of both mitofusins helps in segregating healthy mitochondria from the damaged ones (Twig *et al.,* 2008). p97 is a hexameric AAA+ ATPase that plays a crucial role in ubiquitin-dependent proteolysis (Meyer *et al.,* 2014). Npl4/Ufd1 heterodimer is a cofactor that binds to p97 and to some extent helps the degradation of the MOM proteins during mitophagy (Kimura *et al.,* 2013, Kim *et al.,* 2013). Additionally, the protein levels of Miro1, which is involved in the transport of mitochondria along microtubules, were found to be decreased upon PINK1-Parkin mitophagy induction (Chan *et al.,* 2011). Wang et al. (2011) concluded that the rapid degradation of Miro1 leads to microtubule-dependent mitochondrial trafficking arrest, which prevents the translocation of the damaged mitochondria.

6.6 MODIFIERS OF MITOCHONDRIAL QUALITY CONTROL

Several negative and positive regulators have been discovered to affect the PINK1-Parkin induced mitophagy. Three enzymes are activated stepwise in order to ubiquitinate a substrate, E1 (ubiquitin-activating enzyme), E2 (ubiquitin-conjugating

enzyme) and the final E3 which transfers ubiquitin onto the lysine residue of a substrate (Yamano *et al.,* 2016). Some enzymes of the E2 family that are responsible for the ubiquitin conjunction alter the activation and translocation of Parkin (Fiesel *et al.,* 2014). Two of them, UBE2D and UBE2L3, transfer the ubiquitin moiety directly onto a Parkin catalytic center. In contrast, UBE2R1 regulates Parkin in a negative manner. F-box only protein 7 (Fbxo7), which belongs to the E3 ubiquitin ligase complex, associates with both PINK1 and Parkin and triggers Parkin recruitment to the depolarized mitochondria (Burchell *et al.,* 2013).

Another class of enzymes, namely deubiquitinating enzymes (DUBs), work antagonistically to Parkin E3 ubiquitin ligases *i.e.* they remove the ubiquitin moiety from the substrates and in this way regulate PINK1-Parkin mitophagy (Wu *et al.,* 2004). For instance, the overexpression of the MOM-tethered USP30 (which cleaves K6 and K11-linked chains as well as K48 and K63-linked branched ubiquitin chains) was proved to inhibit mitophagy and its siRNA-mediated knockdown triggers induction of mitophagy (Bingol *et al.,* 2014). Along the same line, overexpression of the cytosolic USP15, which is also responsible for the reduction of K48- and K-63-linked ubiquitin chains, was reported to attenuate mitophagy. Anti-apoptotic Bcl-2, Mcl-1 and Bcl-xL, which are localized to the MOM, impede Parkin translocation leading to suppression of mitophagy (Hollville *et al.,* 2014). Beclin1 is a pro-autophagic protein that was found to interact with PINK1, and the latter interaction leads to the induction of an autophagy response in neuronal cell (Michiorri *et al.,* 2010). Finally, it was reported that some microRNAs become more prominent under chronic mitophagy flux and act as inhibitors of PINK1 expression indicating a negative feedback regulation (Kim *et al.,* 2016).

6.7 PINK1 MUTANTS LEAD TO THE DEVELOPMENT OF PARKINSON'S DISEASE

Parkinson's disease is caused by a loss of dopaminergic neurons in the substantia nigra pars compacta and accumulation of an intracellular protein, α-synuclein. Such pathologies lead to the development of a chronic progressive neurodegenerative disease with several characteristic symptoms *i.e.* bradykinesia, rigidity, tremor and postural instability (Radhakrishnan & Goyal, 2018). Parkinsonism cases are mostly sporadic, however 5-10% of them are of hereditary cause (Lesage & Brice, 2009). Several genes have been identified as causative genes for familial Parkinson's

disease namely α-synuclein, Parkin, PINK1, leucine rich repeat kinase 2 and DJ-1. Mutations in PINK1 cause an autosomal recessive young onset of Parkinson's disease (Hatano *et al.,* 2009). Three mutations found in the MTS region of PINK1 *i.e.* G32R, P52L and A78V were associated with PD (Sim *et al.,* 2012). The first of the aforementioned mutations, G32R was speculated to have an effect on the distribution of the positive charges on the helix. On the other hand, the R68P mutation may result in hindrance of PINK1 translocation due to the reduction of positive charges on the helix. The P52L mutation might lead to the loss of a "kink" or flexibility of the MTS that might result in disordered structural integrity (Sim *et al.,* 2012).

Two PD-associated mutations were found in the transmembrane domain of PINK1 namely R98F and I111S. Both the arginine and isoleucine residues are evolutionary conserved among vertebrates, hence most likely crucial for the maintenance of the structural integrity of the transmembrane α-helix (Sim *et al.,* 2012). Moreover, both mutations could affect the PARL-mediated cleavage. For instance, the R98F mutation interrupted the aforementioned processing and led to the increased levels of the non-cleaved PINK1 in HeLa cells (Jin *et al.,* 2010). Woodroof et al. (2011) found one mutation, C125G, at the region between the TMD and kinase domain that resulted in a decrease of PINK1 kinase activity by 40%. More than 50 mutations in the PINK1 kinase domain were discovered to be associated with PD, however the impact of most of them has not been elucidated yet. Song et al. (2013) investigated several of the mutants using mammalian cells and *Drosophila* model system. The two mutants, human G309D and L347P corresponding to *Drosophila* G426D and L464P, respectively, failed to trigger the translocation of Parkin to the mitochondrial outer membrane. Other PD-related mutants, such as G386A and G409V significantly inhibited PINK1 kinase activity (Woodroof *et al.,* 2011). Two PD-associated mutations were found in the C-terminus of PINK1 *i.e.* A537T and N542S and they were predicted to abolish the regulatory function and/or the ability to maintain structural integrity of the carboxyl terminus of the protein (Sim *et al.,* 2012).

6.8 CROSSTALK OF PINK1-PARKIN WITH OTHER PARKINSON'S DISEASE GENES

Lately, several co-substrates of PINK1 and Parkin have been discovered indicating the sophisticated mechanism that underlies the PINK1 and Parkin-mediated quality control of mitochondria. Kamp et al. (2010) found that pronounced mitochondrial

fragmentation caused by α-synuclein aggregation could be rescued by co-expressing PINK1, Parkin, or DJ-1. In agreement, downregulation or deletion of either PINK1 or Parkin triggered the development of mitochondrial pathologies and made the neurons more susceptible to α-synuclein-induced neurotoxicity. Interestingly, Di Maio et al. (2016) showed that α-synuclein directly binds to the Tom20 import receptor leading to hindered mitochondrial import, which was believed to have a negative effect on PINK1-Parkin pathway.

Fbxo1 is another protein whose mutations were found to cause an early onset of autosomal recessive PD, however, the underlying mechanism has not been yet identified (Burchell *et al.,* 2013). Proteins that contain an F-box domain were shown to target substrates to SCF-type E3-ubiquitin ligase complexes (Skowyra *et al.,* 1997). Burchell et al. (2013) showed that Fbxo1 participates in mitochondrial maintenance by interacting with PINK1 and Parkin. Furthermore, it was found that Fbxo1 depletion negatively affects the translocation of Parkin onto mitochondria as well as ubiquitination of Mitofusin 1 and finally mitophagy. Several other proteins, like Beclin-1 and PARIS, were shown to interact with PINK1. Michiorri et al. (2010) showed that full-length PINK1 interact with pro-autophagic Beclin-1, which leads to enhanced basal and starvation-induced autophagy induction. Lee at al. (2017) demonstrated that PINK1 phosphorylates PARIS, which leads to its ubiquitination and subsequent clearance by Parkin. PARIS functions to repress PGC-1α, a transcriptional coactivator that has its crucial role in the cellular energy metabolism regulation (Shin *et al.,* 2011). Hence, dysfunction of PINK1 or Parkin results in PARIS accumulation and PGC-1α repression which was claimed to have a central effect on dopamine neuron loss. Therefore, PARIS was suggested to be one of the players in pathogenesis of PD (Lee *et al.,* 2017).

6.9 PINK1 IMPORT MECHANISM INTO DEPOLARIZED MITOCHONDRIA

The critical step in PINK1-Parkin mitophagy induction is PINK1 arrest at the outer membrane of unfunctional mitochondria, hence it is important to understand the mechanism of this process. The translocation of various proteins via the TIM23 complex is hindered upon mitochondrial depolarization, which results in cytosolic retention of multiple protein precursors. Under such conditions, PINK1 instead of being retro-translocated, is inserted into the mitochondrial outer membrane. There are three

main published hypotheses regarding the precise location of PINK1 in the MOM of depolarized organelles. The first suggests that PINK1 is laterally released from the TOM complex into the bulk of the outer membrane (Nguyen *et al.,* 2016). The second argues that PINK1 is arrested in the TOM40 lumen from where it can trigger the mitophagy cascade (Hasson *et al.,* 2013), whereas the third proposes that the N-terminal segment of PINK1 could undergo lateral release, but remains bound to the TOM complex and is not released into the bulk of the membrane (Rasool *et al.,* 2021).

In an effort to better understand the interaction of the TOM complex with newly synthesized PINK1 molecules, several studies investigated the role of specific TOM components. Two studies point towards the relevance of TOM7, an accessory protein belonging to the TOM complex, as being a “side gate” for PINK1 membrane insertion (Hasson *et al.,* 2013, Sekine *et al.,* 2019). This suggestion is based on the observation that CCCP treatment of HeLa cells lacking TOM7 failed to induce PINK1 accumulation in the MOM (Sekine *et al.,* 2019). Another factor that was found to be relevant for PINK1 retention in the MOM is the presence of the outer mitochondrial membrane localization signal (OMS) (Okatsu *et al.,* 2015). The OMS comprises a weak hydrophobic segment localized N-terminally to the transmembrane domain of PINK1 and encompassing amino acid residues 70-95. Moreover, it was experimentally proved that upon CCCP depolarization of mitochondria, PINK1(1-90) was still able to insert into the MOM (Okatsu *et al.,* 2015). Sekine et al. (2019) concluded that both TOM7 and OMS are crucial in PINK1 retention, with TOM7 mediating the lateral release of the protein from the TOM40 channel.

Lazarou et al. (2012) showed that PINK1 full-length accumulates in the MOM in the form of high molecular weight (HMW) complexes with the TOM complex at an apparent size of 720 kDa containing at least three TOM subunits: TOM40, TOM20, and TOM22. Additionally, Okatsu et al. (2013) discovered that PINK1 forms dimers in such HMW complexes and is found to be in the phosphorylated forms. Considering all the aforementioned findings, a model was proposed where the TOM complex facilitates accurate orientation of the dimeric PINK1 so that the intermolecular phosphorylation and subsequent activation can occur (Okatsu *et al.,* 2013).

Since PINK1 accumulation at the MOM is the first event that leads to the removal of malfunctional mitochondria, it is of great importance to understand the exact

mechanism of this process, namely the recognition of PINK1 at the MOM as well as its further membrane-integration.

7. RESEARCH OBJECTIVES

Considerable research has been done to understand the biogenesis of PINK1 in healthy as well as damaged mitochondria. Nevertheless, the import pathway of the protein into the malfunctional organelle remains elusive. Recently, a model was proposed in which the TOM complex assures accurate orientation of the dimeric PINK1 enabling its intermolecular phosphorylation which leads to its activation. The latter step is necessary for the induction of mitophagy, which is stimulated by PINK1 and Parkin. Any disturbance in this organellar quality system leads to a failure in removal of compromised mitochondria, which results in the development of neurodegenerative diseases such as Parkinsonism. Hence, studying the import route of PINK1 to the MOM can provide a new insight and potential therapeutic targets to combat such disorders.

Currently, it is unresolved which receptor at the TOM complex is more important for the recognition of PINK1: TOM70 or TOM20. Moreover, also TOM7 was found to play an important role in PINK1 assembly into MOM, however the exact mechanism by which TOM7 contributes to the membrane integration is yet to be discovered. Collectively, there are three hypotheses regarding the precise location of PINK1 at the MOM of non-polarized organelles: 1) PINK1 is laterally released from the TOM complex into the lipid bulk of the MOM, 2) PINK1 is stalled in the lumen of TOM40 pore, and 3) the N-terminal segment of PINK1 undergoes lateral release, but remains bound to the TOM complex.

The main goal of this study was to clarify the aforementioned uncertainties and answer the following questions:

1) Which receptor at the MOM is playing the major role in recognition of PINK1?
2) What is the role of TOM7 in PINK1 association with the TOM complex?
3) Where does PINK1 reside in the OMM?

These questions were addressed in the article “The role of the individual TOM subunits in the association of PINK1 with depolarized mitochondria” (Maruszczak *et al.,* 2022).

8. SUMMARY OF THE RESULTS AND DISCUSSION

The role of the individual TOM subunits in the association of PINK1 with depolarized mitochondria (Maruszczak et al., 2022)

8.1 SUMMARY OF THE RESULTS

PINK1 is a crucial protein in quality control of mitochondria and extensive research was carried out to elucidate its function and biogenesis. The unique feature of the protein is its two different fates depending on mitochondrial fitness. While PINK1 import is relatively well described in healthy organelles (for an extensive review see Sekine & Youle, 2018), the understanding of the pathway that leads to its accumulation at the outer membrane of depolarized organelles is limited. PINK1 arrest at the MOM is essential for activation of mitophagy. Accordingly, the goal of this study was to dissect the individual steps that lead to the correct integration of PINK1 in the MOM.

8.1.1 ASSOCIATION OF PINK1 WITH THE TOM COMPLEX IN DEPOLARIZED MITOCHONDRIA

The first step in studying PINK1 arrest at the MOM was to establish an assay that would allow differention between monomeric soluble PINK1 and membrane-associated protein. Previous research show that upon CCCP treatment of mitochondria, PINK1 co-migrates on BN-PAGE with the TOM complex, forming a stable complex of 700 kDa (Lazarou *et al.,* 2012). To verify this report, I performed an *in vitro* import of radiolabeled PINK1 into CCCP-treated mitochondria isolated from HeLa cells. After the import reaction, the organelles were solubilized with digitonin and analyzed by BN-PAGE and autoradiography. I observed a built-up of a band at approximately 700 kDa (Maruszczak *et al.,* 2022, Fig. 1a). I used two methods to confirm that this radioactive 700 kDa band indeed represents PINK1 associating with the TOM complex: (i) immunodepletion and, (ii) antibody shift.

I could deplete the TOM complex containing PINK1 using TOM22 antibody coupled to protein A beads (Maruszczak *et al.,* 2022, Fig. 1a). To prove the specificity of the assay, I also used antibodies against unrelated mitochondrial proteins, i.e. Cytochrome C and VDAC1 (Maruszczak *et al.,* 2022, S1a). As expected, they did not deplete the PINK1-TOM complex. Furthermore, by incubating solubilized mitochondria

with imported PINK1 with TOM22 antibody, I could detect a size shift on BN-PAGE of the band representing the PINK1-TOM complex. As expected, when the same experiment was performed using an antibody against the unrelated protein ATP5A, the complex did not change its size (Maruszczak *et al.,* 2022, S1b). To check whether the mutations of PINK1 related to Parkinson disease would affect initial PINK1 association with the TOM complex, I imported radiolabeled PINK1 S228A, which is an autohposhorylation site for PINK1, and N-terminally localized glutamine to proline variant (Q126P) into depolarized mitochondria (Maruszczak *et al.,* 2022, Fig. 1c,d). Mutated PINK1 was imported as efficiently as the native protein, which is in line with previous results (Okatsu *et al.,* 2013; Rasool *et al.,* 2021). Collectively, these observations support the usage of an *in vitro* import assay followed by BN-PAGE as a robust and reliable method to study the association of PINK1 with the MOM.

8.1.2 IDENTIFICATION OF TOM70 AS A POTENTIAL RECEPTOR FOR PINK1 IMPORT INTO MITOCHONDRIA

PINK1 is synthesized on cytosolic ribosomes and then has to be targeted to the surface of mitochondria. PINK1 possesses N-terminal mitochondrial targeting sequence and is imported via a presequence pathway into healthy mitochondria (Jin *et al.,* 2010). It is commonly accepted that whereas TOM20 recognizes mainly precursor proteins bearing N-terminal presequences, TOM70 specializes in processing precursors harboring internal hydrophobic segments as well as internal MTSs (Yamano *et al.,* 2008). Interestingly, Kato et al. (2013) showed that PINK1 is recognized by TOM70 receptor in healthy mitochondria. To further investigate the interaction between PINK1 and TOM70, I performed a peptide scan, in which peptides encompassing the N-teminal 140 amino acids of PINK1 were synthsized onto a nitrocellulose membrane (in collaboration with Dr. M. Jung, Homburg). These N-terminal 140 amino acids residues are expected to contain all the targeting and sorting information in PINK1. I excluded the kinase domain in that assay, as I did not expect major import motifs in this part of the protein. The outcome of this assay indicated that Tom70 binds the N-terminus of PINK1 in three segments: MTS, OMS and TMD, indicating the ability of the receptor to recognize internal MTSs as well as hydrophobic segments of PINK1 (Maruszczak *et al.,* 2022, S2a,b).

To further substantiate these interactions, I incubated the cytosolic domain of yeast Tom70 with newly translated radiolabeled PINK1. In parallel, synthesized PINK1 was also incubated with the cytosolic domain of yeast Tom20 as well as glutathione S-transferase (GST), since both proteins were N-terminally tagged with GST. The results showed that PINK1 directly interacts with Tom70, while Tom20 binding was rather weak (Maruszczak *et al.,* 2022, S2c). These findings further support the central role of TOM70 in PINK1 recognition and subsequent import. Lastly, I checked whether the MTS of PINK1 is crucial for its direct interaction with Tom70, by generating a construct of the protein without its presequence. Notably, PINK1 lacking its MTS bound the receptor as efficiently as the one containing it (Maruszczak *et al.,* 2022, S2d).

Interestingly, when I performed a peptide scan assay with purified cytosolic domain of Tom20, I observed binding over the whole length of PINK1 N-terminus (Figure 3). This observation is not surprising, since Sim et al. (2012) predicted that the MTS of PINK1 might encompass amino acids 1-100 of PINK1 as they were predicted to form an amphipathic helix. The apparent discrepancy between the moderate binding of Tom20 as reflected in the peptide scan and the weak binding observed in the *in vitro* pull-down assay might be due to the different experimental set-up. The peptides printed onto the membrane in the peptide scan are available for binding, whereas the N-terminus of PINK1 (as part of the whole protein) might be masked by other elements of the structure.

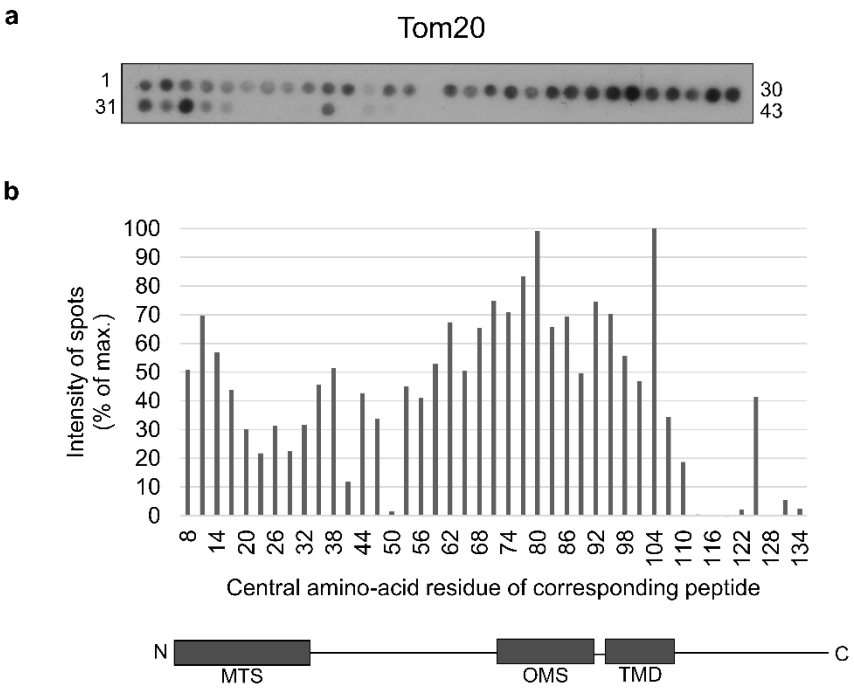

Figure 3. The cytosolic domain of Tom20 interacts with PINK1 in the peptide scan assay. (a) Nitrocellulose membrane containing 15-mer peptides covering amino acid residues 1-140 of PINK1 was incubated with recombinantly expressed cytosolic domain of yeast Tom20. After incubation, the interaction was visualized by immunodecoration using antibody against Tom20 (upper panel). The numbers flanking the panel reflect the serial numbers of the peptides. (b) The intensity of each dot was quantified and the average quantification of three independent experiments were plotted. The dot with the strongest intensity was set as 100%. The numbers on the X-axis reflect the central amino acid residue of each peptide. A schematic representation of the N-terminal region of PINK1 is shown. MTS: mitochondrial targeting signal; OMS: outer mitochondrial membrane localization signal; TMD: transmembrane domain.

8.1.3 TOM70 PLAYS AN IMPORTANT ROLE IN PINK1 RECOGNITION AT THE SURFACE OF MITOCHONDRIAL OUTER MEMBRANE, WHILE THE ROLE OF TOM20 IS MARGINAL

To validate the importance of TOM70 receptor, I performed *in vitro* imports of radiolabeled PINK1 into mitochondria isolated from HeLa cells that were depleted of TOM70. Firstly, I incubated newly translated PINK1 with polarized mitochondria and observed a significant reduction (30%) of the import of PINK1 into organelles depleted from the receptor as compared to control organelles (Maruszczak *et al.,* 2022, Fig. 2c,d). This observation is in agreement with previously published data (Kato *et al.,* 2013). The efficiency of the protein translocation was measured by the formation of 52 kDa band that corresponds to PARL-processed PINK1 (Jin *et al.,* 2010). Furthermore,

I carried out the same experiment with mitochondria depolarized with CCCP prior to the import. PINK1 association with the TOM complex was reduced by 30% in mitochondria depleted of TOM70 as compared to control (Maruszczak *et al*., 2022, Fig. 2e,f).

Although TOM20 did not bind PINK1 as efficiently as TOM70, I could not fully exclude the possibility that it contributes to PINK1 recognition at the MOM. Hence, I performed *in vitro* imports of PINK1 into mitochondria depleted of TOM20. The formation of the 52 kDa PINK1 species was comparable in control and TOM20 KD organelles (Maruszczak *et al.,* 2022, Fig. 3c,d). Upon treatment of mitochondria with CCCP to force PINK1 arrest at the MOM, I could observe 20% reduction of PINK1 association with the TOM complex of TOM20 KD organelles as compared to control (Maruszczak *et al.,* 2022, Fig. 3e,f). These experiments suggest a rather marginal role of TOM20 receptor in the import of PINK1.

Since PINK1 was still imported into mitochondria depleted of either TOM70 or TOM20, I wanted to check whether in the absence of one receptor, the other could take over its role. Hence, I knocked down both proteins in HeLa cells, isolated mitochondria from these cells and performed *in vitro* import into polarized as well as CCCP-treated organelles. The processing of PINK1 by PARL decreased to 80% in TOM70/TOM20 KD, while association of PINK1 with the TOM complex dropped to 40% (Maruszczak *et al.,* 2022, Fig. 4c-f). The drastic reduction of the import, especially in depolarized mitochondria indicates the exchangable roles of both receptors and may indicate that both receptors have stabilizing roles in the association of PINK1 with the TOM complex.

8.1.4 PINK1 ASSOCIATION WITH THE TOM COMPLEX IS REDUCED UPON KNOCK DOWN OF TOM7

TOM7, a small accessory protein of the TOM complex, was found to play a role in the association of PINK1 with the MOM upon depolarization of the organelles (Hasson *et al.,* 2013; Sekine *et al.,* 2019). However, the mechanism by which TOM7 facilitates this process remains unclear. To better understand this issue, I knocked down TOM7 in U2OS cells and isolated mitochondria from these cells. Since I could not find a functional antibody against TOM7, I validated the depletion in three different ways. Firstly, it was previously reported that upon knock down of TOM7, the TOM complex

loses its stability and migrates at apparently lower molecular mass (Kato & Mihara, 2008). Thus, I solubilized mitochondria isolated from control and TOM7 depleted cells and analyzed them via BN-PAGE. Indeed, I could observe altered migration pattern of the TOM complex in the TOM7 KD cells (Maruszczak *et al.,* 2022, Fig. 5a). Secondly, I used scrambled siRNA in parallel to siRNA against TOM7 to exclude any non-specificity. I imported radiolabeled TOM40 into mitochondria isolated from the control cells as well as the cells treated with the specific siRNAs. Notably, TOM40 integrated into the TOM complex in all three cases, however in the TOM7 KD mitochondria, the TOM complex in which TOM40 integrated appeared to migrate lower, as it was seen previously (Maruszczak *et al.,* 2022, Fig. 5b). When the same membrane was decorated with the anibody against TOM40, the endogenous complex also migrated lower and appeared less stable. Thirdly, I performed RT-qPCR as the final validation of the knock down and the results showed dramatically decreased levels of the TOM7 encoding mRNA (data not shown). Taken together, the TOM7 KD presented an expected and constant effect on the TOM complex, assuring that the depletion of the protein was specific.

Since the stability of the TOM complex is compromised in mitochondria from TOM7 KD cells, I tested whether any client protein of this complex will be affected by such hindrance. Hence, I imported radiolabeled matrix-destined pSu9-DHFR into mitochondria isolated from the control and the cells depleted of TOM7. The correct import of pSu9-DHFR was monitored by its processing by MPP. The import of this protein dropped by 20-30% upon TOM7 KD as compared to control (Maruszczak *et al.,* 2022, Fig. 5c,d). The association of PINK1 with the TOM complex in mitochondria depleted of TOM7 showed similar results. (Maruszczak *et al.,* 2022, Fig. 5e,f). To exclude general import deficiency in TOM7 KD cells and prove that the effect is specific to the TOM complex, I imported into the isolated organelles PBR (TSPO), which does not rely on the main translocase for its import into mitochondria (Otera *et al.,* 2007). As expected, the import of PBR did not alter upon TOM7 depletion (Maruszczak *et al.,* 2022, Fig. 5g,h). Hence, it appears that TOM7 KD does not specifically affect PINK1 association, but also other proteins that rely on a stable TOM complex for their import.

Next, I wanted to check whether the double KD of both TOM7 and TOM70 would have a synthetic effect on PINK1 association with the MOM. To this end, I knocked down both proteins in HeLa cells and isolated mitochondria from these cells. I imported

PINK1 into depolarized mitochondria and observed more than 60% reduction of PINK1 association with the TOM complex as compared to control (Maruszczak *et al.,* 2022, Fig. 6b,c). Such drastic effect might be due to the combined effect of both depletions; the absence of the main receptor of PINK1 import into mitochondria and destabilization of the TOM complex in the absence of TOM7.

8.1.5 THE LUMEN OF THE TOM PORE IS CRUCIAL FOR PINK1 ASSOCIATION WITH THE MITOCHONDRIAL OUTER MEMBRANE

The precise PINK1 localization in the TOM complex of depolarized mitochondria remains an open question in the field. There are three hypotheses in the literature on this matter: 1) PINK1 is laterally released from the TOM complex into the bulk of the MOM (Nguyen *et al.,* 2016), 2) PINK1 gets arrested in the TOM40 channel from where it can induce the mitophagy cascade (Hasson *et al.,* 2013) and 3) PINK1 N-terminal segment undergoes lateral release, however remains bound to the TOM complex and is not released into the bulk of MOM (Rasool *et al.,* 2021). TOM40 appears to play a central role in all three situations, hence my aim was to study PINK1 dependence on the TOM40 pore in depolarized mitochondria. To avoid secondary effects of TOM40 KD, as it could result in general disruption of protein import into mitochondria, I used another system that relies on clogging the TOM complex with excess amounts of pSu9-DFHR. The fusion protein consists of the presequence of subunit 9 of F_0-ATPase fused to dihydrofolate reductase (DHFR). If excess of purified pSu9-DHFR is added to isolated mitochondria in the presence of methotrexate (DHFR ligand), then the presequence segment of the protein will translocate into the matrix, however the tightly folded DHFR domain will prevent the import of the DHFR moiety via the TOM complex. In such a situation, the entire presequence import pathway becomes clogged.

Firsty, I imported radiolabeled PINK1 and F1β into polarized mitochondria that were incubated with excess amounts of pSu9-DHFR prior to the import. As expected, since both proteins rely on the TOM and TIM23 complexes for their import, their translocation was acutely affected (Maruszczak *et al.,* 2022, Fig. 7a,b). Furthermore, I also imported radiolabeled TOM40 and observed 40% reduction in its MOM association in mitochondria preincubated with pSu9-DHFR (Maruszczak *et al.,* 2022, Fig. 7c,d). The reduction observed for TOM40 was not as severe as for the

presequence proteins because the biogenesis of TOM40 does not require TIM23 and depends on the TOM and SAM complexes that are more abundant than the TOM/TIM23 supra-complexes. I used PBR as a negative control, since its import should not be affected by the TOM complex blockage. As expected, PBR was imported to the same efficiency in both control and blocked mitochondria (Maruszczak *et al.,* 2022, Fig. 7e,f). Lastly, I imported radiolabeled PINK1 into blocked and CCCP-depolarized mitochondria and observed a drastic reduction of PINK1 association with the TOM complex to less than 40% as compared to control (Maruszczak *et al.,* 2022, Fig. 7g,h). These experiments show that PINK1 uses the lumen of TOM40 for its stable association with the TOM complex.

8.1.6 TcPINK1 APPARENTLY BLOCKS THE TOM PORE IN DEPOLARIZED MITOCHONDRIA

Finally, I aimed to study where in the MOM PINK1 resides upon depolarization of mitochondria. Specifically, I was interested whether it gets released into the bulk of the MOM, arrested in the TOM40 lumen, or remains bound to the TOM complex, however outside the TOM40 barrel. To address this aim, I obtained from the group of Dr. J.F. Trempe the corresponding plasmids and purified recombinant TcPINK1, which was previously used in studies on structure-function relationships of PINK1 (Kumar *et al.,* 2017; Rasool *et al.,* 2018; Okatsu *et al.,* 2018; Rasool *et al.,* 2021). TcPINK1 is more stable than hPINK1, hence it was more suitable to use in my experimental system. Firstly, I checked whether TcPINK1, similarly to hPINK1, associates with the TOM complex upon depolarization. Indeed, radiolabeled TcPINK1 co-migrated with the TOM complex at around 700 kDa (Maruszczak *et al.,* 2022, Fig. 8a). Subsequently, I carried out reciprocal experiments to the ones described above by testing whether TcPINK1 can clog the TOM complex and therefore, inhibit the import of other clients of the TOM complex. To this end, I incubated isolated mitochondria with CCCP and recombinant TcPINK1, and afterwards, reimported TOM40 or hPINK1. Integration of both proteins into the MOM was compromised upon clogging the complex with TcPINK1 (Maruszczak *et al.,* 2022, Fig. 8b-e). Notably, the reduction of the TOM40 membrane integration in mitochondria blocked with pSu9-DHFR and TcPINK1 was similar. This can be expained by either the fact that the kinase domain of PINK1 hinders the access of other substrates to the TOM complex or that PINK1 similarly to pSu9-DHFR occupies the pore of the TOM40 in depolarized mitochondria.

8.2 DISCUSSION

8.2.1 DIFFERENTIAL ROLES OF THE IMPORT RECEPTORS TOM70 AND TOM20

Recent publications enriched our knowledge regarding the spectrum of functions of TOM70. It was known that TOM70 contains a tetratricopeptide structure that along with Hsp70 and Hsp90 chaperones functions in recruitment and recognition of protein clients to mitochondria (Young *et al.,* 2003; Fan *et al.,* 2011; Hoseini *et al.,* 2016). Additional findings showed that the mature parts of mitochondrial precursors might contribute to the efficiency of the protein import into the organelle (Yamamoto *et al.,* 2009; Schendzielorz *et al.,* 2016). Finally, Backes et al. (2018) found that besides the cleavable N-terminal presequence, there are other MTS-like features that can be present in the mature protein parts. These specific protein segments were described as internal MTS-like signals (iMTS-Ls) and were found to specifically interact with TOM70 (Backes *et al.,* 2018). It was found that, similarly to canonical MTS, these iMTS-Ls have low frequencies of glutamate and aspartate and high occurence of hydroxylated or positively-charged amino acids (lysine and arginine). These specific protein segments had low hydrophobicity score and were additionally described as being predominantly helical and of amphipathic nature. Analysis of the primary sequence of PINK1 (in collaboration with Prof. J. Herrmann, TU Kaiserslautern) revealed that the protein contains iMTS-Ls within its N-terminus. A specific tool was used (Schneider *et al.,* 2021; http://hyperweb.bio.uni-kl.de/) and PINK1 segment between amino acids 40-80 was identified with a high score (Figure 4). Since these iMTS-Ls are supposed to interact with TOM70, this prediction fits nicely the results of the peptide scan with Tom70.

PINK1 lacking its first 35 amino acid residues and hence the MTS, was still found to associate with mitochondria, however was retained mainly at the MOM (Okatsu *et al.,* 2015). Hence, it is tempting to speculate that since PINK1 can be imported into both the matrix and stalled within the MOM, it is mainly dependent on TOM70 in depolarized mitochondria. This assumption is supported by three arguments: 1) TOM70 generally recognizes iMTS-Ls, 2) PINK1 contains a putative internal MTS at residues 40-80, and 3) PINK1 variant lacking the first 34 residues is mainly arrested in the MOM. Indeed, my results showed that PINK1 import into depolarized mitochondria depleted of

TOM70 was significantly affected, while TOM20 depletion had lower impact on the association of PINK1 with the MOM.

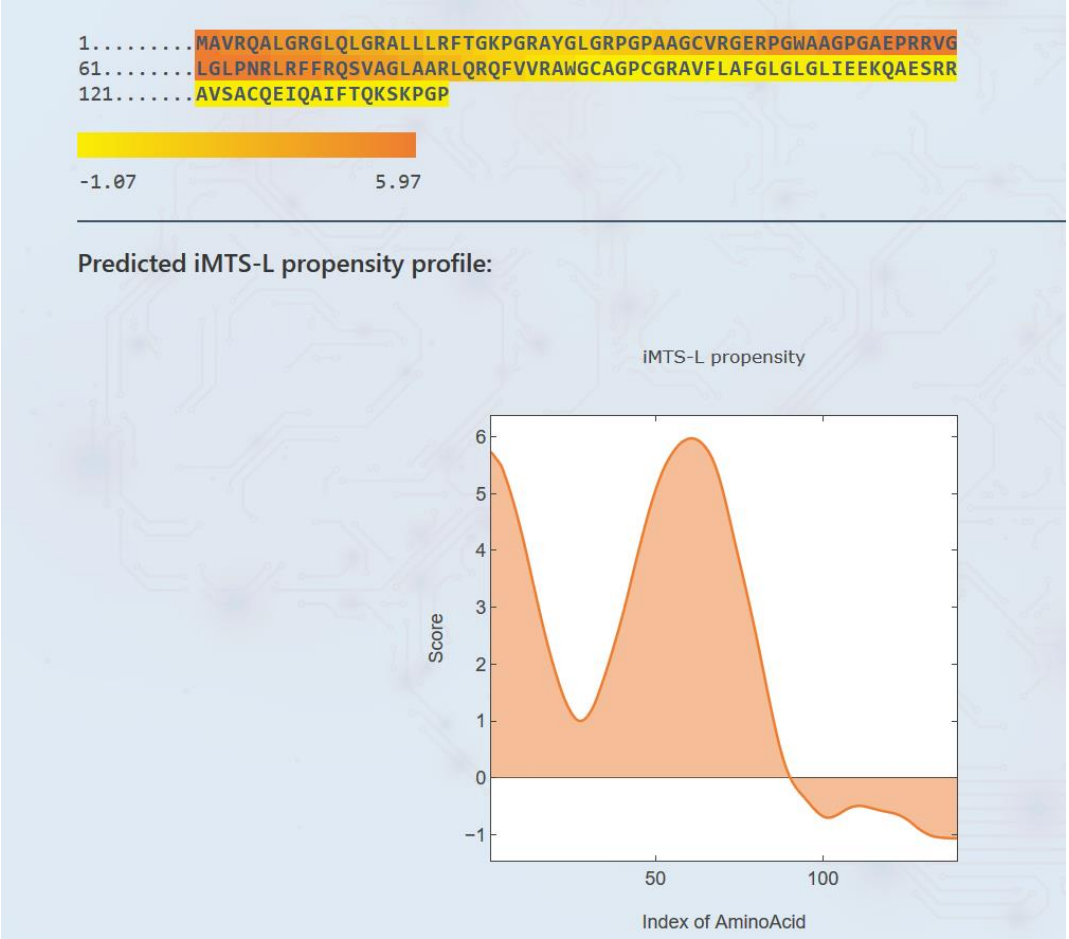

Figure 4. PINK1(1-140) contains iMTS-Ls. PINK1(1-140) amino acid sequence was used for the iMTS-Ls prediction. The probability scores of iMTS-Ls are presented as a coloured heatmap (upper panel). A graphic representation of the smoothed probability for formation of iMTS-L (lower panel).

Recent study by Backes et al. (2021) emphasized the importance of TOM70 ability to tether cytosolic chaperones over its receptor function. Hence, I cannot exclude the possibility that the interaction of PINK1 and TOM70 receptor is due to the recruitment of chaperone-bound PINK1 from the cytosol. However, since TOM70 specifically bound the internal MTS of PINK1 in the peptide scan, I conclude that both assigned roles of TOM70 are important in the initial recruitment of the protein to the surface of the mitochondria as well as the further import into the organelle.

8.2.2 TOM7 ROLE IN PINK1 ASSOCIATION WITH THE MITOCHONDRIAL OUTER MEMBRANE

Recent research postulated an important role of TOM7 in PINK1 stabilization in the MOM (Hasson *et al.,* 2013; Sekine *et al.,* 2019; Rasool *et al.,* 2021). Hasson et al. (2013) reported that in TOM7 knockout (KO) cells, YFP-Parkin failed to translocate to depolarized mitochondria and that mitophagy downstream of Parkin recruitment was acutely affected. Moreover, TOM7 KD in induced pluripotent stem cell (iPS cell) derived neurons resulted in reduced accumulation of endogenous PINK1 as a response to depolarization. Overall the authors concluded that TOM7 stabilizes PINK1 in the MOM, and therefore enables the recruitment of Parkin. When I imported PINK1 into mitochondria depleted from TOM7, I observed only moderate reduction in PINK1 association with mitochondria. The difference between both studies is that Hasson et al. (2013) used cells in which TOM7 was knockout, while in my system I depleted the protein with siRNA. Indeed, in the iPS experiments where TOM7 was knocked down, PINK1 was still accumulating in the MOM, however not to the degree in which it happens in control cells (Hasson *et al.,* 2013). Thus, the presence of small amounts of TOM7 might still be efficient for PINK1 stabilization at the MOM, however in case of complete KO, the arrest is hindered. Hasson et al. (2013) did not observe any difference between the import of Su9-DHFR presursor into control and TOM7 KO mitochondria. In contrast, pSu9-DHFR import was affected in my *in vitro* import system. This reduction might indicate general import problem due to destabilization of the TOM complex in mitochondria isolated from TOM7 KD cells.

The symmetry-driven docking model by Rasool et al. (2021) suggests that N-terminally located NT helix of PINK1 faces TOM7, which causes the PINK1 TM helix to be placed outside the TOM40 pore. Hence, these authors concluded that the N-terminus must be released from the TOM40 via a lateral opening. However, lateral release of substrates from the TOM complex is questionable, since according to the recently published atomic structure of the TOM complex, the β-barrels forming TOM40 appear to be tightly closed (Wang *et al.,* 2020; Guan *et al.,* 2021).

Such modeled interactions of PINK1 with the TOM complex indicate that indeed TOM7 is necesarry for proper positioning of PINK1 in the TOM40 pore. Nevertheless, my results are not in contrast to the ones presented by Rasool et al. (2021), since my

experiments focus on initial biogenesis of PINK1 in the MOM. It was shown that Parkin is not recruited unless PINK1 is properly positioned within the TOM complex, which happens downstream of the events that I investigated. It might be that this specific displacement of PINK1 N-terminus happens only after PINK1 dimer transphosphorylation, which would lead to their activation and hence Parkin recruitment.

8.2.3 PINK1 NEEDS THE LUMEN OF TOM40 FOR ITS ASSOCIATION WITH THE MITOCHONDRIAL OUTER MEMBRANE

The blockage of TOM40 pore with excess substrate in depolarized mitochondria resulted in dramatic reduction in the capacity of PINK1 to form a complex with TOM. This outcome suggests that the lumen of TOM40 is crucial for PINK1 biogenesis at the MOM. To test the hypothesis that PINK1 arrests in the TOM40 pore, I incubated depolarized mitochondria with excess amounts of TcPINK1 and then imported TOM40 and hPINK1 into such treated organelles. The reduction in the membrane integration of both substrate proteins suggests that PINK1 might reside in the TOM40 lumen and block the import pore for other TOM complex substrates. Several additional observations suport this hypothesis: 1) the interaction between PINK1 and TOM complex is strong enough to withstand the solubilization process of mitochondria. Of note, only the core components of the translocase can sustain these conditions, *i.e.* TOM40, TOM22 and the three small subunits TOM5, TOM6 and TOM7, 2) Blockage of the TOM complex by PINK1 prevents the import of other proteins into mitochondria marked for degradation, and 3) PINK1 re-import after recovery of the mitochondrial membrane potential is rather fast (Lazarou *et al.,* 2012), hence it could indicate that it is already localized in the TOM40 pore. Re-translocation from the lipid core of the MOM would require additional steps such as extraction from the membrane and putative re-entering pathway into the TOM complex.

In summary, this research aimed to dissect the individual steps of PINK1 integration into the MOM. To that end, I applied a wide variety of *in vitro* and *in organello* biochemical assays to study the interaction of PINK1 with the TOM complex upon mitochondrial depolarization. My findings emphasize the role of the individual components of the TOM complex in the correct positioning of PINK1, which is a critical

step in mitophagy induction. Overall, the results generated in this study can expand our understanding of the complex mechanism of PINK1 integration into the MOM.

Human Dopaminergic Neurons Lacking PINK1 Exhibit Disrupted Dopamine Metabolism Related to Vitamin B6 Co-Factors (Bus et al., 2020)

8.3 SUMMARY OF THE RESULTS AND DISCUSSION

Loss of function mutations in PINK1 and Parkin are well known to cause an autosomal recessive and early onset of Parkinson disease (PD) (Ge *et al.,* 2020). Both proteins function in the signalling pathway that leads to the removal of damaged mitochondria, hence any hindrance in the process results in the abolition of cell homeostasis (Quinn *et al.,* 2020). The goal of this study was to elucidate the neuronal-specific functions of PINK1 and their implications on the pathomechanism of PD.

Differentiated human midbrain-specific dopaminergic neurons (hDANs) knockout for PINK1 were used as a model system to understand the role of the protein in brain function. Firsty, it was shown by other co-authors that treatment with the potassium ionophore Valinomycin of both control and PINK1 KO hDANs, led to the same accumulation of the autophagy marker, LC3-II. Hence, these findings suggest PINK1 is non-essential for the general autophagy. I measured the import ability of mitochondria isolated from either control or hDANs devoid of PINK1. To that end, I incubated radiolabeled protein precursors of pSu9-DHFR and Fis1 with purified organelles and analyzed their import into isolated mitochondria by SDS-PAGE followed by autoradiography. The import efficiency was not altered in organelles isolated from PINK1 KO hDANs (Bus *et al.,* Fig S3b).

Dopamine release was previously reported to be altered in PINK1 KO mouse striatum (Kitada *et al.,* 2007). Here, via investigating various metabolic pathways, it was found that deficiency of dopamine might be an effect of changed metabolism. The study showed that 3,4-Dihydroxyphenylacetic acid (DOPAC) and dopamine levels were reduced in PINK1 KO hDANs. Dopamine synthesis relies on the active form of vitamin B6, namely pyridoxal phosphate, which is recycled from degraded B6 enzymes in a salvage pathway with the help of Pyridoxine 5′-phosphate oxidase (PNPO) enzyme. This study proposes the anaplerotic aid to the TCA cycle and supporting anabolism via acetyl-CoA that is provided by the precursors of dopamine. Hence, metabolic adaptation to altered environment happens at the cost of lower dopamine synthesis, which is one of the hallmarks of Parkinson disease.

9. REFERENCES

1. Backes, S., Bykov, Y. S., Flohr, T., Räschle, M., Zhou, J., Lenhard, S., Krämer, L., Mühlhaus, T., Bibi, C., Jann, C., Smith, J. D., Steinmetz, L. M., Rapaport, D., Storchová, Z., Schuldiner, M., Boos, F., & Herrmann, J. M. (2021). The chaperone-binding activity of the mitochondrial surface receptor Tom70 protects the cytosol against mitoprotein-induced stress. *Cell Reports*, *35*(1), 108936. doi:10.1016/j.celrep.2021.108936
2. Backes, S., Hess, S., Boos, F., Woellhaf, M. W., Gödel, S., Jung, M., Mühlhaus, T., & Herrmann, J. M. (2018). Tom70 enhances mitochondrial preprotein import efficiency by binding to internal targeting sequences. *Journal of Cell Biology*, *217*(4), 1369–1382. doi:10.1083/jcb.201708044
3. Becker, T., Vögtle, F., Stojanovski, D., & Meisinger, C. (2008). Sorting and assembly of mitochondrial outer membrane proteins. *Biochimica Et Biophysica Acta (BBA) - Bioenergetics,1777*(7-8), 557-563. doi:10.1016/j.bbabio.2008.03.017
4. Bingol, B., Tea, J.S., Phu, L., Reichelt, M., Bakalarski, C.E., Song, Q., Foreman, O., Kirkpatrick, D.S., Sheng, M. (2014). The mitochondrial deubiquitinase USP30 opposes parkin-mediated mitophagy. *Nature, 510*(7505), 370-5. doi: 10.1038/nature13418
5. Burchell, V. S., Nelson, D. E., Sanchez-Martinez, A., Delgado-Camprubi, M., Ivatt, R. M., Pogson, J. H., … Plun-Favreau, H. (2013). The Parkinson's disease-linked proteins Fbxo7 and Parkin interact to mediate mitophagy. *Nature neuroscience*, *16*(9), 1257–1265. doi:10.1038/nn.3489
6. Chan, N. C., Salazar, A. M., Pham, A. H., Sweredoski, M. J., Kolawa, N. J., Graham, R. L., … Chan, D. C. (2011). Broad activation of the ubiquitin-proteasome system by Parkin is critical for mitophagy. *Human molecular genetics*, *20*(9), 1726–1737. doi:10.1093/hmg/ddr048
7. Chenette, E. J. (2011). Sticking to the TCA cycle. *Nature Cell Biology, 13*(10), 1188-1188. doi:10.1038/ncb2361
8. Deas, E., Plun-Favreau, H., Gandhi, S., Desmond, H., Kjaer, S., Loh, S. H., … Wood, N. W. (2011). PINK1 cleavage at position A103 by the mitochondrial protease PARL. *Human molecular genetics*, *20*(5), 867–879. doi:10.1093/hmg/ddq526

9. Di Maio, R., Barrett, P. J., Hoffman, E. K., Barrett, C. W., Zharikov, A., Borah, A., … Greenamyre, J. T. (2016). α-Synuclein binds to TOM20 and inhibits mitochondrial protein import in Parkinson's disease. *Science translational medicine*, *8*(342), 342ra78. doi:10.1126/scitranslmed.aaf3634
10. Fan, A. C., Kozlov, G., Hoegl, A., Marcellus, R. C., Wong, M. J., Gehring, K., & Young, J. C. (2011). Interaction between the Human Mitochondrial Import Receptors Tom20 and Tom70 in Vitro Suggests a Chaperone Displacement Mechanism. *Journal of Biological Chemistry*, *286*(37), 32208–32219. doi:10.1074/jbc.m111.280446
11. Fiesel, F. C., Moussaud-Lamodière, E. L., Ando, M., & Springer, W. (2014). A specific subset of E2 ubiquitin-conjugating enzymes regulate Parkin activation and mitophagy differently. *Journal of cell science*, *127*(Pt 16), 3488–3504. doi:10.1242/jcs.147520
12. Fiorese, C. J., Schulz, A. M., Lin, Y. F., Rosin, N., Pellegrino, M. W., & Haynes, C. M. (2016). The Transcription Factor ATF5 Mediates a Mammalian Mitochondrial UPR. *Current biology: CB, 26*(15), 2037–2043. doi:10.1016/j.cub.2016.06.002
13. Friedman, J. R., & Nunnari, J. (2014). Mitochondrial form and function. *Nature*, *505*(7483), 335–343. doi:10.1038/nature12985
14. Ge, P., Dawson, V. L., & Dawson, T. M. (2020). PINK1 and Parkin mitochondrial quality control: a source of regional vulnerability in Parkinson's disease. *Molecular Neurodegeneration*, *15*(1). doi:10.1186/s13024-020-00367-7
15. Greene, A. W., Grenier, K., Aguileta, M. A., Muise, S., Farazifard, R., Haque, M. E., . . . Fon, E. A. (2012). Mitochondrial processing peptidase regulates PINK1 processing, import and Parkin recruitment. *EMBO Reports, 13*(4), 378-385. doi:10.1038/embor.2012.14
16. Guan, Z., Yan, L., Wang, Q., Qi, L., Hong, S., Gong, Z., Yan, C., & Yin, P. (2021). Structural insights into assembly of human mitochondrial translocase TOM complex. *Cell Discovery*, *7*(1). doi:10.1038/s41421-021-00252-7
17. Ha, Y., Akiyama, Y., & Xue, Y. (2013). Structure and mechanism of rhomboid protease. *The Journal of biological chemistry*, *288*(22), 15430–15436. doi:10.1074/jbc.R112.422378
18. Hasson, S. A., Kane, L. A., Yamano, K., Huang, C. H., Sliter, D. A., Buehler, E., Wang, C., Heman-Ackah, S. M., Hessa, T., Guha, R., Martin, S. E., & Youle, R.

J. (2013). High-content genome-wide RNAi screens identify regulators of parkin upstream of mitophagy. *Nature, 504*(7479), 291–295. doi:10.1038/nature12748

19. Hatano, T., Kubo, S., Sato, S., & Hattori, N. (2009). Pathogenesis of familial Parkinson's disease: New insights based on monogenic forms of Parkinson's disease. *Journal of Neurochemistry,111*(5), 1075-1093. doi:10.1111/j.1471-4159.2009.06403.x
20. Haynes, C. M., Yang, Y., Blais, S. P., Neubert, T. A., & Ron, D. (2010). The Matrix Peptide Exporter HAF-1 Signals a Mitochondrial UPR by Activating the Transcription Factor ZC376.7 in C. elegans. *Molecular Cell, 37*(4), 529-540. doi:10.1016/j.molcel.2010.01.015
21. Hollville, E., Carroll, R.G., Cullen, S.P. & Martin, S.J. (2014). Bcl-2 family proteins participate in mitochondrial quality control by regulating Parkin/PINK1-dependent mitophagy. *Mol Cell, 55*(3), 451–466. doi:10.1016/j.molcel.2014.06.001
22. Horvath, S. E., Rampelt, H., Oeljeklaus, S., Warscheid, B., van der Laan, M., & Pfanner, N. (2015). Role of membrane contact sites in protein import into mitochondria. *Protein science: a publication of the Protein Society*, *24*(3), 277–297. doi:10.1002/pro.2625
23. Hoseini, H., Pandey, S., Jores, T., Schmitt, A., Franz-Wachtel, M., Macek, B., Buchner, J., Dimmer, K. S., & Rapaport, D. (2016). The cytosolic cochaperone Sti1 is relevant for mitochondrial biogenesis and morphology. *The FEBS Journal*, *283*(18), 3338–3352. doi:10.1111/febs.13813
24. Houten, S. M., Violante, S., Ventura, F. V., & Wanders, R. J. (2016). The Biochemistry and Physiology of Mitochondrial Fatty Acid β-Oxidation and Its Genetic Disorders. *Annual Review of Physiology, 78*(1), 23-44. doi:10.1146/annurev-physiol-021115-105045
25. Jin, S. M., Lazarou, M., Wang, C., Kane, L. A., Narendra, D. P., & Youle, R. J. (2010). Mitochondrial membrane potential regulates PINK1 import and proteolytic destabilization by PARL. *Journal of Cell Biology*, *191*(5), 933–942. doi:10.1083/jcb.201008084
26. Kamp, F., Exner, N., Lutz, A. K., Wender, N., Hegermann, J., Brunner, B., … Haass, C. (2010). Inhibition of mitochondrial fusion by α-synuclein is rescued by PINK1, Parkin and DJ-1. *The EMBO journal*, *29*(20), 3571–3589. doi:10.1038/emboj.2010.223

27. Kato, H., Lu, Q., Rapaport, D., & Kozjak-Pavlovic, V. (2013). Tom70 Is Essential for PINK1 Import into Mitochondria. *PLoS ONE*, *8*(3), e58435. doi:10.1371/journal.pone.0058435
28. Kato, H., & Mihara, K. (2008). Identification of Tom5 and Tom6 in the preprotein translocase complex of human mitochondrial outer membrane. *Biochemical and Biophysical Research Communications*, *369*(3), 958–963. doi:10.1016/j.bbrc.2008.02.150
29. Kim, J., Fiesel, F. C., Belmonte, K. C., Hudec, R., Wang, W. X., Kim, C., … Kim, J. (2016). miR-27a and miR-27b regulate autophagic clearance of damaged mitochondria by targeting PTEN-induced putative kinase 1 (PINK1). *Molecular neurodegeneration*, *11*(1), 55. doi:10.1186/s13024-016-0121-4
30. Kim, N. C., Tresse, E., Kolaitis, R. M., Molliex, A., Thomas, R. E., Alami, N. H., … Taylor, J. P. (2013). VCP is essential for mitochondrial quality control by PINK1/Parkin and this function is impaired by VCP mutations. *Neuron*, *78*(1), 65–80. doi:10.1016/j.neuron.2013.02.029
31. Kimura, Y., Fukushi, J., Hori, S., Matsuda, N., Okatsu, K., Kakiyama, Y., . . . Tanaka, K. (2013). Different dynamic movements of wild-type and pathogenic VCPs and their cofactors to damaged mitochondria in a Parkin-mediated mitochondrial quality control system. *Genes to Cells, 18*(12), 1131-1143. doi:10.1111/gtc.12103
32. Kitada, T., Pisani, A., Porter, D. R., Yamaguchi, H., Tscherter, A., Martella, G., Bonsi, P., Zhang, C., Pothos, E. N., & Shen, J. (2007). Impaired dopamine release and synaptic plasticity in the striatum of *PINK1* -deficient mice. *Proceedings of the National Academy of Sciences*, *104*(27), 11441–11446. doi:10.1073/pnas.0702717104
33. Kondapalli, C., Kazlauskaite, A., Zhang, N., Woodroof, H. I., Campbell, D. G., Gourlay, R., … Muqit, M. M. (2012). PINK1 is activated by mitochondrial membrane potential depolarization and stimulates Parkin E3 ligase activity by phosphorylating Serine 65. *Open biology*, *2*(5), 120080. doi:10.1098/rsob.120080
34. Kumar, A., Tamjar, J., Waddell, A. D., Woodroof, H. I., Raimi, O. G., Shaw, A. M., Peggie, M., Muqit, M. M., & van Aalten, D. M. (2017). Structure of PINK1 and mechanisms of Parkinson's disease-associated mutations. *eLife*, *6*. doi:10.7554/elife.29985

35. Kurz, M., Martin, H., Rassow, J., Pfanner, N., & Ryan, M. T. (1999). Biogenesis of Tim proteins of the mitochondrial carrier import pathway: differential targeting mechanisms and crossing over with the main import pathway. *Molecular biology of the cell*, *10*(7), 2461–2474. doi:10.1091/mbc.10.7.2461
36. Lazarou, M., Jin, S. M., Kane, L. A., & Youle, R. J. (2012). Role of PINK1 binding to the TOM complex and alternate intracellular membranes in recruitment and activation of the E3 ligase Parkin. *Developmental cell*, *22*(2), 320–333. doi:10.1016/j.devcel.2011.12.014
37. Lee, Y., Stevens, D. A., Kang, S. U., Jiang, H., Lee, Y. I., Ko, H. S., … Dawson, T. M. (2017). PINK1 Primes Parkin-Mediated Ubiquitination of PARIS in Dopaminergic Neuronal Survival. *Cell reports*, *18*(4), 918–932. doi:10.1016/j.celrep.2016.12.090
38. Lesage, S. & Brice, A. (2009). Parkinson's disease: from monogenic forms to genetic susceptibility factors. *Human Molecular Genetics, 18*(R1), R48–R59. doi: 10.1093/hmg/ddp012
39. Meyer, H., & Weihl, C. C. (2014). The VCP/p97 system at a glance: connecting cellular function to disease pathogenesis. *Journal of Cell Science, 127*(Pt 18), 3877–3883. doi:10.1242/jcs.093831
40. Michiorri, S., Gelmetti, V., Giarda, E., Lombardi, F., Romano, F., Marongiu, R., . . . Casari, G. (2010). The Parkinson-associated protein PINK1 interacts with Beclin1 and promotes autophagy. *Cell Death & Differentiation, 17*(6), 962-974. doi:10.1038/cdd.2009.200
41. Muqit, M. M., Abou-Sleiman, P. M., Saurin, A. T., Harvey, K., Gandhi, S., Deas, E. . . . Latchman, D. S. (2006). Altered cleavage and localization of PINK1 to aggresomes in the presence of proteasomal stress. *Journal of Neurochemistry, 98*(1), 156-169. doi:10.1111/j.1471-4159.2006.03845.x
42. Narendra, D. P., Jin, S. M., Tanaka, A., Suen, D. F., Gautier, C. A., Shen, J., … Youle, R. J. (2010). PINK1 is selectively stabilized on impaired mitochondria to activate Parkin. *PLoS biology*, *8*(1), e1000298. doi:10.1371/journal.pbio.1000298
43. Neupert, W. & Herrmann, J.M. (2007). Translocation of proteins into mitochondria. *Annu Rev Biochem., 76*, 723-49. doi: 10.1146/annurev.biochem.76.052705.163409

44. Nguyen, T. N., Padman, B. S., & Lazarou, M. (2016). Deciphering the Molecular Signals of PINK1/Parkin Mitophagy. *Trends in Cell Biology*, *26*(10), 733–744. https://doi.org/10.1016/j.tcb.2016.05.008
45. Nolen, B., Yun, C.Y., Wong, C.F., McCammon, J.A., Fu, X.D., Ghosh, G. (2001). The structure of Sky1p reveals a novel mechanism for constitutive activity. *Nat Struct Biol., 8*(2), 176-83. doi: 10.1038/84178
46. Nunnari, J., & Suomalainen, A. (2012). Mitochondria: in sickness and in health. *Cell*, *148*(6), 1145–1159. doi:10.1016/j.cell.2012.02.035
47. Okatsu, K., Kimura, M., Oka, T., Tanaka, K. & Matsuda, N. (2015). Unconventional PINK1 localization mechanism to the outer membrane of depolarized mitochondria drives Parkin recruitment. *Journal of Cell Science*. Published. doi:10.1242/jcs.161000
48. Okatsu, K., Oka, T., Iguchi, M., Imamura, K., Kosako, H., Tani, N., … Matsuda, N. (2012). PINK1 autophosphorylation upon membrane potential dissipation is essential for Parkin recruitment to damaged mitochondria. *Nature communications*, *3*, 1016. doi:10.1038/ncomms2016
49. Okatsu, K., Sato, Y., Yamano, K., Matsuda, N., Negishi, L., Takahashi, A., Yamagata, A., Goto-Ito, S., Mishima, M., Ito, Y., Oka, T., Tanaka, K., & Fukai, S. (2018). Structural insights into ubiquitin phosphorylation by PINK1. *Scientific Reports*, *8*(1). doi:10.1038/s41598-018-28656-8
50. Okatsu, K., Uno, M., Koyano, F., Go, E., Kimura, M., Oka, T. … Matsuda, N. (2013). A dimeric PINK1-containing complex on depolarized mitochondria stimulates Parkin recruitment. *The Journal of biological chemistry*, *288*(51), 36372–36384. doi:10.1074/jbc.M113.509653
51. Ordureau, A., Sarraf, S. A., Duda, D. M., Heo, J. M., Jedrychowski, M. P., Sviderskiy, V. O., … Harper, J. W. (2014). Quantitative proteomics reveal a feedforward mechanism for mitochondrial PARKIN translocation and ubiquitin chain synthesis. *Molecular cell*, *56*(3), 360–375. doi:10.1016/j.molcel.2014.09.007
52. Osellame, L. D., Blacker, T. S., & Duchen, M. R. (2012). Cellular and molecular mechanisms of mitochondrial function. *Best practice & research. Clinical endocrinology & metabolism*, *26*(6), 711–723. doi:10.1016/j.beem.2012.05.003
53. Otera, H., Taira, Y., Horie, C., Suzuki, Y., Suzuki, H., Setoguchi, K., Kato, H., Oka, T., & Mihara, K. (2007). A novel insertion pathway of mitochondrial outer

membrane proteins with multiple transmembrane segments. *Journal of Cell Biology*, *179*(7), 1355–1363. doi:10.1083/jcb.200702143

54. Quinn, P. M. J., Moreira, P. I., Ambrósio, A. F., & Alves, C. H. (2020). PINK1/PARKIN signalling in neurodegeneration and neuroinflammation. *Acta Neuropathologica Communications*, *8*(1). doi:10.1186/s40478-020-01062-w
55. Radhakrishnan, D.M. & Goyal, V. (2018). Parkinson's disease: A review. *Neurology India, 66*(7), 26-35. doi: 10.4103/0028-3886.226451
56. Rasool, S., Soya, N., Truong, L., Croteau, N., Lukacs, G. L., & Trempe, J. (2018). PINK 1 autophosphorylation is required for ubiquitin recognition. *EMBO Reports*, *19*(4). doi:10.15252/embr.201744981
57. Rasool, S., Veyron, S., Soya, N., Eldeeb, M. A., Lukacs, G. L., Fon, E. A., & Trempe, J. F. (2021). Mechanism of PINK1 activation by autophosphorylation and insights into assembly on the TOM complex. *Molecular Cell*. Published. doi:10.1016/j.molcel.2021.11.012
58. Rojansky, R., Cha, M. Y., & Chan, D. C. (2016). Elimination of paternal mitochondria in mouse embryos occurs through autophagic degradation dependent on PARKIN and MUL1. *eLife*, *5*, e17896. doi:10.7554/eLife.17896
59. Sarraf, S. A., Raman, M., Guarani-Pereira, V., Sowa, M. E., Huttlin, E. L., Gygi, S. P., & Harper, J. W. (2013). Landscape of the PARKIN-dependent ubiquitylome in response to mitochondrial depolarization. *Nature*, *496*(7445), 372–376. doi:10.1038/nature12043
60. Schendzielorz, A. B., Schulz, C., Lytovchenko, O., Clancy, A., Guiard, B., Ieva, R., van der Laan, M., & Rehling, P. (2016). Two distinct membrane potential–dependent steps drive mitochondrial matrix protein translocation. *Journal of Cell Biology*, *216*(1), 83–92. doi:10.1083/jcb.201607066
61. Schmidt, O., Pfanner, N., & Meisinger, C. (2010). Mitochondrial protein import: from proteomics to functional mechanisms. *Nature Reviews Molecular Cell Biology*, *11*(9), 655–667. doi:10.1038/nrm2959
62. Schneider, K., Zimmer, D., Nielsen, H., Herrmann, J. M., & Mühlhaus, T. (2021). iMLP, a predictor for internal matrix targeting-like sequences in mitochondrial proteins. *Biological Chemistry*, *402*(8), 937–943. doi:10.1515/hsz-2021-0185
63. Schulz, C., Schendzielorz, A., & Rehling, P. (2015). Unlocking the presequence import pathway. *Trends in Cell Biology, 25*(5), 265-275. doi:10.1016/j.tcb.2014.12.001

64. Sekine, S., Wang, C., Sideris, D. P., Bunker, E., Zhang, Z., & Youle, R. J. (2019). Reciprocal Roles of Tom7 and OMA1 during Mitochondrial Import and Activation of PINK1. *Molecular Cell, 73*(5). doi:10.1016/j.molcel.2019.01.002
65. Sekine, S., & Youle, R. J. (2018). PINK1 import regulation; a fine system to convey mitochondrial stress to the cytosol. *BMC Biology, 16*(1). doi:10.1186/s12915-017-0470-7
66. Sharpe, H. J., Stevens, T. J., & Munro, S. (2010). A comprehensive comparison of transmembrane domains reveals organelle-specific properties. *Cell*, *142*(1), 158–169. doi:10.1016/j.cell.2010.05.037
67. Shin, J. H., Ko, H. S., Kang, H., Lee, Y., Lee, Y. I., Pletinkova, O., … Dawson, T. M. (2011). PARIS (ZNF746) repression of PGC-1α contributes to neurodegeneration in Parkinson's disease. *Cell*, *144*(5), 689–702. doi:10.1016/j.cell.2011.02.010
68. Silvestri, L., Caputo, V., Bellacchio, E., Atorino, L., Dallapiccola, B., Valente, E. M., & Casari, G. (2005). Mitochondrial import and enzymatic activity of PINK1 mutants associated to recessive parkinsonism. *Human Molecular Genetics, 14*(22), 3477-3492. doi:10.1093/hmg/ddi377
69. Sim, C., Gabriel, K., Mills, R., Culvenor, J., & Cheng, H. (2012). Analysis of the regulatory and catalytic domains of PTEN-induced kinase-1 (PINK1). *Human Mutation*, *33*(10), 1408-1422. doi: 10.1002/humu.22127
70. Skowyra, D., Craig, K. L., Tyers, M., Elledge, S. J., & Harper, J. (1997). F-Box Proteins Are Receptors that Recruit Phosphorylated Substrates to the SCF Ubiquitin-Ligase Complex. *Cell,91*(2), 209-219. doi:10.1016/s0092-8674(00)80403-1
71. Song, S., Jang, S., Park, J., Bang, S., Choi, S., Kwon, K. Y., … Chung, J. (2013). Characterization of PINK1 (PTEN-induced putative kinase 1) mutations associated with Parkinson disease in mammalian cells and Drosophila. *The Journal of biological chemistry*, *288*(8), 5660–5672. doi:10.1074/jbc.M112.430801
72. Song, Z., Chen, H., Fiket, M., Alexander, C., & Chan, D. C. (2007). OPA1 processing controls mitochondrial fusion and is regulated by mRNA splicing, membrane potential, and Yme1L. *The Journal of cell biology*, *178*(5), 749–755. doi:10.1083/jcb.200704110

73. Stojanovski, D., Bragoszewski, P., & Chacinska, A. (2012). The MIA pathway: A tight bond between protein transport and oxidative folding in mitochondria. *Biochimica Et Biophysica Acta (BBA) - Molecular Cell Research, 1823*(7), 1142-1150. doi:10.1016/j.bbamcr.2012.04.014
74. Tanaka, A., Cleland, M. M., Xu, S., Narendra, D. P., Suen, D. F., Karbowski, M., & Youle, R. J. (2010). Proteasome and p97 mediate mitophagy and degradation of mitofusins induced by Parkin. *The Journal of cell biology*, *191*(7), 1367–1380. doi:10.1083/jcb.201007013
75. Tasaki, T., Mulder, L. C., Iwamatsu, A., Lee, M. J., Davydov, I. V., Varshavsky, A., … Kwon, Y. T. (2005). A family of mammalian E3 ubiquitin ligases that contain the UBR box motif and recognize N-degrons. *Molecular and cellular biology*, *25*(16), 7120–7136. doi:10.1128/MCB.25.16.7120-7136.2005
76. Tasaki, T., Sriram, S. M., Park, K. S., & Kwon, Y. T. (2012). The N-end rule pathway. *Annual review of biochemistry*, *81*, 261–289. doi:10.1146/annurev-biochem-051710-093308
77. Twig, G., Elorza, A., Molina, A. J., Mohamed, H., Wikstrom, J. D., Walzer, G., … Shirihai, O. S. (2008). Fission and selective fusion govern mitochondrial segregation and elimination by autophagy. *The EMBO journal*, *27*(2), 433–446. doi:10.1038/sj.emboj.7601963
78. Unoki, M., & Nakamura, Y. (2001). Growth-suppressive effects of BPOZ and EGR2, two genes involved in the PTEN signaling pathway. *Oncogene, 20*(33), 4457-4465. doi:10.1038/sj.onc.1204608
79. Valente, E., Abou-Sleiman, P., Caputo, V., Miratul M. K. Muqit, Harvey, K., Gispert, S., . . . Wood, N. (2004). Hereditary Early-Onset Parkinson's Disease Caused by Mutations in PINK1. *Science, 304*(5674), 1158-1160. doi: 10.1126/science.1096284
80. Vincow, E. S., Merrihew, G., Thomas, R. E., Shulman, N. J., Beyer, R. P., MacCoss, M. J., & Pallanck, L. J. (2013). The PINK1-Parkin pathway promotes both mitophagy and selective respiratory chain turnover in vivo. *Proceedings of the National Academy of Sciences of the United States of America*, *110*(16), 6400–6405. doi:10.1073/pnas.1221132110
81. Wang, W., Chen, X., Zhang, L., Yi, J., Ma, Q., Yin, J., Zhuo, W., Gu, J., & Yang, M. (2020). Atomic structure of human TOM core complex. *Cell Discovery*, *6*(1). doi:10.1038/s41421-020-00198-2

82. Wang, X., Winter, D., Ashrafi, G., Schlehe, J., Wong, Y. L., Selkoe, D., … Schwarz, T. L. (2011). PINK1 and Parkin target Miro for phosphorylation and degradation to arrest mitochondrial motility. *Cell*, *147*(4), 893–906. doi:10.1016/j.cell.2011.10.018
83. Whitworth, A. J., Lee, J. R., Ho, V. M., Flick, R., Chowdhury, R., & McQuibban, G. A. (2008). Rhomboid-7 and HtrA2/Omi act in a common pathway with the Parkinson's disease factors Pink1 and Parkin. *Disease models & mechanisms*, *1*(2-3), 168–173. doi:10.1242/dmm.000109
84. Wiedemann, N., & Pfanner, N. (2017). Mitochondrial Machineries for Protein Import and Assembly. *Annual Review of Biochemistry, 86*(1), 685-714. doi:10.1146/annurev-biochem-060815-014352
85. Woodroof, H. I., Pogson, J. H., Begley, M., Cantley, L. C., Deak, M., Campbell, D. G., … Muqit, M. M. (2011). Discovery of catalytically active orthologues of the Parkinson's disease kinase PINK1: analysis of substrate specificity and impact of mutations. *Open biology, 1*(3), 110012. doi:10.1098/rsob.110012
86. Wu, X., Yen, L., Irwin, L., Sweeney, C., & Carraway, K. L., 3rd (2004). Stabilization of the E3 ubiquitin ligase Nrdp1 by the deubiquitinating enzyme USP8. *Molecular and cellular biology*, *24*(17), 7748–7757. doi:10.1128/MCB.24.17.7748-7757.2004
87. Yamamoto, H., Fukui, K., Takahashi, H., Kitamura, S., Shiota, T., Terao, K., Uchida, M., Esaki, M., Nishikawa, S. I., Yoshihisa, T., Yamano, K., & Endo, T. (2009). Roles of Tom70 in Import of Presequence-containing Mitochondrial Proteins. *Journal of Biological Chemistry*, *284*(46), 31635–31646. doi:10.1074/jbc.m109.041756
88. Yamano, K., & Youle, R. J. (2013). PINK1 is degraded through the N-end rule pathway. *Autophagy*, *9*(11), 1758–1769. doi:10.4161/auto.24633
89. Yamano, K., Matsuda, N., & Tanaka, K. (2016). The ubiquitin signal and autophagy: An orchestrated dance leading to mitochondrial degradation. *EMBO Reports, 17*(3), 300-316. doi:10.15252/embr.201541486
90. Yamano, K., Yatsukawa, Y. I., Esaki, M., Hobbs, A. E. A., Jensen, R. E., & Endo, T. (2008). Tom20 and Tom22 Share the Common Signal Recognition Pathway in Mitochondrial Protein Import. *Journal of Biological Chemistry*, *283*(7), 3799–3807. doi:10.1074/jbc.m708339200

91. Yoo, Y. S., Park, Y. Y., Kim, J. H., Cho, H., Kim, S. H., Lee, H. S., … Cho, H. (2015). The mitochondrial ubiquitin ligase MARCH5 resolves MAVS aggregates during antiviral signalling. *Nature communications*, *6*, 7910. doi:10.1038/ncomms8910
92. Youle, R. J., & van der Bliek, A. M. (2012). Mitochondrial Fission, Fusion, and Stress. *Science*, *337*(6098), 1062–1065. doi:10.1126/science.1219855
93. Young, J. C., Hoogenraad, N. J., & Hartl, F. (2003). Molecular Chaperones Hsp90 and Hsp70 Deliver Preproteins to the Mitochondrial Import Receptor Tom70. *Cell*, *112*(1), 41–50. doi:10.1016/s0092-8674(02)01250-3
94. Zhou, C., Huang, Y., Shao, Y., May, J., Prou, D., Perier, C., … Przedborski, S. (2008). The kinase domain of mitochondrial PINK1 faces the cytoplasm. *Proceedings of the National Academy of Sciences of the United States of America*, *105*(33), 12022–12027. doi:10.1073/pnas.0802814105

10. ACKNOWLEDGMENTS

First of all, I would like to thank my PhD supervisor Prof. Dr. Doron Rapaport for giving me the opportunity to complete the doctoral degree in his group. I am grateful for his constant advice and contagious passion for mitochondria. His openness and trust have given me a lot of scientific confidence. Mostly, I am grateful to him for giving me the freedom to decide which way I wanted my project to go and always encouraging me to proceed with new ideas, while still always being available for short scientific discussions. I would like to extend my gratitude to my thesis advisory committee, Prof. Dr. Maya Schuldiner, Prof. Dr. Tassula Proikas-Cezanne and Dr. Kai Steffan Dimmer for their valuable input. I would like to additionally thank Prof. Dr. Maya Schuldiner and her group for hosting me during my scientific internship and sharing very productive as well as fun time in Israel.

Now I would like to thank Elena for constant technical support and brilliant jokes that we shared. To Anasuya for excellent life support and extreme kindness. To Fenja, another life supporter, especially when making sure that I attend MOMbrane seminars. To Jialin for showing me infinite patience and understanding as well as teaching InkScape and baking best vegan cakes. To Layla for sharing her life philosophy, kindness and patience as well as passion for sport and providing the first pet, Zaatar, to the whole group. To Nitya for sharing the obsession on animals and our plan to be volunteers is the African wild animal sanctuary. To Vitasta for understanding the physical pain, especially knees and shoulders and her devotion to her friends as well as always making me laugh. To Roza for realization that we are one person, sharing all interests and feministic views. To Zach and John, newly arriving boys in the group, for immediately finding themselves in women's environment, for their great sense of humour and kindness. Generally, to all the group for not only sharing the lab life but also private time and great friendship that came out of this PhD.

I would also like to thank my friends for always being there for me. Biggest thanks go to Vakis for being the best partner during tough times as well as the best parents that one can have, for their infinite trust and support.

11. APPENDIX

ACCEPTED PAPERS

1. Bus, C., Zizmare, L., Feldkaemper, M., Geisler, S., Zarani, M., Schaedler, A., Klose, F., Admard, J., Mageean, C. J., Arena, G., Fallier-Becker, P., Ugun-Klusek, A., **Maruszczak, K. K.**, Kapolou, K., Schmid, B., Rapaport, D., Ueffing, M., Casadei, N., Krüger, R., . . . Fitzgerald, J. C. (2020). Human Dopaminergic Neurons Lacking PINK1 Exhibit Disrupted Dopamine Metabolism Related to Vitamin B6 Co-Factors. *iScience*, *23*(12), 101797. https://doi.org/10.1016/j.isci.2020.101797

2. **Maruszczak, K. K.**, Jung, M., Rasool, S., Trempe, J. F., & Rapaport, D. (2022). The role of the individual TOM subunits in the association of PINK1 with depolarized mitochondria. *Journal of Molecular Medicine*, *100*(5), 747–762. https://doi.org/10.1007/s00109-022-02191-6

iScience

CellPress
OPEN ACCESS

Article

Human Dopaminergic Neurons Lacking PINK1 Exhibit Disrupted Dopamine Metabolism Related to Vitamin B6 Co-Factors

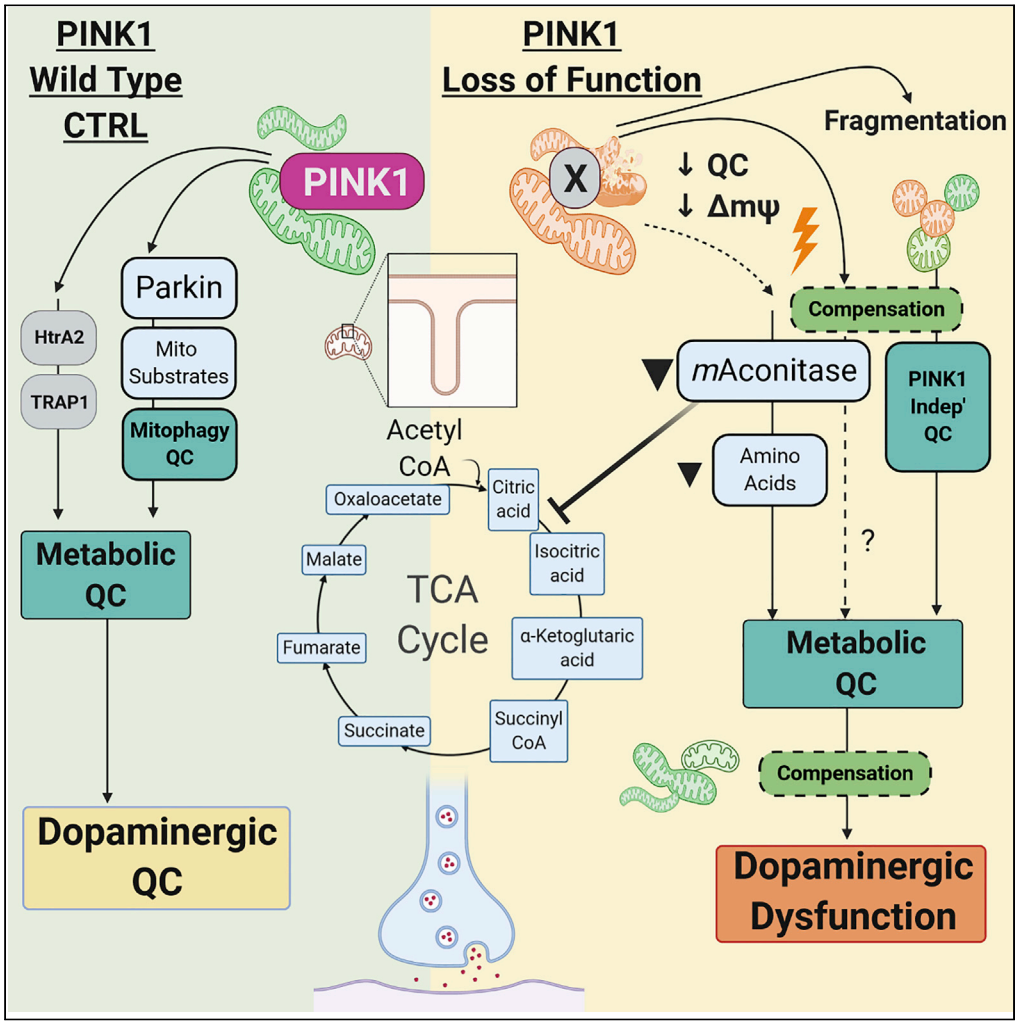

Christine Bus, Laimdota Zizmare, Marita Feldkaemper, ..., Christoph Trautwein, Christian J. Gloeckner, Julia C. Fitzgerald

julia.fitzgerald@uni-tuebingen.de

HIGHLIGHTS

PINK1 KO hDANs do not undergo ionophore-induced mitophagy yet CI remains active

PINK1 KO impacts the TCA cycle via *m*Aconitase leading to depletion of key amino acids

PINK1 KO silences *PNPO*, which provides essential biological co-factors

Dopamine pools and neurotransmitter uptake are reduced by PINK1 loss of function

Bus et al., iScience *23*, 101797
December 18, 2020
https://doi.org/10.1016/j.isci.2020.101797

iScience

CellPress
OPEN ACCESS

Article

Human Dopaminergic Neurons Lacking PINK1 Exhibit Disrupted Dopamine Metabolism Related to Vitamin B6 Co-Factors

Christine Bus,[1,2,14] Laimdota Zizmare,[3,14] Marita Feldkaemper,[4] Sven Geisler,[1] Maria Zarani,[1] Anna Schaedler,[1,5] Franziska Klose,[6] Jakob Admard,[7] Craig J. Mageean,[2,6] Giuseppe Arena,[8] Petra Fallier-Becker,[9] Aslihan Ugun-Klusek,[10] Klaudia K. Maruszczak,[11] Konstantina Kapolou,[1,5] Benjamin Schmid,[1] Doron Rapaport,[11] Marius Ueffing,[4,6] Nicolas Casadei,[7] Rejko Krüger,[8,12] Thomas Gasser,[1,2] Daniela M. Vogt Weisenhorn,[13] Philipp J. Kahle,[1,2] Christoph Trautwein,[3] Christian J. Gloeckner,[2,6] and Julia C. Fitzgerald[1,15,*]

SUMMARY

PINK1 loss-of-function mutations cause early onset Parkinson disease. PINK1-Parkin mediated mitophagy has been well studied, but the relevance of the endogenous process in the brain is debated.

Here, the absence of PINK1 in human dopaminergic neurons inhibits ionophore-induced mitophagy and reduces mitochondrial membrane potential. Compensatory, mitochondrial renewal maintains mitochondrial morphology and protects the respiratory chain. This is paralleled by metabolic changes, including inhibition of the TCA cycle enzyme *m*Aconitase, accumulation of NAD$^+$, and metabolite depletion. Loss of PINK1 disrupts dopamine metabolism by critically affecting its synthesis and uptake. The mechanism involves steering of key amino acids toward energy production rather than neurotransmitter metabolism and involves cofactors related to the vitamin B6 salvage pathway identified using unbiased multi-omics approaches.

We propose that reduction of mitochondrial membrane potential that cannot be controlled by PINK1 signaling initiates metabolic compensation that has neurometabolic consequences relevant to Parkinson disease.

INTRODUCTION

PINK1 mutations are the second most frequent cause of early onset Parkinson disease (PD), and *PINK1* variants have been found in sporadic PD (Gandhi and Plun-Favreau, 2017; Klein et al., 2006). PINK1 PD has an early occurrence of L-DOPA-associated dyskinesia, slow disease progression, and absence of cognitive impairment (Schiesling et al., 2008; Valente et al., 2004). Affective and psychotic symptoms are also frequently a part of the clinical presentation (Steinlechner et al., 2007).

Homozygous *Pink1* knockout (KO) mice, *drosophila*, zebrafish, and PINK1 KO human cancer cells indicate that loss of PINK1 causes mitochondrial dysfunction, altered mitochondrial morphology, disturbed mitochondrial quality control, as well as iron and calcium toxicity (Esposito et al., 2013; Gautier et al., 2008; Gispert et al., 2009; Heeman et al., 2011; Julienne et al., 2017; Moisoi et al., 2014; Parganlija et al., 2014; Requejo-Aguilar et al., 2014; Villa et al., 2017; Vives-Bauza et al., 2010). PINK1 *in vivo* models are phenotypically mild, with neurodegeneration only observed in PINK1 KO zebrafish (Anichtchik et al., 2008; Soman et al., 2017). Dopamine release and synaptic plasticity alterations have been reported in *PINK1* KO mouse striatum (Kitada et al., 2007).

PINK1 is a serine/threonine kinase targeted to mitochondria acting in a pathway together with another PD gene product, the E3-ubiquitin ligase Parkin (Clark et al., 2006; Park et al., 2006), to regulate mitophagy (Geisler et al., 2010; Narendra et al., 2008, 2010a). Upon loss of mitochondrial membrane potential or accumulation of misfolded proteins, PINK1 stabilizes on the outer mitochondrial membrane (Jin et al., 2010; Jin and Youle, 2013; Narendra et al., 2010a). PINK1 then phosphorylates ubiquitin at Ser65 to activate Parkin (Kane et al., 2014; Kazlauskaite et al., 2014; Koyano et al., 2014). Parkin ubiquitinylates mitochondrial outer

[1]Department of Neurodegenerative Diseases, Centre of Neurology and Hertie Institute for Clinical Brain Research, University of Tübingen, Otfried Müller Strasse 27, 72076, Tübingen, Germany

[2]DZNE – German Center for Neurodegenerative Diseases, Tübingen, Germany

[3]Werner Siemens Imaging Center, Department of Preclinical Imaging and Radiopharmacy, University of Tübingen, Tübingen, Germany

[4]Institute for Ophthalmic Research, Centre for Ophthalmology, University of Tübingen, Tübingen, Germany

[5]Graduate School of Cellular and Molecular Neuroscience, University of Tübingen, Tübingen, Germany

[6]Core Facility for Medical Bioanalytics, University of Tübingen, Center for Ophthalmology, Institute for Ophthalmic Research, Tübingen, Germany

[7]NGS Competence Center Tübingen, Institute of Medical Genetics and Applied Genomics, University of Tübingen, Germany

[8]Translational Neuroscience, Luxembourg Centre for Systems Biomedicine (LCSB), University of Luxembourg, Luxembourg

[9]Institute of Pathology and Neuropathology, University of Tübingen, Tübingen, Germany

[10]School of Science and Technology, Nottingham

Continued

membrane proteins such as Mitofusins (Gegg et al., 2010) and Miro (Birsa et al., 2014). Miro1 is also suggested to be phosphorylated by PINK1 and is important for mitochondrial movement and arrest (Wang et al., 2011b). The buildup of ubiquitin chains on the outer mitochondrial membrane acts as a signal for the recruitment of autophagy receptors (Geisler et al., 2010; Lazarou et al., 2015; Wong and Holzbaur, 2014) important for mitochondrial clustering (Narendra et al., 2010b; Okatsu et al., 2010). Some *in vivo* studies have shown that PINK1 is not required for basal mitophagy in neurons (McWilliams et al., 2018; Lee et al., 2018) or in human platelets (Walsh et al., 2018) but the topic is controversial (for an extensive review see Chu, 2019; Cummins and Gotz, 2018).

The pathogenic action of PINK1 mutations could be cell-type specific. PINK1 is highly expressed in the brain but it is also expressed throughout the rest of the body and has been associated with disease mechanisms in several tissues (Wang et al., 2018; Guo et al., 2019) including the progression of some cancers (Berthier et al., 2011; Villa et al., 2017). PINK1 is expressed predominantly in neurons (Blackinton et al., 2007) and myelinating oligodendrocytes (Zhang et al., 2014b). First studies in PINK1 PD patient stem-cell-derived neurons described defective Parkin recruitment to mitochondria and enhanced mitochondrial biogenesis (Seibler et al., 2011).

PINK1 has been shown to have a diverse catalog of biological functions beyond but not exclusive of mitophagy. PINK1 may play important roles at endoplasmic reticulum (ER) contact sites and in ER stress (Gelmetti et al., 2017; Torres-Odio et al., 2017; Celardo et al., 2016) and also in interactions with MIRO-1, VDAC, Grp78, TRAP1 and mitofusins (McLelland et al., 2018; Kane and Youle, 2011; Grossmann et al., 2019; Geisler et al., 2010; Shoshan-Barmatz et al., 2004). PINK1 has been shown to regulate calcium (Gandhi et al., 2009; Heeman et al., 2011; Soman et al., 2017), iron toxicity (Allen et al., 2013a; Esposito et al., 2013; Horowitz and Greenamyre, 2010; Li et al., 2018), and lipids (Ivatt et al., 2014). Recently PINK1 has been shown to modulate STING-induced inflammation (Sliter et al., 2018) and innate immunity (West et al., 2015; Matheoud et al., 2019; Sliter et al., 2018; Mouton-Liger et al., 2018).

In this study, our aim was to understand the neuronal-specific functions of PINK1 and how this is relevant to Parkinson disease etiology. We differentiated human midbrain specific neurons and showed that PINK1 is not required for maintenance of the mitochondrial networks nor for mitochondrial respiration but rather the fine tuning of mitochondrial matrix metabolism. These alterations may compensate for low mitochondrial quality but ultimately impact neuronal morphogenesis, neurotransmitter homeostasis, and dopamine neuron function.

RESULTS

Homozygous *PINK1* Knockout in Human iPSCs Does Not Inhibit Differentiation of Midbrain-Specific Dopaminergic Neurons (hDANs) but Inhibits Ionophore-Induced Mitophagy

We generated induced pluripotent stem cells (iPSCs) from a healthy female individual that we previously characterized (Reinhardt et al., 2013b) and then introduced a homozygous deletion of *PINK1* using a TALEN directed to Exon 1 (Figure 1A). Twenty-eight to thirty-five days old human midbrain-specific dopaminergic neurons (hDANs) were derived via neural precursor cells (NPCs) using a differentiation protocol we previously described (Reinhardt et al., 2013a). We selected two clonal iPSC lines with no random integration where no *PINK1* transcripts upstream or downstream of the gene edit could be detected (Figure S1A). We stained independent hDAN differentiations for MAP2, a marker of mature neurons, and also, tyrosine hydroxylase (TH), dopamine transporter (DAT), and forkhead box protein A2 (FOXA2), which are markers of mature dopaminergic neurons (Figures S1B and 1B). There are higher amounts of dopaminergic markers TH and DAT for the PINK1 KO lines ($p < 0.0001$). Notably, TH content is significantly more variable in PINK1 KO hDANs ($p = 0.0206$). Gene expression markers TH, MAP2, DAT, FOXA2 were measured alongside markers MAO-A and MAO-B (catecholamine degradation), VGlut1 (glutaminergic neurons), SYP (synaptic marker), and TPH2 (highly expressed in serotonergic neurons). TH and vGlut expression were increased ($p < 0.005$) and TPH2 and MAP2 decreased ($p < 0.005$) in PINK1 KO hDANs compared with their isogenic control (Figure 1C). The proportion of TH-positive neurons in 2D, iPSC-derived hDAN differentiations varies significantly. Because the aim of the protocol is to derive dopaminergic neurons, implicit bias cannot be ruled out during imaging even though counting is blinded. Fully automated procedures and developmental studies *in vivo* will be beneficial. We can conclude that PINK1 KO does not inhibit the differentiation of TH-positive, dopaminergic neurons from NPC intermediates.

Trent University, Nottingham, UK

[11]Interfaculty Institute of Biochemistry, University of Tübingen, Tübingen, Germany

[12]Transversal Translational Medicine, Luxembourg Institute of Health (LIH), Strassen, Luxembourg

[13]Helmholtz Zentrum München, German Research Center for Environmental Health, Institute of Developmental Genetics, Munich-Neuherberg, Germany

[14]These authors contributed equally

[15]Lead Contact

*Correspondence: julia.fitzgerald@uni-tuebingen.de

https://doi.org/10.1016/j.isci.2020.101797

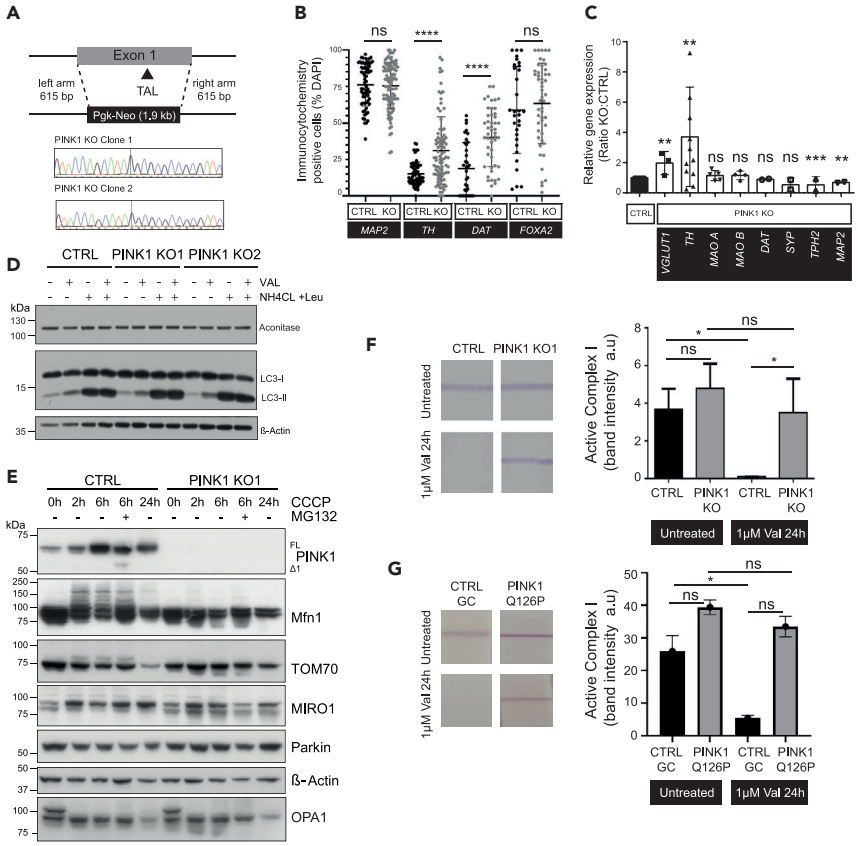

Figure 1. Homozygous *PINK1* Knockout in Human iPSCs Does Not Inhibit Differentiation of hDANs but Inhibits Ionophore-Induced Mitophagy

(A) Scheme showing removal of PINK1 exon 1 (homozygous) using TALEN gene editing in healthy iPSCs. Sequence confirmation of two clonal lines.

(B) Percentage of hDANs in a field of view positive for MAP2, FOXA2, TH, and DAT using immunocytochemistry. Each point on the graph is a technical replicate (nDiff = 4, error bars = SD). ns = not significant, **** = $p < 0.0001$ (Mann Whitney U-test).

(C) Relative gene expression of neuronal markers in PINK1 KO hDANs compared with the healthy control (nDiff = 4, except vGlut, nDiff = 3, error bars = SD). ns = not significant, TH ** = p0.0063 (t test), vGlut ** = p0.0022, TPH2 *** = $p < 0.0002$, MAP2 ** = p0.0043 (all Mann Whitney U-test).

(D) Western blots showing autophagic flux (LC3-II accumulation (C)an LC3-I, mAconitase, and β-actin) in untreated CTRL and PINK1 KO hDANs and those stimulated by Valinomycin (Val, 1µM, 24 h) or NH_4CL (20mM, 4 h) and Leupeptin (Leu, 200µM, 4 h) or both treatments together. nDiff = 3.

(E) Western blots in CTRL and PINK1 KO hDANs untreated or following 10µM CCCP treatment for 0, 2, 6 and 24 h −/+ proteasome inhibition (MG132, 10µM, 6 h). nDiff = 3.

(F) CI dipstick assay for active CI in CTRL and PINK1 KO hDANs treated with or without 1µM Valinomycin for 24 h (left panel). Quantification of dipstick band (nDiff = 3). ns = not significant, * = $p < 0.05$, error bars = SD (t test).

(G) CI dipstick assay for active CI in gene-corrected (GC) CTRL and PINK1 Q126P hDANs treated with or without 1µM valinomycin for 24 h (left panel). Quantification of dipstick band (nDiff = 3). ns = not significant, * = p0.023, error bars = SD (Mann Whitney U-test).

We treated hDANs with the potassium ionophore Valinomycin (Val, 1µM, 24 h) or lysosomal inhibitors (NH_4CL 20mM with Leupeptin (Leu), 200µM for 4 h) and measured autophagic flux using Western blotting for LC3-I/II in combination with mitochondrial aconitase (*m*Aconitase) and β-actin as loading controls. Valinomycin and NH_4Cl induced LC3-II accumulation in control and PINK1 KO hDANs to the same extent (Figure 1D), meaning that PINK1 is dispensable for general autophagy. Neither treatment led to significant depletion of *m*Aconitase (Figure 1D), suggesting that removal of the mitochondrial matrix was not induced under these conditions in hDANs. We then assessed markers of canonical, CCCP ionophore-induced mitophagy in hDANs with the addition of the proteasome inhibitor MG132 at 6 h. PINK1 accumulates in

control hDANs over the CCCP time course peaking at 6 h (Figure 1E) in line with previous work. The ubiquitination and degradation of mitochondrial outer membrane (MOM) proteins Mitofusin1 (Mfn1) and TOM70 was almost absent in PINK1 KO hDANs (Figure 1E), confirming previous work in non-neuronal cells that PINK1 is required for CCCP-induced ubiquitinylation and degradation of Mfn1. The MOM protein and PINK1 substrate MIRO-1 accumulates in all hDAN lines following CCCP treatment (Figure 1E). After 6-h CCCP and proteasomal inhibition MIRO-1 levels were lower in PINK1 KO hDANs (Figure 1E), suggesting that PINK1 could stabilize MIRO-1 during late stages of CCCP-induced mitophagy. Steady state Parkin levels remain unaffected by PINK1 KO (Figure 1E). There was some loss of the OPA-long form and more OPA-short form in CCCP-induced PINK1 KO hDANs consistent with mitochondrial fragmentation at very early stages of mitophagy (Figure 1E).

The potassium ionophore Valinomycin, as CCCP, induces PINK1-Parkin-mediated mitophagy (Rakovic et al., 2019; Zhang et al., 2014a) and was our ionophore of choice to induce mitophagy in hDANs. Because of the 24-h treatment window, it allowed us to optimize a 24-h period of antioxidant withdrawal (removal of potent antioxidants from the neuronal maturation media), which we established for all readouts. In line with previous work in hDANs, ionophores do not induce the turnover of all mitochondrial markers equally. We observe little influence of depolarization on matrix proteins, so we measured the amount of active protein at the inner mitochondrial membrane (IMM) using NADH dehydrogenase (CI). Using PINK1 KO and PINK1 Q126P patient hDAN isogenic lines, we immunoprecipitated CI from fresh lysates and then quantified the conversion of NADH given as a substrate using a simple dipstick assay. We found no significant differences in active CI between the lines under basal conditions (Figures 1F and 1G). Mitophagy induced by Valinomycin depletes active CI in control hDANs after 24 h but not in PINK1 KO nor PINK1 Q126P hDANs (Figures 1F and 1G), suggesting that PINK1-dependent mitophagy (but not PINK1 *per se*) is relevant for complex I activity in hDANs.

PINK1 Knockout hDANs Exhibit Normal Mitochondrial Morphology but Defective ER Calcium Release and Reduced Mitochondrial Membrane Potential

We used electron microscopy (EM) to look for qualitative structural changes to the mitochondria in hDANs devoid of PINK1. EM images from independent hDAN differentiations (PINK KO 1 and PINK KO 2) showed no notable differences in mitochondrial size, shape, or abundance (Figure 2A). Removal of mitochondria following 24-h Valinomycin treatment occurred in control hDANs but not in PINK1 KO hDANs receiving the same treatment (Figure 2A). We observed the presence of round membranous structures in PINK1 KO hDANs, particularly in those treated with the ionophore (indicated by black arrows, Figure 2A). We employed live cell imaging with baculovirus gene transfer into mammalian cells (Bacmam Mito dsRed) on mature hDANs (Figures 2B and S2A) to quantify mitochondrial abundance and morphology. We found no significant differences between PINK1 KO and CTRL hDANs mitochondrial morphology (Figures 2B and S2A). Only PINK1 KO neuronal precursor cells (NPCs) have reduced mitochondrial area per cell compared with isogenic controls (Figure 2B), suggesting mitochondrial fragmentation may be important for neurons to overcome the loss of PINK1 during differentiation. Next, we measured the lifetime (or turnover) of mitochondria using MitoTimer live cell imaging. PINK1 KO causes significantly lower red/green MitoTimer ratio compared with controls, indicating shorter lifespan of the expressed mitochondrial protein and points to mitochondrial renewal in hDANs (Figure S2B). Increased TOM22 fluorescence in flow cytometry (Figure S2C), increased PGC1α levels (Figure S2D), and altered SDHA (nuclear encoded)/MTCO1 (mtDNA encoded) ratio (Figure S2E) support the notion that hDANS lacking PINK1 may employ piecemeal mitochondrial renewal. Statistical significance could only be assigned in the case of PINK1 KO hDANs for the SDHA/MTCO1 mitobiogenesis test after the addition of Valinomycin (Figure S2E).

PINK1 loss of function has previously been associated with calcium toxicity (Gandhi et al., 2009). We measured cytosolic calcium levels using live imaging in PINK1 KO and control following the addition of thapsigargin to release calcium from ER stores. Control hDANs release calcium into the cytosol, which is then buffered. PINK1 KO hDANs respond minimally to thapsigargin stimulation compared with control hDANs (Figure 2C). Response to thapsigargin normalized to the baseline is shown because baseline cytosolic calcium levels were on average higher in control hDANs compared with PINK1 KO (Figure S2F).

Mitochondrial membrane potential ($\Delta\psi$m) is an indicator of mitochondrial function and health. We used the mitochondrial toxin rotenone and FCCP acute treatments to lower the $\Delta\Psi$m further in living cells. We found lower $\Delta\Psi$m in untreated PINK1 KO hDANs compared with controls using flow cytometry (Figure 2D, left

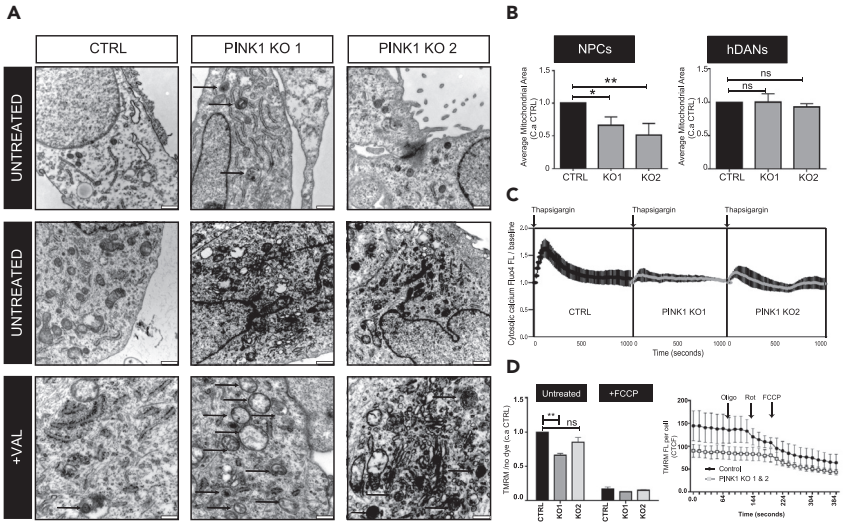

Figure 2. PINK1 Knockout hDANs Exhibit Normal Mitochondrial Morphology but Defective ER Calcium Release and Reduced Mitochondrial Membrane Potential

(A) Electron microscope images of hDANs untreated or treated with valinomycin (Val, 1μM, 24 h). Representative images (nDiff = 3). Black arrows point to membranous structures.

(B) Average mitochondrial area in neuronal progenitor cells (NPCs) and hDANs from live cell imaging (nDiff = 4, error bars = SD). ns = not significant, * = $p < 0.05$, ** = $p < 0.005$ (Mann Whitney U-test).

(C) Cytosolic calcium in response to the addition of thapsigargin during live cell imaging measured by Fluo4 dye fluorescence in hDANs. The total corrected cell fluorescence is shown (nDiff = 4, error bars = SD).

(D) Left panel. Mean average mitochondrial membrane potential ($\Delta\Psi$m) (flow cytometry TMRM fluorescence) for untreated hDANs and those treated acutely with 10μM CCCP (nDiff = 3). Right panel, mean average $\Delta\Psi$m (live cell kinetic imaging, corrected total cell fluorescence, CTCF). Acute treatment with sequential addition of Oligomycin (Oligo), Rotenone (Rot), and FCCP (nDiff = 3, error bars = SD). ** = $p < 0.0026$. ns = not significant (t test).

panel) and live cell imaging (Figure 2D, right panel). Under baseline conditions the $\Delta\Psi$m was reduced by approximately 25%–30% in PINK1 KO hDANs ($p < 0.0001$, endpoint PINK1 KO1 only, and $p < 0.0001$, live imaging corrected total cell fluorescence). Together the pH gradient and the membrane potential constitute an electrochemical proton gradient, which exerts the proton-motive force needed to generate ATP. We show part depolarization in untreated PINK1 KO hDANs, and it is not clear to what extent mitochondrial membrane depolarization is protective and at what point irreversible damage occurs. ATP levels in PINK1 KO hDANs were similar to their control (Figure S2G).

PINK1 KO Impedes *m*Aconitase and Reduces Distinct Metabolite Pools but Does Not Inhibit Respiration in hDANs

Low $\Delta\Psi$m could indicate dysfunctional mitochondrial respiration but basal mitochondrial oxygen consumption was surprisingly elevated over healthy hDANs and respiratory capacity unaffected (Figure 3A). Perhaps one significant observation is that PINK1 KO hDANs are capable of consuming more oxygen than their healthy controls when uncoupled (Figure 3A). Mild uncoupling is used by cells to reduce their oxidative burden. hDANs also prefer glycolysis (indicated by a small increase in extracellular acidification rate, ECAR) when mitochondrial respiration is minimalized (Figure 3A). The substrates pyruvate, glucose, and glutamine are given to the hDANs in the base media before measurement of basal oxygen consumption; therefore, we asked whether mitochondrial substrates could be a limiting factor in PINK1 KO hDANs.

First, we measured the activity of complex I (CI) of the respiratory chain because CI dysfunction has previously been associated with PINK1-Parkinson disease (Morais et al., 2014; Pogson et al., 2014; Vos et al., 2017). Using NADH and coenzyme Q10 as substrates, CI enzyme activity is not significantly affected by loss of PINK1 in hDANs (Figure 3B). We normalize CI activity rates to citrate synthase activity to account for differences in mitochondrial mass and remove any non-CI-specific consumption of NADH by completely inhibiting CI with rotenone in the same set. Because we observed an overall increase (p =

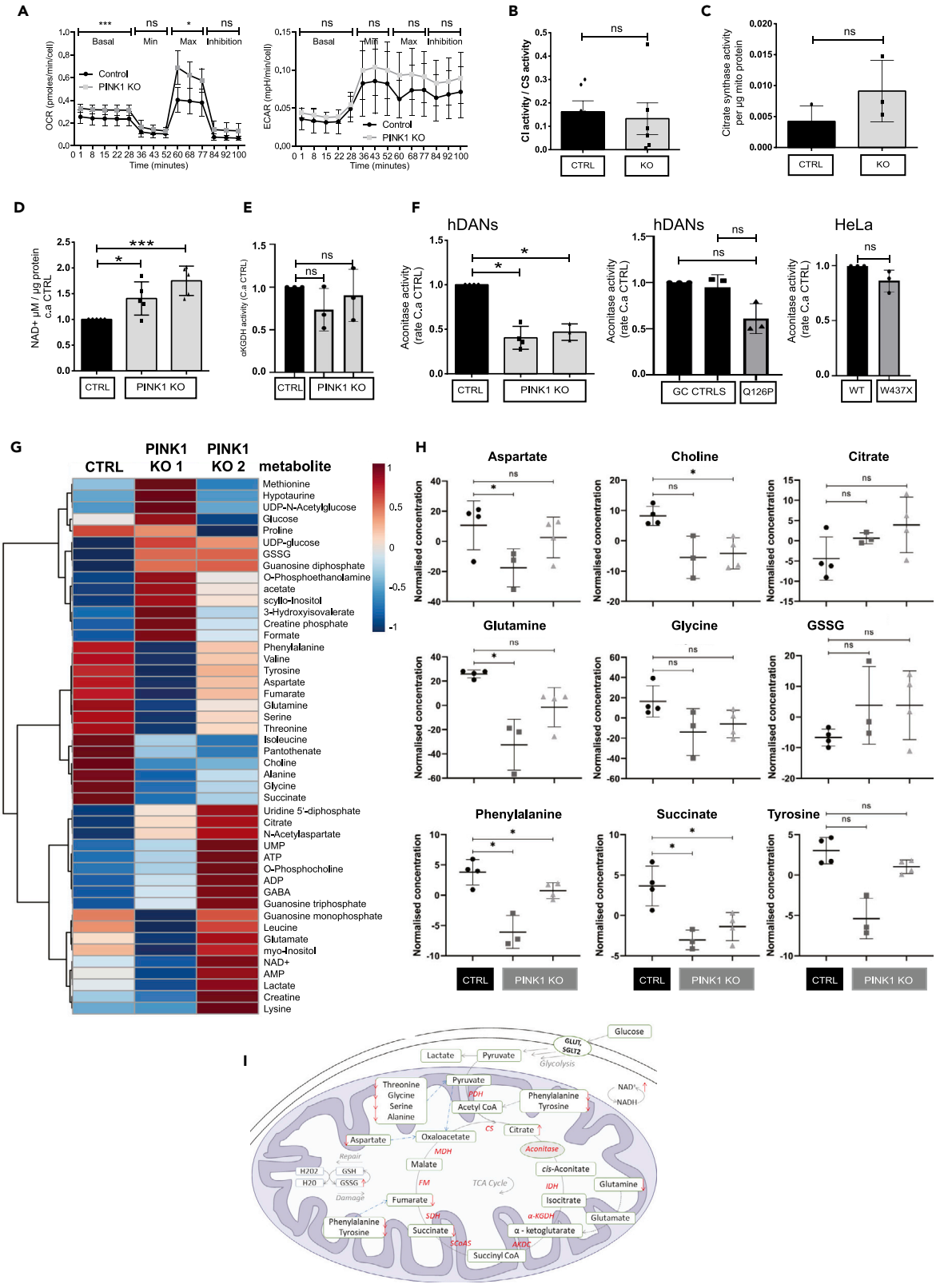
A
B
C
D
E
F
G
H
I
Basal
Min
Max
Inhibition
Control
PINK1 KO
OCR (pmoles/min/cell)
ECAR (mpH/min/cell)
Time (minutes)
CI activity / CS activity
Citrate synthase activity per µg mito protein
CTRL
KO
NAD+ µM / µg protein c.a CTRL
αKGDH activity (C.a CTRL)
Aconitase activity (rate C.a CTRL)
hDANs
HeLa
GC CTRLS
Q126P
WT
W437X
CTRL
PINK1 KO 1
PINK1 KO 2
metabolite
Methionine
Hypotaurine
UDP-N-Acetylglucose
Glucose
Proline
UDP-glucose
GSSG
Guanosine diphosphate
O-Phosphoethanolamine
acetate
scyllo-Inositol
3-Hydroxyisovalerate
Creatine phosphate
Formate
Phenylalanine
Valine
Tyrosine
Aspartate
Fumarate
Glutamine
Serine
Threonine
Isoleucine
Pantothenate
Choline
Alanine
Glycine
Succinate
Uridine 5'-diphosphate
Citrate
N-Acetylaspartate
UMP
ATP
O-Phosphocholine
ADP
GABA
Guanosine triphosphate
Guanosine monophosphate
Leucine
Glutamate
myo-Inositol
NAD+
AMP
Lactate
Creatine
Lysine
Normalised concentration
Aspartate
Choline
Citrate
Glutamine
Glycine
GSSG
Phenylalanine
Succinate
Tyrosine
Glucose
GLUT, SGLT2
Glycolysis
Pyruvate
Lactate
PDH
Acetyl CoA
Threonine
Glycine
Serine
Alanine
Phenylalanine
Tyrosine
NAD+
NADH
CS
Citrate
Oxaloacetate
Aspartate
MDH
Aconitase
cis-Aconitate
Malate
Repair
Damage
H2O2
H2O
GSH
GSSG
FM
TCA Cycle
IDH
Isocitrate
Glutamine
Glutamate
Fumarate
SDH
α-KGDH
α - ketoglutarate
Succinate
SCoAS
AKDC
Succinyl CoA

Figure 3. PINK1 KO Impedes *m*Aconitase Activity and Reduces Distinct Amino Acid Pools but Does Not Inhibit Respiration in hDANs

(A) Respiratory analyses of OCR (oxygen consumption rate, left panel) and ECAR (extracellular acidification rate, middle panel) in hDANs. Basal = basal respiration, min = minimal respiration, max = maximal respiration, ns = not significant. *** = p0.0004, * = p0.0158 (nDiff = 4, error bars = SD, t test).

(B) Complex I (CI) enzyme activity normalized to citrate synthase (CS) activity. ns = not significant, (nDiff = 6, error = SD, t test).

(C) Citrate synthase enzyme activity normalized to total protein concentration of the mitochondrial preparation. ns = not significant (nDiff = 3, t test).

(D) NAD^+ concentration of hDANs normalized to total protein and to the healthy control. * = p0.0222, *** = p0.0004. (nDiff = 5, error bars = SD, t test).

(E) Alpha-ketoglutarate dehydrogenase enzyme activity in mitochondrial preparations of PINK1 KO hDANs normalized to µg protein of mitochondria and healthy control. ns = not significant (nDiff = 3, t test).

(F) Aconitase enzyme activity in of PINK1 KO (left panel) and Q126P hDANs (middle panel) with respective controls and wildtype plus W437X HeLa cells (right panel). ns = not significant, * = $p < 0.05$ (nDiff = 3, HeLa n = 3, t test).

(G) A heatmap, generated with MetaboAnalyst, illustrates the Control and PINK KO clone 1 and 2 group relative average metabolite concentration changes. All metabolites were quantified by NMR-based metabolomics. Red indicates high concentrations and blue indicates low concentrations. The metabolites with similar concentration pattern have been grouped together.

(H) NMR metabolomics analysis-based scatterplots were generated for metabolites related to citric acid (TCA, Krebs) cycle and general mitochondria activity. One-way ANOVA & post-hoc tests (Fischer's LSD) were applied to the three-group comparison dataset with adjusted p value (FDR—false discovery rate) cutoff at p0.05. Metabolites tyrosine (p0.0005), phenylalanine (p0.0007), glutamine (p0.0025), and succinate (p0.0042) were reported with the highest significant p values. The t test was applied for individual pair comparison. Where = $p < 0.05$ and ns = not significant.

(I) Mitochondria metabolic pathways illustration focused on the TCA cycle, GSH repair/damage, and NAD+/NADH pool. Red arrows highlight the quantified metabolite concentration changes in PINK1 KO hDANs. Gray arrows indicate the reaction flow; blue long dash arrows show anaplerotic reactions.

0.22 not significant) in citrate synthase enzyme activity (Figure 3C) in PINK1 KO hDANs, we cannot rule out that alterations to mitochondrial dynamics is masking susceptibility to CI function. Nor can we rule out that the availability of substrates to the electron transport chain is an important physiological factor since substrates are given in such assays. Therefore, we looked more closely at wider energy metabolism in PINK1 KO hDANs. The NAD^+ pool was significantly elevated (Figure 3D), suggestive of metabolic compensation or flexibility.

α-ketoglutarate dehydrogenase (αKGDH) is a key, rate-limiting enzyme of the citric acid cycle and a redox sensor. We found no significant alterations to αKGDH activity (Figure 3E). The most notable impact of PINK1 KO was a drastic reduction in the activity of the citric acid cycle enzyme *m*-Aconitase, by around 60% ($p < 0.05$) compared with control hDANs (Figure 3F, left panel). The trend was replicated in PINK1 PD patient hDANs (Q126P) and HeLa PINK1 loss-of-function W437X cells (Figure 3F, middle and right panels). We used a coupled assay for *m*Aconitase that includes the second catalytic step of the reaction requiring iron. mAconitase catalyzes the isomerization of citrate to isocitrate and possesses a 4Fe-4S iron–sulfur cluster. The iron transport protein STEAP3 and the mitochondrial iron transporter Mitoferrin were upregulated in PINK1 KO hDANs (Figure S3A). PINK1 KO hDANs were able to import the radiolabeled proteins ^{35}S-pSU9-DHFR and ^{35}S-Fis1, suggesting relatively normal protein import function into mitochondria (Figure S3B). We recorded no significant levels of cytosolic ROS or changes in reduced glutathione levels in the presence or absence of several stressors (Figure S3C). Citrate or pyruvate transport could also be affected by the mitochondrial proton gradient (Bender and Martinou, 2016).

Nuclear magnetic resonance (NMR) spectroscopy-based metabolomics analysis enabled us to identify a buildup of citrate, which is in-line with reduced *m*Aconitase activity (Figures 3G and 3H). Overall, 46 metabolites from different chemical compound groups and pathways were quantified. We show the average metabolite concentrations in each PINK1 KO and CTRL; however, most of them did not have statistically significant changes (Figure 3G). NMR detected increased levels of oxidized glutathione (GSSG), GDP, and UDP in PINK1 KO hDANs (Figures 3G and 3H).

PINK1 KO hDANs tend to have reduced amino acid pools (shown in the heatmap in Figure 3G), with phenylalanine ($p = 0.0007$, one-way ANOVA), tyrosine ($p = 0.0005$, one-way ANOVA), and glutamine ($p = 0.0025$, one-way ANOVA) having significantly reduced concentrations compared with isogenic control, which has implications for protein synthesis and neurotransmitter metabolism (especially dopamine, which is synthesized from tyrosine).

Reduced glutamine is particularly relevant for antioxidant defense, inflammation, lipid metabolism, and many other metabolic pathways. We also observed significantly reduced succinate levels ($p = 0.0042$, one-way ANOVA), which has implications for mitochondrial respiration and antioxidant status for example. Phenylalanine and succinate were significantly reduced ($p =< 0.016$ and $p =< 0.023$ respectively, using t tests) in PINK1 KO clones compared with control hDANs (Figures 3G, 3H, and S4C).

Principle component analysis (PCA) of the metabolomics data shows that PINK1 KO hDAN clones 1 and 2 vary in metabolic profile (Figure S4A) but sPLSDA suggested distinct group differences (Figures S4B and S4C). Since changes in glutamine levels are associated with neuronal differentiation, we mined the data for the compounds most associated with glutamate (Figure S4D). Here again the phenylalanine and tyrosine were highlighted. PINK1 KO hDANs may utilize succinate and glutamate for energy production. Hormetic dose response to amino acids is known to regulate lifespan and neuronal differentiation and could point toward a compensatory metabolic shift in an attempt to reduce oxidative burden and maintain ATP output. The overall NAD^+ concentration was increased significantly in one PINK1 KO clone, which correlates well with the Figure 3D biochemical assay (Figure S4E). PINK1 KO-induced changes in mitochondrial metabolism are depicted in the diagram in Figure 3I. Whether reduced *m*Aconitase activity is the primary cause of the metabolite changes is still unclear. Glucose, lactate, and pyruvate concentrations were also quantified, yet there were no significant metabolic changes between the control and PINK1 KOs (Figure S4E). Buildup of citrate and a general depletion of metabolites following *m*Aconitase in the citric acid cycle point toward compensatory utilization of amino acids and possibly anaplerotic usage of phenylalanine and tyrosine.

Gene Expression Analysis Highlights the Relevance of PINK1 in Vitamin B6 Salvage and Neuronal-Specific Processes

We hypothesized that the observed metabolic changes due to loss of PINK1 in hDANs could be indirect compensation for reduced mitochondrial quality. We then sought to identify genes relevant to PINK1 in hDANs that could further decipher mechanisms in hDANs. RNAs were deep sequenced in the basal state and following treatment with 1μM Valinomycin (24 h). We compared the top significantly regulated genes ($p < 0.03$) for genotype and treatment. Colored squares show the gene expression as per-row normalized (scaled and centered, i.e. mean = 0, standard deviation = 1) cpm (counts per million) as a measure for gene expression strength (Figure 4A). The raw CPM and Log2FC expression datasets are available as a supplementary Excel file (Table S1). Those significantly regulated genes were used for unbiased pathway analysis using GOrilla (http://cbl-gorilla.cs.technion.ac.il/), a tool for identifying enriched gene ontology (GO) terms. The list of all genes sequenced in the hDANs was used as the background input. The top 15, most significant (ranked by FDR-q-value) GO process terms for the PINK1 KO genotype include tissue development, nervous system development, and cell differentiation (Figure 4B, upper panel graph). For PINK1 KO hDANs challenged with Valinomycin, all GO process significant terms are listed in the table (Figure 4B lower panel, table) and include extracellular structure organization and negative regulation of developmental process. The most significant differentially expressed gene was Pyridoxine-5′-phosphate oxidase (*PNPO*), an enzyme of the vitamin B_6 salvage pathway, important for many cellular functions including amino acid metabolism and neurotransmitter metabolism. *PNPO* gene expression was virtually silenced in PINK1 KO hDANs compared with control. Searching by PNPO-associated pathways, we used Ingenuity software (Qiagen) to find relevant pathways, which included dopamine metabolism. The software plotted all gene expression changes in the dopamine pathway (Figure 4B, bottom right scheme. Red = increased expression and green = decreased expression in PINK1 KO hDANs compared with control). There was a significant and remarkable downregulation of *PNPO* expression ($p < 0.0001$) in both PINK1 KO NPCs and in hDANs (Figure 4C).

Both unbiased metabolite and expression analysis pointed toward PINK1 involvement in dopaminergic differentiation and neuronal-specific regulation. The RNA sequencing analysis for the dopamine synthesis pathway is shown in Figure 4D. We measured the expression of genes involved in dopamine and neurotransmitter metabolism in RNA prepared from the following isogenic models: PINK1 KO hDANs, PINK1 Q126P Parkinson disease patient hDANs (the Q126P mutation is located just after the transmembrane domain of PINK1 (94–110 aa)), HeLa cells gene edited with PINK1 loss-of-function mutation (*PINK1* W437X, kinase domain), three PINK1 Q456X Parkinson disease patient hDAN lines with corresponding gene-corrected controls (*PINK1* Q456X, kinase domain), and PINK1 KO mouse striatum. Statistically significant gene changes occurred for *PNPO* (*PINK1 KO* and *Q456X*), dopa decarboxylase (*Q126P*), and tryptophan hydroxylase 1 (*TPH1, Q126P*) (Figure 4D). TH expression was not significantly different but PINK1 Q126P hDANs were more variable than the gene corrected control (p0.000013). We also measured expression of TPH2 (serotonin biosynthesis), PDXK (pyridoxal kinase, this gene was also unaffected according to RNA sequencing) and DNAJC12 (a co-chaperone together with HSP70 responsible for the proper folding of phenylalanine hydroxylase), which were not significantly altered in any of the PINK1 models. These data confirm reduced PNPO expression occurs in human neurons where PINK1 is

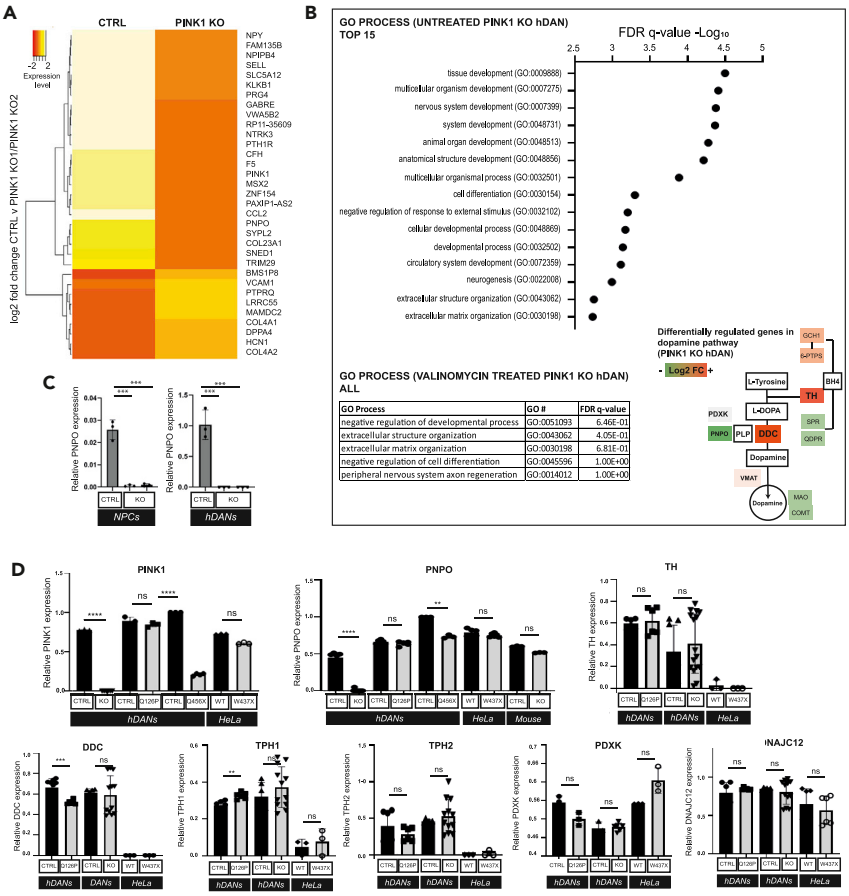

Figure 4. Gene Expression Analysis Highlights the Relevance of PINK1 in Vitamin B6 Salvage and Dopamine Pathways

(A) Deep RNA sequencing revealed disregulated genes. Log2FC of top significant hits ($p < 0.03$) in regard to genotype (PINK1 KO vs control hDANs) or treatment (untreated and 1μM Valinomycin) (n = 3, nDiff = 1), gene expression as per-row normalized (mean = 0, SD = 1) counts per million (cpm).

(B) Pathway analysis of top regulated genes to identify enriched gene ontology (GO) terms with regard to the genotype (upper panel, graph ranked GO terms by significance-FDR q-value) and treatment (10μM Valinomycin, lower left panel, all GO terms listed in table with significance-FDR q-value). Dopamine pathway heatmap of Log2FC gene expression changes in PINK1 KO hDANS compared with control (lower right panel, n = 3, nDiff = 1).

(C) Confirmation of the downregulated *PNPO* expression in PINK1 KO NPCs and hDANs with respective controls by qRT-PCR. *** = $p < 0.0001$ (nDiff = 3, error bars = SD, t test).

(D) qRT-PCR expression analysis of selected genes in the pathway in PINK1 KO, PINK1 Q126P PD hDANs, PINK1 HeLa W437X, and for PNPO PINK1 Q456X PD-derived hDANs (Patient n = 3) and PINK1 KO mouse ventral midbrain (n = 3) with respective isogenic controls. (nDiff = 3, error bars = SD). ns = not significant, PINK1 exon 1–2 (**** = $p < 0.0001$ for PINK1 KO versus CTRL and PINK1 Q456X versus GC CTRL), PNPO (**** = $p < 0.0001$ for PINK1 versus CTRL, ** = p0.0027 for PINK1 Q456X versus GC CTRL), DDC (*** = p0.0010 for PINK1 Q126P versus GC CTRL), TPH1 (** = p0.0035 for Q126P versus GC CTRL). All t test.

significantly depleted. It remains unclear whether depletion of PINK1 or reduced PINK1 kinase function is driving the effect on PNPO.

Combined Proteomic and Transcriptomic Pathway Analyses Highlight Metabolic Role of PINK1

To further identify pathways or interactors that could link PINK1 to neuronal metabolism, we performed quantitative proteomics across independent PINK1 KO hDAN differentiations using crude mitochondrial preparations (Figure S5A). The final assay library contained 3,951 protein IDs including ambiguous hits.

The library contained 3,413 proteins covered by at least one proteotypic peptide. According to MitoCarta2.0 (Calvo et al., 2016), 761 of those proteins were annotated as mitochondrial proteins, which allowed a 65% coverage of the reference mitochondrial proteome. Based on the extracted peptide/protein abundances we calculated the Log2 fold change (Log2FC) values for the control versus PINK1 KO clone 1 and then again for PINK1 KO clone 2 and marked all those proteins that showed significant Log2FC in both PINK1 KO clones. To list the top proteomic hits for PINK1, we removed significant hits between −1.75 and +1.75 to be able to list them in Figure 5A. No other filtering was applied, and the raw mean Log2FC data and list of all significant hits are available as a supplementary Excel file (Table S2). We performed pathway analysis of the top hits against the assay library (Figure 5B). The most significant (FDR-q-value) GO process terms included movement of cell or subcellular components, amide biosynthetic process, cellular amide metabolic process, and peptide biosynthetic process (the top 25 GO process terms are ranked in Figure 5B). These terms point toward PINK1 loss of function in hDAN affecting development and differentiation and metabolism. We overlapped the top regulated genes with top regulated proteins and ranked them by fold change for PINK1 KO. One hundred fourty-four IDs common to both PINK1 KO clones differ from the control (Figure 5C). This list was subjected to pathway analysis against the proteome using Gorilla, and again the top 25 significant GO terms were ranked by FDR-q-value (Figure 5D). Here, core metabolic GO process terms were enriched.

Alternative pathway analysis of proteomic data using Qiagen Ingenuity plotted the interactions between annotated biological pathways (Figure S5D). These data highlight processes relevant to neurons and synapses: androgen signaling, synaptic long-term depression, axonal guidance, CREB signaling, GABA signaling, and EF2 signaling (Figure S5D). The iron sulfur cluster containing calcium-binding protein NECAB2 (also known as MitoNEET) was consistently and significantly more abundant in PINK1 KO hDANs (+2.4 Log2FC, Figure 5A) and was confirmed by Western blotting (Figure S5B). Proteomic data were used to rank disease or function terms and revealed cell migration, severe psychological disorder, and mood disorder for PINK1 KO (Figure S5C).

PINK1 Is Required for Maintenance of Dopamine Pools and Proper Neurotransmitter Uptake in Human Neurons

We next investigated neurotransmitters and dopamine homeostasis in PINK1 hDAN models following data from the unbiased omics approaches. We measured the neurotransmitter content of the hDANs using high-pressure liquid chromatography (HPLC). Short-term and low-dose L-DOPA treatment allows measurement of dopamine (DA) and DA flux accurately. The PINK1 KO hDANs have significantly reduced DOPAC (20-fold reduction, $p < 0.0049$, *n*Diff = 8) and DA levels (6-fold reduction, p0.0026, *n*Diff = 8) (Figure 6A). The ratio of DOPAC/DA was also reduced but not HVA/DA, implicating a role for PINK1 at the presynapse (Figure 6B). We controlled for the number of dopaminergic neurons in the heterogeneous hDAN cultures by monitoring TH at mRNA and protein level in each independent differentiation and HPLC experiment. TH levels vary but not decrease in PINK1 KO hDANs (Figure 6C) HPLC samples, ruling out the possibility that loss of TH positive neurons is responsible for the loss of DA and its metabolites. DA levels inside hDANs and in the media could not be replenished by blocking DA degradation (Figure 6D). Data are not normalized, as hDANs were counted prior to HPLC measurement. Endogenous dopamine is difficult to detect in 2D cultures and requires large hDAN numbers but we measured 0.69 $\pm$ 0.355 ng dopamine per ml in untreated control hDANs (nDiff = 3) and 0.245 $\pm$ 0.122 ng dopamine per ml in untreated PINK1 KO hDANs (KO1 and KO2, nDiff = 4). MAO A and B enzyme activity and MAO-A protein levels were not significantly affected by PINK1 KO (Figure 6H). These data suggest that synthesis or uptake of dopamine, and not degradation, is the major factor contributing to the phenotype. To rule out major oxidation of DA to its Quinone form, which is not detectable by HPLC, we measured total oxidized catecholamines and did not observe any significant differences in the absence or presence of L-DOPA (Figure 6I).

Next, we measured neurotransmitter (NT) uptake by giving a labeled substrate and found it was significantly impaired in PINK1 KO hDANs (Figure 6E). This could not be rescued by inhibition of the monoamine uptake into vesicles (VMAT inhibition), DA synthesis via TH (TH inhibition), or DA degradation (COMT/MAO inhibition) (Figure 6F). This was replicated in PINK1 Q126P hDANs (Figure 6G). Addition of pyridoxal phosphate (PLP) rescue was not feasible because of its ubiquitous inclusion in neuronal base medias. Addition of tetrahydrobiopterin (BH_4) improved NT uptake across all hDAN preparations (Figure 6G). Unlike PLP, which is required for many, diverse biochemical reactions including amino acid conversion, BH_4 is an essential cofactor for aromatic amino acid hydroxylases, alkylglycerol monooxygenase, and nitric oxide

A TOP DIFFERENTIALLY REGULATED PROTEINS (PINK1 KO hDAN)

Protein name	Gene name	Mean Log2FC
Elongation factor 1-alpha 2	EEF1A2	4.192420094
UPF0317 protein C14orf159, mitochondrial	C14orf159	4.157141138
Neurosecretory protein VGF	VGF	3.8658334
Galectin-3	LGALS3	3.25878559
Sulfhydryl oxidase 2	QSOX2	2.878469142
Succinyl-CoA:3-ketoacid coenzyme A transferase 1/2, mitochondrial	OXCT1/2	2.846974378
Carbamoyl-phosphate synthase, mitochondrial	CPS1	2.843917478
Carbonic anhydrase 5B, mitochondrial	CA5B	2.605060207
Succinyl-CoA:3-ketoacid coenzyme A transferase 1, mitochondrial	OXCT1	2.590537888
Junctional adhesion molecule A	F11R	2.584196471
Slit homolog 1 protein	SLIT1	2.469430945
Histone H1.0;Histone H1.0, N-terminally processed	H1F0	2.443224143
N-terminal EF-hand calcium-binding protein 2	NECAB2	2.388285213
Cryptic family protein 1B;Cryptic protein	CFC1;CFC1B	2.34695718
NF-kappa-B inhibitor-interacting Ras-like protein 2	NKIRAS2	2.321456868
Glycine dehydrogenase (decarboxylating), mitochondrial	GLDC	2.211895812
1-phosphatidylinositol 4,5-bisphosphate phosphodiesterase delta-1	PLCD1	2.196720717
Phenylalanine--tRNA ligase, mitochondrial	FARS2	2.134816732
Band 4.1-like protein 5	EPB41L5	2.114930143
Multidrug resistance-associated protein 1	ABCC1	2.079568599
Nicotinate-nucleotide pyrophosphorylase [carboxylating]	QPRT	2.079059777
Mitochondrial fission process protein 1	MTFP1	1.935806295
Pyruvate dehydrogenase (acetyl-transferring)] kinase isozyme 1/2	PDK1;PDK2	1.924509606
Dihydroxyacetone phosphate acyltransferase	GNPAT	1.840879971
Fumarylacetoacetate hydrolase domain-containing protein 2A/2B	FAHD2A/2B	1.837931817
Acyl-coenzyme A thioesterase 13	ACOT13	1.822779947
Armadillo repeat-containing protein 1	ARMC1	1.817550467
Branched-chain-amino-acid aminotransferase, mitochondrial	BCAT2	1.801050485
40S ribosomal protein S24	RPS24	1.77797224

Protein name	Gene name	Mean Log2FC
Major prion protein	PRNP	-1.80624209
Voltage-dependent calcium channel subunit alpha-2/delta-2	CACNA2D2	-1.807879035
T1-TrpRS;T2-TrpRS;Tryptophan--tRNA ligase, cytoplasmic	WARS	-1.901320942
T-complex protein 1 subunit alpha/delta	CCT4;TCP1	-1.904381452
Follistatin-related protein 1	FSTL1	-1.981035678
Calponin-2	CNN2	-1.994760166
ATP-binding cassette sub-family A member 8	ABCA8	-2.004429944
Coronin-1A	CORO1A	-2.059196673
Prenylcysteine oxidase-like	PCYOX1L	-2.064975164
Vasorin	VASN	-2.107535902
Phostensin	PPP1R18	-2.148819609
Polypeptide N-acetylgalactosaminyltransferase 10	GALNT10	-2.154130218
C-type mannose receptor 2	MRC2	-2.16529882
Caldesmon	CALD1	-2.318425112
Gap junction alpha-1 protein	GJA1	-2.39525254
Ephrin type-A receptor 2	EPHA2	-2.405345654
Prolyl 3-hydroxylase 3	LEPREL2	-2.468191654
Myopalladin;Palladin	MYPN;PALLD	-2.631420683
Epidermal growth factor receptor	EGFR	-2.759726181
SPATS2-like protein	SPATS2L	-2.908308718
Heat shock protein beta-1	HSPB1	-2.921190835
Neurofilament light polypeptide	NEFL	-2.959022345
Receptor-type tyrosine-protein phosphatase O	PTPRO	-3.192127725
Actin, alpha/gamma	ACTA1; ACTG2	-3.300479796
Actin, alpha/alpha	ACTA1;ACTA2	-3.471660464
Nucleoside diphosphate kinase, mitochondrial	NME4	-3.509311273
Glypican-4;Secreted glypican-4	GPC4	-3.521926984
Tropomyosin alpha-1 chain;Tropomyosin beta chain	TPM1;TPM2	-3.532751322
Integrin alpha-1	ITGA1	-3.619241666
Collectin-12	COLEC12	-3.756430396
Tropomyosin alpha-1 chain	TPM1	-3.827982433
Collagen alpha-1(XI) chain	COL11A1	-3.872735863
Collagen alpha-1(III) chain	COL3A1	-4.123005226
Myosin regulatory light polypeptide 9	MYL9	-4.515445514
Collagen alpha-1(XII) chain	COL12A1	-4.892665194
Collagen alpha-1(I) chain	COL1A1	-5.803406489

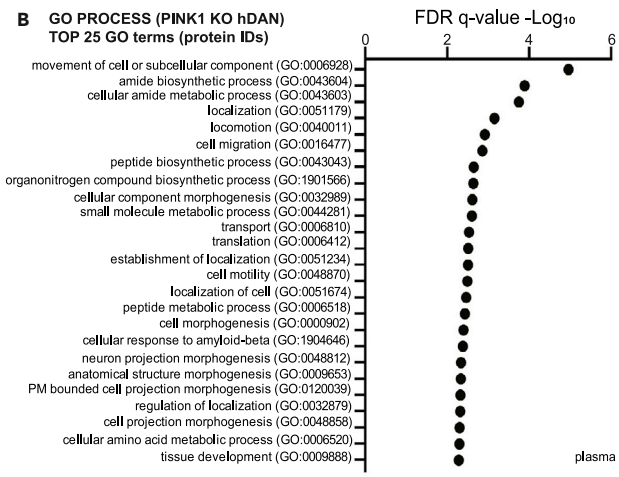

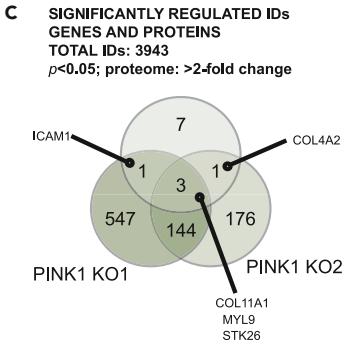

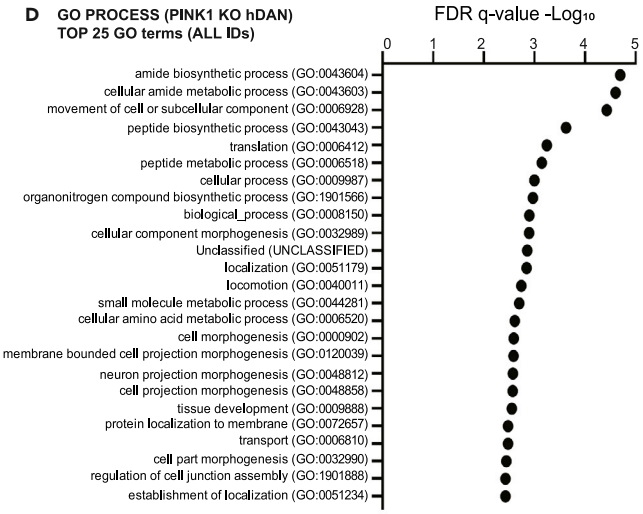

Figure 5. Combined Proteomic and Transcriptomic Pathway Analyses Highlight Metabolic Role of PINK1

(A) Top differentially abundant proteins (mean Log2 fold change), significantly changed in both PINK1 KO1 and PINK1 KO2 hDANs (nDiff = 3, t test).

(B) Unbiased pathway analysis of differentially abundant proteins to generate the top 25 GO process terms for untreated PINK1 KO hDANs (nDiff = 3) based on significance (FDR-q-value).

(C) Overlap of differentially regulated genes and proteins from transcriptomics and proteomics comparing CTRL and PINK1 KO hDANs.

(D) Unbiased pathway analysis of differentially regulated ID (genes and proteins) to generate the top 25 GO process terms for untreated PINK1 KO hDANs based on significance (FDR-q-value).

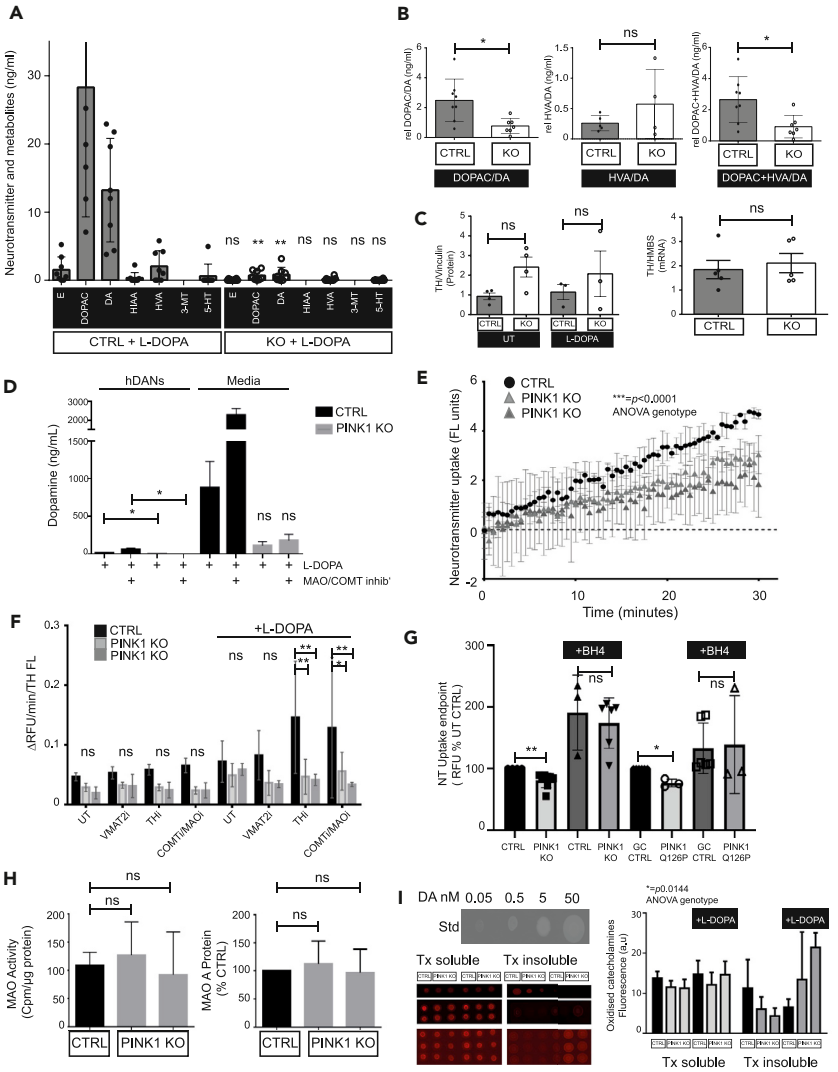

Figure 6. PINK1 Is Required for Maintenance of Dopamine Pools and Proper Neurotransmitter Uptake in Human Neurons

(A) Concentration of neurotransmitters and metabolites epinephrine (E), 3,4-dihydroxyphenylacetic acid (DOPAC), dopamine (DA), 5-hydroxyindoleacetic acid (HIAA), homovanillic acid (HVA), 3-methoxytyramine (3-MT), and 5-hydroxytryptamine/serotonin (5-HT) in hDANs treated with L-DOPA 50µM for 24 h. ** = p0.0045 (DOPAC), p0.0023 (DA), ns = not significant. (nDiff = 8, error bars = SD, t test).

(B) Ratios of DOPAC/DA, HVA/DA, and DOPAC plus HVA/DA. * = p0.0130 (DOPAC/DA), p0.0144 (DOPAC + HVA/DA), ns = not significant (nDiff = 8, error bars = SD, t test).

(C) Tyrosine hydroxylase (TH) protein levels (left panel) and gene expression (right panel) in hDAN aliquots from each HPLC experiments. ns = not significant (nDiff = 4, error bars = SD, t test).

(D) Dopamine concentration in hDANs and in cell culture supernatants treated with L-DOPA for 24 h with or without inhibition of dopamine degradation via COMT and MAOA/B (MOA/COMT inhib'). ** = p0.0036 (L-DOPA, CTRL versus KO), p0.046 (DOPAC + MAOi, CTRL versus KO), ns = not significant (nDiff = 4, error bars = SD, t test).

(E) Neurotransmitter uptake in hDANs measured by the fluorescence of the labeled amine converted inside hDANs only. * = p < 0.0001 (nDiff = 3, error bars = SD, two-way ANOVA).

(F) Quantification of neurotransmitter uptake in hDANs with or without acute inhibition of TH activity (THi), VMAT2 activity (VMAT2i), and COMT and MAOA/B activity (COMTi/MAOi) with or without 24-h 50µM L-DOPA treatment. The rate of uptake is normalized to the amount of TH staining in the well to account for hDAN number. ** = p0.0071 (*L-DOPA + THi, KO1), ** = p0.0048 (*L-DOPA + THi, KO2), * = p0.049 (*L-DOPA + COMTi/MAOi versus KO1), ** = p0.010 (*L-DOPA + COMTi/MAOi vs KO2) (nDiff = 3, t test).

Figure 6. *Continued*

(G) Neurotransmitter uptake in untreated or BH4-treated PINK1 KO and Q126P hDANs with respective isogenic and gene corrected (GC) controls ** = p0.0024 (untreated CTRL versus PINK1 KO), * = p0.023 (untreated GC CTRL versus PINK1 Q126P), ns = not significant. (nDiff = 3, error bars = SD, t test).

(H) MAO A/B activity in hDANs measured by the deamination of a radiolabeled tyramine substrate (left panel) and MAO-A protein levels normalized to GAPDH marker and the healthy control (right panel) ns = not significant (nDiff = 3, error bars = SD, t test).

(I) Catecholamine oxidation in hDANs with or without 50μM L-DOPA treatment for 24 h, showing results for soluble and insoluble fractions. Left panel pictures of blots with oxidized catecholamines. Right panel mean fluorescence signal (a.u.) of oxidized catechols in hDANs (representative blots, nDiff = 3). Two-way ANOVA found significance across the genotypes (* = p0.144), including all the conditions.

synthases and therefore indispensable for the production of catecholamine neurotransmitters including dopamine.

DISCUSSION

Homozygous PINK1 KO causes a significant catecholamine deficit in human mid-brain-specific neurons. The loss of dopamine cannot be attributed to any significant absence of TH-positive neurons in the same hDAN cultures used for catecholamine detection, although TH expression varied across differentiations. Reduced dopamine pools are not a result of increased degradation by monoamine oxidases. Dopamine oxidation remains a possible explanation as we detected increased catecholamine oxidation, but this was inconsistent and in Triton insoluble fractions of PINK1 KO hDANs with L-DOPA treatment. It will be interesting to study whether neuromelanin levels are increased with the advent of mid-brain-specific organoid models. One interesting possibility is that the dopamine deficiency could be caused by mitochondrial metabolism. We show that loss of PINK1-mitochondrial quality control reduces mitochondrial membrane potential and *m*Aconitase activity, yet this is compensated to maintain the mitochondrial networks and meet energy demand. Routing of phenylalanine and tyrosine into the TCA cycle and to acetyl-CoA reduces the pool of precursors for neurotransmitter synthesis. The fact that PINK1 also plays an important role in mitochondrial metabolism in cancer and is highly expressed in non-neuronal brain cells demonstrates that one main function of PINK1 is to help maintain the metabolic quality of mitochondria.

Although PINK1 maintains general mitochondrial quality, it is dispensable for the maintenance of mitochondrial networks and mitochondrial structure in human neurons. This is in line with prior evidence that mitochondrial turnover can occur independently of PINK1 (McWilliams et al., 2018; Lee et al., 2018; Allen et al., 2013a).

Loss of PINK1-mediated, mitochondrial quality control does, however, impair mitochondrial health, seen here by reduced mitochondrial membrane potential. The mitochondrial membrane potential contributes to the proton-motive force needed to generate energy and therefore is seen as a mitochondrial dysfunction. However, the situation might be more complex because mild depolarization and uncoupling has been shown to be beneficial for longevity. Depolarization can trigger stress responses and mitochondrial signaling that are necessary for adaption and reducing oxidative burden. Even small changes to mitochondrial membranes are important for adapting and regulating redox (Vyssokikh et al., 2020) and fueling dopamine release (Graves et al., 2020).

Our data confirm PINK1's role in canonical, ionophore-induced mitophagy while highlighting the relevance of mitochondrial quality control mechanisms that could occur independently of PINK1 (Soubannier et al., 2012; Pickles et al., 2018). Mitochondrial fragmentation occurs in PINK1 KO NPCs but is not observed in the mature hDANs. This supports the model that mitochondrial dynamics can protect healthy mitochondrial domains from elimination when left unchecked by the PINK1-Parkin pathway (Burman et al., 2017; Exner et al., 2007; Ziviani et al., 2010).

Here, we show that PINK1 is dispensable for complex I activity in hDANs. Even in the presence of ionophores, complex I in PINK1 KO hDANs still actively consumes NADH. This observation is in contrast to several studies showing that PINK1 is needed for phosphorylation of complex I (Morais et al., 2014) and reduced complex I activity in PINK1 models and PD patients (Pogson et al., 2014; Flones et al., 2017; Schapira et al., 1989). Our data are obtained from neurons derived from stem cells where the gene knockout has been introduced and therefore does not rule out the possibility that complex I could become impaired

during aging, nor does it take into account the influence of substrate availability, influence of the complete respiratory chain, different states of respiration, lipids, and membrane architecture (Vos et al., 2017). In our study, the depletion of succinate, but not NADH or complex I, points to the relevance of succinate dehydrogenase (complex II) in tuning of respiration and reducing oxidative burden. The mitochondrial matrix protein TRAP1 modulates complex II activity (Sciacovelli et al., 2013) and has previously been shown to act downstream of PINK1 (Fitzgerald et al., 2017; Pridgeon et al., 2007).

PINK1 orchestrates diverse quality control mechanisms (Geisler et al., 2010, Narendra et al., 2010a, Wang et al., 2011a, Sliter et al., 2018, Lai et al., 2015), yet discovery of novel *bonefide* PINK1 substrates in human neurons remains elusive. We show that *m*Aconitase activity and PNPO expression are greatly inhibited by PINK1 KO in neurons. Direct physical interaction between PINK1 and these candidates is unlikely considering their location. The transport of mitochondrial metabolites to the mitochondrial matrix could be a key factor. Other mitochondrial proteins previously described as interactors of PINK1, such as complex I, MIRO-1, or TRAP1, could also be involved in PINK1-metabolic control (Esposito et al., 2013; Morais et al., 2014; Pridgeon et al., 2007; Wang et al., 2011a). The calcium-binding, iron sulfur cluster protein NECAB2 (also known as mitoNEET) and the mitochondrial NDP kinase NME4 identified in this study are interesting candidates for PINK1 interaction.

PINK1 mediates iron homeostasis (Esposito et al., 2013; Kang et al., 2019; Wan et al., 2020; Allen et al., 2013b). The PINK1-PARK2 pathway regulates mitochondrial iron accumulation through affecting SLC25A37 and SCL25A28 degradation, contributing to the abnormal metabolism that supports pancreatic tumor development (Li et al., 2018). Iron is needed for *m*Aconitase activity and must be actively transported into the mitochondrial matrix by mitoferrin, which is upregulated in PINK1 KO hDANs. We propose iron availability in the mitochondrial matrix is responsible for reduced *m*Aconitase activity in PINK1 KO hDANs. Since we do not observe a significant buildup of fumarate nor loss of pyruvate, we can rule out inhibition of *m*Aconitase by succination via fumarate (Ternette et al., 2013). Citrate availability and utilization has been demonstrated for *m*Aconitase role in cancer metabolism. In contrast to certain cancers that permit citrate isomerization at the expense of fatty acid synthesis, PINK1 KO neurons inhibit *m*Aconitase activity, thus promoting fatty acid synthesis. This is important for the mitochondrial and cell membranes and for β-oxidation.

Loss of PINK1 initially induces benign biochemical and metabolic responses and mitochondrial compensation. These biochemical changes are, however, particularly relevant for dopaminergic neurons. Nucleotide and amino acid metabolism were highlighted in metabolomics, transcriptomics, and proteomics experiments in PINK1 KO hDANs. GO terms such as "amide metabolism" describing central metabolic processes ranked the highest when combining the most significant gene and protein changes due to PINK1 KO. Amide metabolism is important in the synthesis of key biochemical intermediates including proteins and lipids and an active component of coenzymes, including CoA.

Amino acids regulate the target of rapamycin (TOR) pathway and are important in aging, inflammation, and neurodegeneration (Auburger et al., 2017; De Simone et al., 2013), reviewed in (Neinast et al., 2019). Phenylalanine and tyrosine, two amino acids reduced in PINK1 KO hDANs, precede tyrosine hydroxylase conversion of tyrosine to L-DOPA, which is the rate-limiting step in the synthesis of dopamine. Dopamine and DOPAC levels are significantly reduced by PINK1 KO in hDANs. Dopamine synthesis also requires pyridoxal phosphate (PLP), the active form of vitamin B6 and a product of the vitamin B6 salvage pathway via PNPO, which is silenced in PINK1 KO hDANs. We suggest that altered dopamine metabolism in PINK1 KO hDANs is due to restriction of its precursors because they are urgently required elsewhere to provide an anaplerotic lifeline to the TCA and support anabolism via acetyl-CoA. The role of PNPO is complex. Silencing of PNPO expression in PINK1 KO NPCs that do not yet express TH or other dopaminergic markers suggests this is tied to the early mitochondrial compensation events resulting from loss of PINK1. Loss of PINK1 expression or kinase function is required for reduced PNPO expression because the PINK1 Q126P point mutation has no effect. High PLP levels can shut down PNPO expression in negative feedback loop, and it is possible that there is an inverse correlation between PINK1 levels and PLP. High PLP levels might be needed for feeding the TCA cycle with amino acid catabolites generated via transamination reactions. The fact that PINK1 Q126P PD hDANS develop neurotransmitter defects without significant reduction of PNPO expression suggests that PNPO silencing here is a relevant to understanding the mechanism but not the biological cause.

Tetrahydrobiopterin (BH_4) is a crucial cofactor in catecholamine metabolism. Here, BH_4 promotes the uptake of catecholamines into neurons. Rescue of catecholamine uptake in PINK1 KO hDANs by BH_4 shows that the uptake defect is secondary since the uptake assay provides a synthetic, exogenous substrate. Because ferrous iron reduces the BH_3 radical back to BH_4 (Berka et al., 2004), the link between PINK1 and Iron and PINK1 and metabolic cofactors needs further elucidation.

Dopamine degradation by MAO and COMT was not significantly affected by loss of PINK1 (we observed significant fluctuations of MAO abundance at the gene and protein level but it was not consistent). TH levels were also highly fluctuating in PINK1 KO hDANs differentiations. TH cofactor biosynthesis is regulated by BH_4 and phenylalanine. These data point toward steering of phenylalanine and tyrosine toward energy metabolism in the mitochondria away from dopamine synthesis.

Whether PINK1 can directly control dopamine metabolism at the mitochondrial outer membrane and mitochondrial-ER contact sites through phosphorylation is an interesting question but so far there is no biochemical evidence. Until candidates are proven, we must assume that it is the loss of mitochondrial quality control and altered MOM landscape that induces metabolic changes. PINK1 involvement in the transport of iron and fine tuning of mitochondrial membranes can mediate such biochemical changes and the consequences go beyond mitophagy in dopaminergic neurons.

Limitations of the Study

- The lack of reliable antibodies to pull down endogenous PINK1 in hDANs limits the biochemical confirmation of PINK1 interactors. Further work using endogenous gene editing of PINK1 in iPSCs and phospho-targeted proteomics is needed.
- It was not possible to reintroduce wild-type human PINK1 into PINK1 KO hDANs to confirm key finding were due to PINK1 KO. Viral transduction is required and low transfection efficiency in iPSC-derived neurons masks any rescue effects without the ability to sort living cells. Introducing antibiotic resistance is limited by the TALEN.

Resource and Availability

Lead Contact

Julia C. Fitzgerald. Hertie Institute for Clinical Brain Research, University of Tübingen, Otfried Müller Strasse 27, Tübingen, 72,076, Germany. Tel: +497071 2981971. Email: julia.fitzgerald@uni-tuebingen.de.

Materials Availability

Please contact us for more information, information on methods, and if you would like to request any materials.

Data and Code Availability

Full Proteomics and transcriptomics peptide and gene lists are deposited and available online at Mendeley Data: Fitzgerald, Julia C. (2020), "Bus et al. iScience. PINK1 hDANs", Mendeley Data, V1, https://doi.org/10.17632/5xv2kwg2c2.1.

High-quality electron microscopy images and other relevant datasets are available at Mendeley Data or on request.

METHODS

All methods can be found in the accompanying Transparent Methods supplemental file.

SUPPLEMENTAL INFORMATION

Supplemental Information can be found online at https://doi.org/10.1016/j.isci.2020.101797.

ACKNOWLEDGMENTS

We greatly acknowledge funding from the Germany Ministry of Education and Research (BMBF) e:Med Demonstrator project MitoPD (FKZ 031A430A). JCF greatly acknowledges support from The German

Research Council (DFG), Research Training Group (RTG) MOMbrane–GRK 2364, And also, The German Center for Neurodegenerative Diseases (DZNE) and The Michael J Fox Foundation for Parkinson's Research (MJFF-15744).

AU-K is supported by Nottingham Trent University Independent Research Fellowship Scheme (UK). This work was supported by research grants from Fonds National de Recherche de Luxembourg (FNR) within the National Center for Excellence in Research on Parkinson's disease (NCER-PD) and MiRisk project [C17/BM/11676395] for RK and GA. DM and KM also acknowledge DFG-RTG MOMbrane (GRK 2364). DVW acknowledges support from the German Science Foundation within the Collaborative Research Centre (CRC) 870, and the Initiative and Network Fund of the Helmholtz Association within the 'ExNet-0041-Phase2-3 ("SyNergy-HMGU")' project.

We would like to thank the iPS cell facility at the HMGU Munich and Annerose Kurz-Drexler as well as Dr. Florian Giesert for generating the hiPSCs and the respective gene-corrected line derived from patients carrying the PINK1 Q126P mutation. We also thank Christine Klein and Philipp Seibler (University of Lübeck, Germany) who kindly shared the human iPSC lines from PD patients carrying the PINK1 Q456X mutation and Jens Schwamborn and Javier Jarazo (LCSB, University of Luxembourg, Luxembourg) for kindly providing their corresponding gene-corrected controls to prepare RNA. We would like to acknowledge The Werner Siemens Imaging Center (WSIC) and Bernd Pichler for access to the NMR spectroscopy for the metabolomics experiments. We thank students and interns in the Fitzgerald lab (Malina John, Max Mattheuer and Lisa Schwarz) who contributed toward establishing and optimizing methodologies. Also E. Ellen Billett for critical review.

AUTHOR CONTRIBUTIONS

Conceptualization, JCF; Methodology, JCF, CB, BS, CJG, CT, DV-W, DR; Validation, JCF, CB, MZ, AS, GA.; Formal Analysis, JCF, MF, AS, CB, KK, CJG, PF-B, AU-K, JA, LZ, CT; Investigation, JCF, CB, MF, SG, MZ, LS, CB, KK, NC, PF-B, AS, FK, CM, JA, AU-K, LZ, KM, GA, CT; Writing—Original Draft, JCF; Writing—Review & Editing, JCF, SG, PK, AU-K, LZ, CB; Visualization, JCF, PK, SG, CJG, CB, JA, LZ, NC; Funding Acquisition, JCF, CJG, MU, RK, TG. and PK; Resources, TG, MU, NC, CT; Supervision, JCF, TG.

DECLARATION OF INTERESTS

The authors declare no conflict of interest.

Received: February 26, 2020
Revised: August 7, 2020
Accepted: November 10, 2020
Published: December 18, 2020

REFERENCES

Allen, G.F., Toth, R., James, J., and Ganley, I.G. (2013a). Loss of iron triggers PINK1/Parkin-independent mitophagy. EMBO Rep. *14*, 1127–1135.

Allen, G.F., Ullah, Y., Hargreaves, I.P., Land, J.M., and Heales, S.J. (2013b). Dopamine but not l-dopa stimulates neural glutathione metabolism. Potential implications for Parkinson's and other dopamine deficiency states. Neurochem. Int. *62*, 684–694.

Anichtchik, O., Diekmann, H., Fleming, A., Roach, A., Goldsmith, P., and Rubinsztein, D.C. (2008). Loss of PINK1 function affects development and results in neurodegeneration in zebrafish. J. Neurosci. *28*, 8199–8207.

Auburger, G., Sen, N.E., Meierhofer, D., Basak, A.N., and Gitler, A.D. (2017). Efficient prevention of neurodegenerative diseases by depletion of starvation response factor Ataxin-2. Trends Neurosci. *40*, 507–516.

Bender, T., and Martinou, J.C. (2016). The mitochondrial pyruvate carrier in health and disease: to carry or not to carry? Biochim. Biophys. Acta *1863*, 2436–2442.

Berka, V., Yeh, H.C., Gao, D., Kiran, F., and Tsai, A.L. (2004). Redox function of tetrahydrobiopterin and effect of L-arginine on oxygen binding in endothelial nitric oxide synthase. Biochemistry *43*, 13137–13148.

Berthier, A., Navarro, S., Jimenez-Sainz, J., Rogla, I., Ripoll, F., Cervera, J., and Pulido, R. (2011). PINK1 displays tissue-specific subcellular location and regulates apoptosis and cell growth in breast cancer cells. Hum. Pathol. *42*, 75–87.

Birsa, N., Norkett, R., Wauer, T., Mevissen, T.E.T., Wu, H.C., Foltynie, T., Bhatia, K., Hirst, W.D., Komander, D., Plun-Favreau, H., and Kittler, J.T. (2014). Lysine 27 ubiquitination of the mitochondrial transport protein Miro is dependent on serine 65 of the parkin ubiquitin ligase. J. Biol. Chem. *289*, 14569–14582.

Blackinton, J.G., Anvret, A., Beilina, A., Olson, L., Cookson, M.R., and Galter, D. (2007). Expression of PINK1 mRNA in human and rodent brain and in Parkinson's disease. Brain Res. *1184*, 10–16.

Burman, J.L., Pickles, S., Wang, C., Sekine, S., Vargas, J.N.S., Zhang, Z., Youle, A.M., Nezich, C.L., Wu, X., Hammer, J.A., and Youle, R.J. (2017). Mitochondrial fission facilitates the selective mitophagy of protein aggregates. J. Cell Biol. *216*, 3231–3247.

Calvo, S.E., Clauser, K.R., and Mootha, V.K. (2016). MitoCarta2.0: an updated inventory of mammalian mitochondrial proteins. Nucleic Acids Res. *44*, D1251–D1257.

Celardo, I., Costa, A.C., Lehmann, S., Jones, C., Wood, N., Mencacci, N.E., Mallucci, G.R., Loh, S.H., and Martins, L.M. (2016). Mitofusin-mediated ER stress triggers neurodegeneration in pink1/parkin models of Parkinson's disease. Cell Death Dis. *7*, e2271.

Chu, C.T. (2019). Multiple pathways for mitophagy: a neurodegenerative conundrum for Parkinson's disease. Neurosci. Lett. *697*, 66–71.

Clark, I.E., Dodson, M.W., Jiang, C., Cao, J.H., Huh, J.R., Seol, J.H., Yoo, S.J., Hay, B.A., and Guo, M. (2006). Drosophila pink1 is required for mitochondrial function and interacts genetically with parkin. Nature *441*, 1162–1166.

Cummins, N., and Gotz, J. (2018). Shedding light on mitophagy in neurons: what is the evidence for PINK1/Parkin mitophagy in vivo? Cell. Mol. Life Sci. *75*, 1151–1162.

Esposito, G., Vos, M., Vilain, S., Swerts, J., De Sousa Valadas, J., Van Meensel, S., Schaap, O., and Verstreken, P. (2013). Aconitase causes iron toxicity in Drosophila pink1 mutants. PLoS Genet. *9*, e1003478.

Exner, N., Treske, B., Paquet, D., Holmstrom, K., Schiesling, C., Gispert, S., Carballo-Carbajal, I., Berg, D., Hoepken, H.H., Gasser, T., et al. (2007). Loss-of-function of human PINK1 results in mitochondrial pathology and can be rescued by parkin. J. Neurosci. *27*, 12413–12418.

Fitzgerald, J.C., Zimprich, A., Berrio, D.A.C., Schindler, K.M., Maurer, B., Schulte, C., Bus, C., Hauser, A.K., Kubler, M., Lewin, R., et al. (2017). Metformin reverses TRAP1 mutation-associated alterations in mitochondrial function in Parkinson's disease. Brain *140*, 2444–2459.

Flones, I.H., Fernandez-Vizarra, E., Lykouri, M., Brakedal, B., Skeie, G.O., Miletic, H., Lilleng, P.K., Alves, G., Tysnes, O.B., Haugarvoll, K., et al. (2017). Neuronal complex I deficiency occurs throughout the Parkinson's disease brain, but is not associated with neurodegeneration or mitochondrial DNA damage. Acta Neuropathol. *135*, 409–425.

Gandhi, S., and Plun-Favreau, H. (2017). Mutations and mechanism: how PINK1 may contribute to risk of sporadic Parkinson's disease. Brain *140*, 2–5.

Gandhi, S., Wood-Kaczmar, A., Yao, Z., Plun-Favreau, H., Deas, E., Klupsch, K., Downward, J., Latchman, D.S., Tabrizi, S.J., Wood, N.W., et al. (2009). PINK1-associated Parkinson's disease is caused by neuronal vulnerability to calcium-induced cell death. Mol. Cell *33*, 627–638.

Gautier, C.A., Kitada, T., and Shen, J. (2008). Loss of PINK1 causes mitochondrial functional defects and increased sensitivity to oxidative stress. Proc. Natl. Acad. Sci. U S A *105*, 11364–11369.

Gegg, M.E., Cooper, J.M., Chau, K.Y., Rojo, M., Schapira, A.H.V., and Taanman, J.W. (2010). Mitofusin 1 and mitofusin 2 are ubiquitinated in a PINK1/parkin-dependent manner upon induction of mitophagy. Hum. Mol. Genet. *19*, 4861–4870.

Geisler, S., Holmstrom, K.M., Skujat, D., Fiesel, F.C., Rothfuss, O.C., Kahle, P.J., and Springer, W. (2010). PINK1/Parkin-mediated mitophagy is dependent on VDAC1 and p62/SQSTM1. Nat. Cell Biol. *12*, 119–131.

Gelmetti, V., De Rosa, P., Torosantucci, L., Marini, E.S., Romagnoli, A., Di Rienzo, M., Arena, G., Vignone, D., Fimia, G.M., and Valente, E.M. (2017). PINK1 and BECN1 relocalize at mitochondria-associated membranes during mitophagy and promote ER-mitochondria tethering and autophagosome formation. Autophagy *13*, 654–669.

Gispert, S., Ricciardi, F., Kurz, A., Azizov, M., Hoepken, H.H., Becker, D., Voos, W., Leuner, K., Muller, W.E., Kudin, A.P., et al. (2009). Parkinson phenotype in aged PINK1-deficient mice is accompanied by progressive mitochondrial dysfunction in absence of neurodegeneration. PLoS One *4*, e5777.

Graves, S.M., Xie, Z., Stout, K.A., Zampese, E., Burbulla, L.F., Shih, J.C., Kondapalli, J., Patriarchi, T., Tian, L., Brichta, L., et al. (2020). Dopamine metabolism by a monoamine oxidase mitochondrial shuttle activates the electron transport chain. Nat. Neurosci. *23*, 15–20.

Grossmann, D., Berenguer-Escuder, C., Bellet, M.E., Scheibner, D., Bohler, J., Massart, F., Rapaport, D., Skupin, A., Fouquier D'herouel, A., Sharma, M., et al. (2019). Mutations in RHOT1 disrupt endoplasmic reticulum-mitochondria contact sites interfering with calcium homeostasis and mitochondrial dynamics in Parkinson's disease. Antioxid. Redox Signal. *31*, 1213–1234.

Guo, T., Liu, T., Sun, Y., Liu, X., Xiong, R., Li, H., Li, Z., Zhang, Z., Tian, Z., and Tian, Y. (2019). Sonodynamic therapy inhibits palmitate-induced beta cell dysfunction via PINK1/Parkin-dependent mitophagy. Cell Death Dis. *10*, 457.

Heeman, B., Van Den Haute, C., Aelvoet, S.A., Valsecchi, F., Rodenburg, R.J., Reumers, V., Debyser, Z., Callewaert, G., Koopman, W.J., Willems, P.H., and Baekelandt, V. (2011). Depletion of PINK1 affects mitochondrial metabolism, calcium homeostasis and energy maintenance. J. Cell Sci. *124*, 1115–1125.

Horowitz, M.P., and Greenamyre, J.T. (2010). Mitochondrial iron metabolism and its role in neurodegeneration. J. Alzheimers Dis. *20*, S551–S568.

Ivatt, R.M., Sanchez-Martinez, A., Godena, V.K., Brown, S., Ziviani, E., and Whitworth, A.J. (2014). Genome-wide RNAi screen identifies the Parkinson disease GWAS risk locus SREBF1 as a regulator of mitophagy. Proc. Natl. Acad. Sci. U S A *111*, 8494–8499.

Jin, S.M., and Youle, R.J. (2013). The accumulation of misfolded proteins in the mitochondrial matrix is sensed by PINK1 to induce PARK2/Parkin-mediated mitophagy of polarized mitochondria. Autophagy *9*, 1750–1757.

Jin, S.M., Lazarou, M., Wang, C., Kane, L.A., Narendra, D.P., and Youle, R.J. (2010). Mitochondrial membrane potential regulates PINK1 import and proteolytic destabilization by PARL. J. Cell Biol. *191*, 933–942.

Julienne, H., Buhl, E., Leslie, D.S., and Hodge, J.J.L. (2017). Drosophila PINK1 and parkin loss-of-function mutants display a range of non-motor Parkinson's disease phenotypes. Neurobiol. Dis. *104*, 15–23.

Kane, L.A., and Youle, R.J. (2011). PINK1 and Parkin flag Miro to direct mitochondrial traffic. Cell *147*, 721–723.

Kane, L.A., Lazarou, M., Fogel, A.I., Li, Y., Yamano, K., Sarraf, S.A., Banerjee, S., and Youle, R.J. (2014). PINK1 phosphorylates ubiquitin to activate Parkin E3 ubiquitin ligase activity. J. Cell Biol. *205*, 143–153.

Kang, R., Xie, Y., Zeh, H.J., Klionsky, D.J., and Tang, D. (2019). Mitochondrial quality control mediated by PINK1 and PRKN: links to iron metabolism and tumor immunity. Autophagy *15*, 172–173.

Kazlauskaite, A., Kondapalli, C., Gourlay, R., Campbell, D.G., Ritorto, M.S., Hofmann, K., Alessi, D.R., Knebel, A., Trost, M., and Muqit, M.M.K. (2014). Parkin is activated by PINK1-dependent phosphorylation of ubiquitin at Ser(65). Biochem. J. *460*, 127–139.

Kitada, T., Pisani, A., Porter, D.R., Yamaguchi, H., Tscherter, A., Martella, G., Bonsi, P., Zhang, C., Pothos, E.N., and Shen, J. (2007). Impaired dopamine release and synaptic plasticity in the striatum of PINK1-deficient mice. Proc. Natl. Acad. Sci. U S A *104*, 11441–11446.

Klein, C., Grunewald, A., and Hedrich, K. (2006). Early-onset parkinsonism associated with PINK1 mutations: frequency, genotypes, and phenotypes. Neurology *66*, 1129–1130.

Koyano, F., Okatsu, K., Kosako, H., Tamura, Y., Go, E., Kimura, M., Kimura, Y., Tsuchiya, H., Yoshihara, H., Hirokawa, T., et al. (2014). Ubiquitin is phosphorylated by PINK1 to activate parkin. Nature *510*, 162.

Lai, Y.C., Kondapalli, C., Lehneck, R., Procter, J.B., Dill, B.D., Woodroof, H.I., Gourlay, R., Peggie, M., Macartney, T.J., Corti, O., et al. (2015). Phosphoproteomic screening identifies Rab GTPases as novel downstream targets of PINK1. EMBO J. *34*, 2840–2861.

Lazarou, M., Sliter, D.A., Kane, L.A., Sarraf, S.A., Wang, C.X., Burman, J.L., Sideris, D.P., Fogel, A.I., and Youle, R.J. (2015). The ubiquitin kinase PINK1 recruits autophagy receptors to induce mitophagy. Nature *524*, 309.

Lee, J.J., Sanchez-Martinez, A., Zarate, A.M., Beninca, C., Mayor, U., Clague, M.J., and Whitworth, A.J. (2018). Basal mitophagy is widespread in Drosophila but minimally affected by loss of Pink1 or parkin. J. Cell Biol. *217*, 1613–1622.

Li, C., Zhang, Y., Cheng, X., Yuan, H., Zhu, S., Liu, J., Wen, Q., Xie, Y., Liu, J., Kroemer, G., et al. (2018). PINK1 and PARK2 suppress pancreatic tumorigenesis through control of mitochondrial iron-mediated immunometabolism. Dev. Cell *46*, 441–455.e8.

Matheoud, D., Cannon, T., Voisin, A., Penttinen, A.M., Ramet, L., Fahmy, A.M., Ducrot, C., Laplante, A., Bourque, M.J., Zhu, L., et al. (2019). Intestinal infection triggers Parkinson's disease-like symptoms in Pink1(-/-) mice. Nature *571*, 565–569.

Mclelland, G.L., Goiran, T., Yi, W., Dorval, G., Chen, C.X., Lauinger, N.D., Krahn, A.I., Valimehr, S., Rakovic, A., Rouiller, I., et al. (2018). Mfn2 ubiquitination by PINK1/parkin gates the p97-

dependent release of ER from mitochondria to drive mitophagy. Elife *7*, e32866.

Mcwilliams, T.G., Prescott, A.R., Montava-Garriga, L., Ball, G., Singh, F., Barini, E., Muqit, M.M.K., Brooks, S.P., and Ganley, I.G. (2018). Basal mitophagy occurs independently of PINK1 in mouse tissues of high metabolic demand. Cell Metab. *27*, 439–449.e5.

Moisoi, N., Fedele, V., Edwards, J., and Martins, L.M. (2014). Loss of PINK1 enhances neurodegeneration in a mouse model of Parkinson's disease triggered by mitochondrial stress. Neuropharmacology *77*, 350–357.

Morais, V.A., Haddad, D., Craessaerts, K., De Bock, P.J., Swerts, J., Vilain, S., Aerts, L., Overbergh, L., Grunewald, A., Seibler, P., et al. (2014). PINK1 loss-of-function mutations affect mitochondrial complex I activity via NdufA10 ubiquinone uncoupling. Science *344*, 203–207.

Mouton-Liger, F., Rosazza, T., Sepulveda-Diaz, J., Ieang, A., Hassoun, S.M., Claire, E., Mangone, G., Brice, A., Michel, P.P., Corvol, J.C., and Corti, O. (2018). Parkin deficiency modulates NLRP3 inflammasome activation by attenuating an A20-dependent negative feedback loop. Glia *66*, 1736–1751.

Narendra, D., Tanaka, A., Suen, D.F., and Youle, R.J. (2008). Parkin is recruited selectively to impaired mitochondria and promotes their autophagy. J. Cell Biol. *183*, 795–803.

Narendra, D.P., Jin, S.M., Tanaka, A., Suen, D.F., Gautier, C.A., Shen, J., Cookson, M.R., and Youle, R.J. (2010a). PINK1 is selectively stabilized on impaired mitochondria to activate Parkin. Plos Biol. *8*, e1000298.

Narendra, D.P., Kane, L.A., Hauser, D.N., Fearnley, I.M., and Youle, R.J. (2010b). p62/SQSTM1 is required for Parkin-induced mitochondrial clustering but not mitophagy; VDAC1 is dispensable for both. Autophagy *6*, 1090–1106.

Neinast, M., Murashige, D., and Arany, Z. (2019). Branched chain amino acids. Annu. Rev. Physiol. *81*, 139–164.

Okatsu, K., Saisho, K., Shimanuki, M., Nakada, K., Shitara, H., Sou, Y., Kimura, M., Sato, S., Hattori, N., Komatsu, M., et al. (2010). p62/SQSTM1 cooperates with Parkin for perinuclear clustering of depolarized mitochondria. Genes to Cells *15*, 887–900.

Parganlija, D., Klinkenberg, M., Dominguez-Bautista, J., Hetzel, M., Gispert, S., Chimi, M.A., Drose, S., Mai, S., Brandt, U., Auburger, G., and Jendrach, M. (2014). Loss of PINK1 impairs stress-induced autophagy and cell survival. PLoS One *9*, e95288.

Park, J., Lee, S.B., Lee, S., Kim, Y., Song, S., Kim, S., Bae, E., Kim, J., Shong, M., Kim, J.M., and Chung, J. (2006). Mitochondrial dysfunction in Drosophila PINK1 mutants is complemented by parkin. Nature *441*, 1157–1161.

Pickles, S., Vigie, P., and Youle, R.J. (2018). Mitophagy and quality control mechanisms in mitochondrial maintenance. Curr. Biol. *28*, R170–R185.

Pogson, J.H., Ivatt, R.M., Sanchez-Martinez, A., Tufi, R., Wilson, E., Mortiboys, H., and Whitworth, A.J. (2014). The complex I subunit NDUFA10 selectively rescues Drosophila pink1 mutants through a mechanism independent of mitophagy. PLoS Genet. *10*, e1004815.

Pridgeon, J.W., Olzmann, J.A., Chin, L.S., and Li, L. (2007). PINK1 protects against oxidative stress by phosphorylating mitochondrial chaperone TRAP1. PLoS Biol. *5*, e172.

Rakovic, A., Ziegler, J., Martensson, C.U., Prasuhn, J., Shurkewitsch, K., Konig, P., Paulson, H.L., and Klein, C. (2019). PINK1-dependent mitophagy is driven by the UPS and can occur independently of LC3 conversion. Cell Death Differ. *26*, 1428–1441.

Reinhardt, P., Glatza, M., Hemmer, K., Tsytsyura, Y., Thiel, C.S., Hoing, S., Moritz, S., Parga, J.A., Wagner, L., Bruder, J.M., et al. (2013a). Derivation and expansion using only small molecules of human neural progenitors for neurodegenerative disease modeling. PLoS One *8*, e59252.

Reinhardt, P., Schmid, B., Burbulla, L.F., Schondorf, D.C., Wagner, L., Glatza, M., Hoing, S., Hargus, G., Heck, S.A., Dhingra, A., et al. (2013b). Genetic correction of a LRRK2 mutation in human iPSCs links parkinsonian neurodegeneration to ERK-dependent changes in gene expression. Cell Stem Cell *12*, 354–367.

Requejo-Aguilar, R., Lopez-Fabuel, I., Fernandez, E., Martins, L.M., Almeida, A., and Bolanos, J.P. (2014). PINK1 deficiency sustains cell proliferation by reprogramming glucose metabolism through HIF1. Nat. Commun. *5*, 4514.

Schapira, A.H., Cooper, J.M., Dexter, D., Jenner, P., Clark, J.B., and Marsden, C.D. (1989). Mitochondrial complex I deficiency in Parkinson's disease. Lancet *1*, 1269.

Schiesling, C., Kieper, N., Seidel, K., and Kruger, R. (2008). Review: Familial Parkinson's disease–genetics, clinical phenotype and neuropathology in relation to the common sporadic form of the disease. Neuropathol. Appl. Neurobiol. *34*, 255–271.

Sciacovelli, M., Guzzo, G., Morello, V., Frezza, C., Zheng, L., Nannini, N., Calabrese, F., Laudiero, G., Esposito, F., Landriscina, M., Defilippi, P., Bernardi, P., and Rasola, A. (2013). The mitochondrial chaperone TRAP1 promotes neoplastic growth by inhibiting succinate dehydrogenase. Cell Metab. *17*, 988–999.

Seibler, P., Graziotto, J., Jeong, H., Simunovic, F., Klein, C., and Krainc, D. (2011). Mitochondrial Parkin recruitment is impaired in neurons derived from mutant PINK1 induced pluripotent stem cells. J. Neurosci. *31*, 5970–5976.

Shoshan-Barmatz, V., Zalk, R., Gincel, D., and Vardi, N. (2004). Subcellular localization of VDAC in mitochondria and ER in the cerebellum. Biochim. Biophys. Acta *1657*, 105–114.

de Simone, R., Vissicchio, F., Mingarelli, C., De Nuccio, C., Visentin, S., Ajmone-Cat, M.A., and Minghetti, L. (2013). Branched-chain amino acids influence the immune properties of microglial cells and their responsiveness to pro-inflammatory signals. Biochim. Biophys. Acta *1832*, 650–659.

Sliter, D.A., Martinez, J., Hao, L., Chen, X., Sun, N., Fischer, T.D., Burman, J.L., Li, Y., Zhang, Z., Narendra, D.P., et al. (2018). Parkin and PINK1 mitigate STING-induced inflammation. Nature *561*, 258–262.

Soman, S., Keatinge, M., Moein, M., Da Costa, M., Mortiboys, H., Skupin, A., Sugunan, S., Bazala, M., Kuznicki, J., and Bandmann, O. (2017). Inhibition of the mitochondrial calcium uniporter rescues dopaminergic neurons in pink1(-/-) zebrafish. Eur. J. Neurosci. *45*, 528–535.

Soubannier, V., Mclelland, G.L., Zunino, R., Braschi, E., Rippstein, P., Fon, E.A., and Mcbride, H.M. (2012). A vesicular transport pathway shuttles cargo from mitochondria to lysosomes. Curr. Biol. *22*, 135–141.

Steinlechner, S., Stahlberg, J., Volkel, B., Djarmati, A., Hagenah, J., Hiller, A., Hedrich, K., Konig, I., Klein, C., and Lencer, R. (2007). Co-occurrence of affective and schizophrenia spectrum disorders with PINK1 mutations. J. Neurol. Neurosurg. Psychiatry *78*, 532–535.

Ternette, N., Yang, M., Laroyia, M., Kitagawa, M., O'Flaherty, L., Wolhulter, K., Igarashi, K., Saito, K., Kato, K., Fischer, R., Berquand, A., Kessler, B.M., Lappin, T., Frizzell, N., Soga, T., Adam, J., and Pollard, P.J. (2013). Inhibition of mitochondrial aconitase by succination in fumarate hydratase deficiency. Cell Rep *3*, 689–700.

Torres-Odio, S., Key, J., Hoepken, H.H., Canet-Pons, J., Valek, L., Roller, B., Walter, M., Morales-Gordo, B., Meierhofer, D., Harter, P.N., et al. (2017). Progression of pathology in PINK1-deficient mouse brain from splicing via ubiquitination, ER stress, and mitophagy changes to neuroinflammation. J. Neuroinflammation *14*, 154.

Valente, E.M., Abou-Sleiman, P.M., Caputo, V., Muqit, M.M., Harvey, K., Gispert, S., Ali, Z., Del Turco, D., Bentivoglio, A.R., Healy, D.G., et al. (2004). Hereditary early-onset Parkinson's disease caused by mutations in PINK1. Science *304*, 1158–1160.

Villa, E., Proics, E., Rubio-Patino, C., Obba, S., Zunino, B., Bossowski, J.P., Rozier, R.M., Chiche, J., Mondragon, L., Riley, J.S., et al. (2017). Parkin-independent mitophagy controls chemotherapeutic response in cancer cells. Cell Rep. *20*, 2846–2859.

Vives-Bauza, C., Zhou, C., Huang, Y., Cui, M., De Vries, R.L., Kim, J., May, J., Tocilescu, M.A., Liu, W., Ko, H.S., et al. (2010). PINK1-dependent recruitment of Parkin to mitochondria in mitophagy. Proc. Natl. Acad. Sci. U S A *107*, 378–383.

Vos, M., Geens, A., Bohm, C., Deaulmerie, L., Swerts, J., Rossi, M., Craessaerts, K., Leites, E.P., Seibler, P., Rakovic, A., et al. (2017). Cardiolipin promotes electron transport between ubiquinone and complex I to rescue PINK1 deficiency. J. Cell Biol. *216*, 695–708.

Vyssokikh, M.Y., Holtze, S., Averina, O.A., Lyamzaev, K.G., Panteleeva, A.A., Marey, M.V., Zinovkin, R.A., Severin, F.F., Skulachev, M.V., Fasel, N., et al. (2020). Mild depolarization of the inner mitochondrial membrane is a crucial component of an anti-aging program. Proc. Natl. Acad. Sci. U S A *117*, 6491–6501.

Walsh, T.G., Van Den Bosch, M.T.J., Lewis, K.E., Williams, C.M., and Poole, A.W. (2018). Loss of the mitochondrial kinase PINK1 does not alter platelet function. Sci. Rep. *8*, 14377.

Wan, Z., Xu, J., Huang, Y., Zhai, Y., Ma, Z., Zhou, B., and Cao, Z. (2020). Elevating bioavailable iron levels in mitochondria suppresses the defective phenotypes caused by PINK1 loss-of-function in Drosophila melanogaster. Biochem. Biophys. Res. Commun. *532*, 285–291.

Wang, X., Winter, D., Ashrafi, G., Schlehe, J., Wong, Y., Selkoe, D., Rice, S., Steen, J., Lavoie, M., and Schwarz, T. (2011a). PINK1 and parkin Target Miro for phosphorylation and degradation to arrest mitochondrial motility. Mol. Biol. Cell *22*, 893–906.

Wang, X.N., Winter, D., Ashrafi, G., Schlehe, J., Wong, Y.L., Selkoe, D., Rice, S., Steen, J., Lavoie, M.J., and Schwarz, T.L. (2011b). PINK1 and parkin Target Miro for phosphorylation and degradation to arrest mitochondrial motility. Cell *147*, 893–906.

Wang, Y., Tang, C.Y., Cai, J., Chen, G.C., Zhang, D.S., Zhang, Z.H., and Dong, Z. (2018). PINK1/Parkin-mediated mitophagy is activated in cisplatin nephrotoxicity to protect against kidney injury. Cell Death Dis. *9*, 1113.

West, A.P., Khoury-Hanold, W., Staron, M., Tal, M.C., Pineda, C.M., Lang, S.M., Bestwick, M., Duguay, B.A., Raimundo, N., Macduff, D.A., et al. (2015). Mitochondrial DNA stress primes the antiviral innate immune response. Nature *520*, 553–557.

Wong, Y.C., and Holzbaur, E.L. (2014). Optineurin is an autophagy receptor for damaged mitochondria in parkin-mediated mitophagy that is disrupted by an ALS-linked mutation. Proc. Natl. Acad. Sci. U S A *111*, E4439–E4448, https://doi.org/10.1073/pnas.1405752111.

Zhang, C., Lee, S., Peng, Y., Bunker, E., Giaime, E., Shen, J., Zhou, Z., and Liu, X. (2014a). PINK1 triggers autocatalytic activation of Parkin to specify cell fate decisions. Curr. Biol. *24*, 1854–1865.

Zhang, Y., Chen, K., Sloan, S.A., Bennett, M.L., Scholze, A.R., O'keeffe, S., Phatnani, H.P., Guarnieri, P., Caneda, C., Ruderisch, N., et al. (2014b). An RNA-sequencing transcriptome and splicing database of glia, neurons, and vascular cells of the cerebral cortex. J. Neurosci. *34*, 11929–11947.

Ziviani, E., Tao, R.N., and Whitworth, A.J. (2010). Drosophila parkin requires PINK1 for mitochondrial translocation and ubiquitinates mitofusin. Proc. Natl. Acad. Sci. U S A *107*, 5018–5023.

iScience, Volume *23*

Supplemental Information

Human Dopaminergic Neurons Lacking PINK1 Exhibit Disrupted Dopamine Metabolism Related to Vitamin B6 Co-Factors

Christine Bus, Laimdota Zizmare, Marita Feldkaemper, Sven Geisler, Maria Zarani, Anna Schaedler, Franziska Klose, Jakob Admard, Craig J. Mageean, Giuseppe Arena, Petra Fallier-Becker, Aslihan Ugun-Klusek, Klaudia K. Maruszczak, Konstantina Kapolou, Benjamin Schmid, Doron Rapaport, Marius Ueffing, Nicolas Casadei, Rejko Krüger, Thomas Gasser, Daniela M. Vogt Weisenhorn, Philipp J. Kahle, Christoph Trautwein, Christian J. Gloeckner, and Julia C. Fitzgerald

Transparent Methods

Ethics statement and data protection

All procedures were in accordance and approved by the ethical board at The University of Tübingen and according to the international standards defined in the declaration of Helsinki. Human samples were obtained with consent and prior ethical approval at The University of Tübingen and the Hertie Institute for Clinical Brain Research Biobank number 146/2009B01. Medical Faculty of the University of Tübingen (https://www.medizin.uni-tuebingen.de/de/medizinische-fakultaet/ethikkommission).

RAW sequences of RNA and peptides will not be made freely available according to EU and German data protection laws to protect the identity of the healthy donor used as an isogenic control in this study. See data availability below.

Generation of human induced pluripotent stem cells (hiPSCs) and *PINK1* knockout

hiPSCs were cultured in self-made E8 media on Vitronectin (VTN-N, Gibco) coated cell culture dishes. iPSCs from a healthy individual that were previously characterized (Reinhardt et al., 2013) were transfected with a TALEN and a homologous construct for *PINK1* exon1 using an Amaxa Nucleofector II with the Stem cell Nucleofection Kit (both from Lonza). The transfected iPSCs were plated on VTN-N –coated 10cm dishes in E8 medium containing 10 µM ROCK inhibitor Y27632. Homologous recombined iPSC colonies were selected with 250 µg/ml G418 (Biochrome) or 10 µgml-1 Blasticidin (InvivoGen) in the second round of TALEN

transfection and re-plated in 12-well plates. Resistant iPSC colonies were characterized by sequencing, qRT-PCR and Western blot to confirm successful homozygous gene knockout. TALENs were designed with the online tool TAL Effector Nucleotide Targeter 2.0 (Cornell University) and generated using a cloning protocol adapted from (Cermak et al., 2011). The following RVD sequences were used for the TALEN monomers: HD HD NI NH NH NG NH NI NH HD NH NH NH NH HD and NI NH HD NG HD HD NH NG HD HD NG HD HD NH HD. Colony-PCR after the first TALEN reaction was conducted with the primers pCR8_F1 (5'-TTGATGCCTGGCAGTTCCCT-3') and pCR8_R1 (5'-CGAACCGAACAGGCTTATGT-3'). After the second Golden Gate reaction the colony-PCR was performed with the primers TAL_F1 (5'-TTGGCGTCGGCAAACAGTGG-3') and TAL_R2 (5'-GGCGACGAGGTGGTCGTTGG-3').

Generation of *PINK1* Q126P hiPSCs and subsequent gene correction

Human fibroblasts were derived from a skin biopsy of a female PD patient with a *PINK1* Q126P mutation in Tübingen of which the family was previously described (Prestel et al., 2008). Human samples were obtained with consent and prior ethical approval at The University of Tübingen and the Hertie Institute for Clinical Brain Research Biobank. The *PINK1* Q126P 15167 hiPSC line was generated using the CoMIP 4in1 method. Reprogramming and characterization (pluripotency, stability of karyotype, and differentiation potential was performed in the iPSC Core Facility of Helmholz Zentrum München. PINK1 Q126P hiPSCs were gene corrected using pCAG-Cas9 vector (Addgene plasmid 84918) and a donor vector carrying a cassette

flanked by a *PINK1* 5'homology arm containing the g.155732C>A and a 3' homology arm. The hiPSCs and the gene corrected line were kindly provided through collaboration with Daniela M. Vogt Weisenhorn and Wolfgang Wurst (Helmholtz Zentrum München, German Research Center for Environmental Health, Institute of Developmental Genetics, Munich-Neuherberg, Germany) as part of a BMBF MitoPD project.

Derivation of NPCs from iPSCs and differentiation into mature, human, mid-brain specific dopaminergic neurons (hDANs)

Mature hDANs were generated from iPSCs via neural progenitor cells (NPC) intermediates using a protocol adapted from (Reinhardt et al., 2013a). The healthy control line (K7.1) has been previously fully characterized and described (Reinhardt et al., 2013a). Two distinct PINK1 KO iPSC clones devoid of PINK1 transcript were used in this study (PINK1 KO1-Δ8.9 and PINK1 KO2-Δ40.7). Briefly, lPSCs were maintained in E8 medium. For the generation of embryoid bodies (EBs), iPSCs were cultured in '50:50 base medium' (one to one mixture of DMEM Hams F12 (#FG4815 Biochrome/Millipore): Neurobasal® medium (#21103-049 Gibco/Thermo Scientific), 1X Penicillin/Streptomycin (Biochrome/Millipore), 1X GlutaMAX supplement Thermo Scientific), 1X B27 supplement (Gibco/Thermo Scientific) and 1X N2 supplement (Gibco/Thermo)) plus the addition of 10µM SB431542 (Sigma, SB), 1µM dorsomorphin, 3µM CHIR99021 (CHIR, Axon) and 0.5µM pumorphamine (PMA, Alexis) on uncoated 6-well cell culture plates. EBs were then transferred to Matrigel (Corning)-coated 6-well plates in NPC maintenance media ('50:50 base medium' plus the addition of 150µM Ascorbic Acid (AA, Sigma), 3µM CHIR, 0.5µM PMA).

After several passages NPCs were cultivated in NPC priming medium (‘50:50 base medium’ plus the addition of 150µM AA and 3µM CHIR99021). Differentiation of confluent NPCs was initiated by cultivation in a patterning medium for seven days (‘50:50 base medium’ plus the addition of 10ng/mL FGF8 (Peprotech), 1µM PMA, 200µM AA, 20ng/mL BDNF (Peprotech). The differentiating neurons were matured in maturation media (’50:50 base medium’ plus the addition of 10ng/mL BDNF, 10ng/mL GDNF (Peprotech), 1ng/mL TGFß-III (Peprotech), 200µM AA, 500 µM dbcAMP (Applichem) and 10µM DAPT (Sigma).

Removal of antioxidant supplements and apoptosis inhibitors

hDANs require N2 and B27 supplements (GIBCO) and ascorbic acid in their culture media. We also routinely use apoptosis inhibitors for splitting and plating NPCs and hDANs, Prior to all experiments, the maturation medium was replaced 24h before the experiment with ‘N2 medium’ (using 50:50 base media without the B27 supplement or ascorbic acid) to reduce excessive amounts of antioxidants in the media that could quench phenotypes. Also, no apoptosis inhibitors such as APOI/ROCK inhibitor were used after the final plating of the hDANs throughout maturation.

Immunofluorescence staining

Mature hDANs were cultivated on Matrigel-coated glass coverslips and fixed with 4% (w/v) paraformaldehyde (PFA, Sigma) in phosphate buffered saline (PBS) for 15 min at room temperature (RT). Permeabilization with ice-cold, neat methanol for 5 min at

-20°C. After washing with 0.01% (v/v) Tween in PBS (PBS-T), the fixed hDANs were blocked with 5% (v/v) normal goat serum in PBS-T for 1h at RT. Afterwards the cells were washed again and incubated overnight at 4°C with the primary antibody in 2.5% (v/v) serum in PBS-T. On the following day the cells were incubated with the secondary fluorescent antibody (#A32721, #A11070, #A21449, #A11010 all from Molecular probes/Thermo Scientific) for 2h at RT in darkness and nuclei stained with DAPI (Sigma). Coverslips were mounted in mounting medium (Dako) on glass slides. Immunofluorescence was imaged using an AxioVert fluorescence microscope (Zeiss). MAP2 (AbCam ab5392) (n=diff5), TH (AbCam ab112) (n=diff5), FOXA2 (Millipore AB4125) (nDiff 3), DAT (Millipore MAB369) (nDiff3). Statistics Figure 1B**:** Blinded IF images were counted manually (IF positive cell as a percent of total cells in a field of view). All values were listed in Graphpad Prism in columns (nDiff=4). The number of % IF positive values from each field of view are as follows; CTRL MAP2 (68), PINK1 KO clones 1 and 2, MAP2 (98), CTRL FOXA2 (31), PINK1 KO clones 1 and 2 FOXA2 (49), CTRL TH (68), PINK1 KO clones 1 and 2, TH (89), CTRL DAT (37) and PINK1 KO clones 1 and 2, DAT (49). Ten outliers were removed by Graphpad Prism (all from CTRL TH). Significance test; All data sets was tested for normal Gaussian distribution using Graphpad Prism (D'Agostino & Pearson test). FOXA2 data was normally distributed and the Unpaired t-test used (ns = not significant). For the remaining non-normally distributed data, the non-parametric Mann Whitney U-test was used. **** = $p<0.0001$. Levene's test of unequal variance was performed in Excel followed by single ANOVA (TH marker CTRL v PINK1 KO p0.0206).

Quantitative Reverse Transcription PCR (qRT-PCR)

RNA was isolated from mature hDANs (and NPCs) using a RNeasy Mini Kit (QIAGEN), including the on-column DNA digestion step. A one-step qRT-PCR was performed on 0.1-1µg RNA (equalized to the same imput amount) with the QuantiTect SYBR Green RT-PCR Kit (QIAGEN) on a LightCycler®480 (Roche). The relative expression levels were calculated with the $2^{-\Delta}$ method, based on a biological reference and housekeeping genes (GAPDH and HMBS) for normalization. Statistics Figure 1C: All ΔΔCt gene of interest/GAPDH were normalised to the CTRL in each case. All values were listed in Graphpad Prism in columns (nDiff=4, except vGlut nDiff = 3). The number of values; CTRL (12), PINK1 KO clones 1 and 2 vGLUT (3), PINK1 KO clones 1 and 2 TH (12), PINK1 KO clones 1 and 2 MAO-A, (11), PINK1 KO clones 1 and 2, MAO-B (10), PINK1 KO clones 1 and 2, DAT (6), PINK1 KO clones 1 and 2, SYP (6), PINK1 KO clones 1 and 2 THP2 (5) and PINK1 KO clones 1 and 2, MAP2 (6). One outlier was removed by Graphpad Prism (from THP2). Significance test; All data sets were tested for normal Gaussian distribution using Graphpad Prism (D'Agostino & Pearson test). TH (**=p0.0063), MAO-A (ns = not significant) and MAO-B (ns = not significant) data were normally distributed and the unpaired T-test used. For the remaining data normality could not be assigned due to low n, the non-parametric Mann Whitney U-test was used. vGlut (**=p0.0022), TPH2 (*** = p<0.0002), MAP2 (**=p0.0043). Statistics Figure 4C and 4D: All ΔΔCt gene of interest/GAPDH were listed in Graphpad Prism in columns. One column was made for both PINK1 KO clones. The data was not normalized to the control in each PINK1 line (except for PINK1 Q456X where there are 3 patients, the ΔΔCt data is normalized to each corresponding gene corrected control line). No outliers were removed by Graphpad Prism. Significance test; assuming normal distribution with

unequal standard deviation, the student's t test with Welch correction was performed. PINK1 exon 1-2 (****=*p*<0.0001 for PINK1 KO v CTRL and PINK1 Q456X v GC CTRL), PNPO (****=*p*<0.0001 for PINK1 v CTRL, **=*p*0.0027 for PINK1 Q456X v GC CTRL), DDC (***=*p*0.0010 for PINK1 Q126P v GC CTRL), TPH1 (**=*p*0.0035 for Q126P v GC CTRL). All t test comparisons were made for all other CTRL and PINK1 lines individually shown for each gene and were not statistically significant. Then all the ΔΔCt values for each gene were listed in two columns in Graphpad Prism (all CTRL/WT v all PINK1 KO/mutation) and each data set for each gene was tested for Gaussian distribution using the D'Agostino & Pearson test. The student's t test with Welch correction; PINK1 (****p<0.0001), DDC (ns=p0.0773), TPH1 (ns=p0.1055), TPH2 (ns=p0.7855), PDXK (ns=p0.8046), DNAJC12 (ns=p0.8663). The non-parametric Mann Whitney U-test; PNPO (*=p0.0192), TH (ns = p0.53). nDiff=3. Levene's variance test was performed in Excel followed by single ANOVA (TH expression GC v Q126P, p0.0000137).

Primer sequences

DNAJC12 (FW:TCACCCAGACAAGCATCCTGA, RV: TTACCTCTGACAACCCAGTGC); **TPH1** (FW: AACCCATGCTTGCAGAGAGT, RV: GCCACAGGACGGATGGAAAA); **TPH2** (FW: GTGGATGTGGCCATGGGTTA, RV: TGGAGAGCTCCCGGAATACA), **PDXK** (FW: GGGATTTGAGATTGACGCGG, RV: GGGACGTACATCGAGCCTTC); **DDC** (FW:GAGCCAGACACGTTTGAGGA, RV: TAGGCGAAGAAGTAGGGGCT); **PNPO** (hFW: AGTCGAAAAGGAAAAGAGCTG; hRV: GGCGGGAGTGGAAGTAG), (msFW:CTGAACCGTCAGGTGCGTGTGGAAGGC,

msRV:AAGGTGCAAGTCTCTCATACACCCAGTCT); **TH** (FW: TGTCTGAGGAGCCTGAGATTCG; RV: GCTTGTCCTTGGCGTCACTG); **PINK1** (exon 1 FW: GGGTCGAGCGCTGCTGCTGCGCTT; exon 2 FW: TCCGGGGGCCCCTGCCTTCC; exon 4 RV: TTGCTTGGGACCTCTCTTGG); **vGLUT1** (FW: GAGTGGCAGTACGTGTTCCT; RV: TCCATTTCGCTGTCGTCACT); **MAO-A** (FW: GCCCTGTGGTTCTTGTGGTATGT; RV: TGCTCCTCACACCAGTTCTTCTC); **MAO-B** (FW: ACTCGTGTGCCTTTGGGTTCAG; RV: TGCTCCTCACACCAGTTCTTCTC); **DAT** (FW: CAAAAGCTGCTTTCCATGGCACACT; RV: CGGCTCCCACCGAGCATTACACT); **SYP** (FW: CAGGGTGGGGCTTAGAATGG; RV: GTGTGTGTGGTGGGGTGCTT); **MAP2** (FW: CCGTGTGGACCATGGGGCTG; RV: GTCGTCGGGGTGATGCCACG); **CP** (FW:CTTAACAGCACCTGGAAGTG; RV:TTGTGAAGGAGGCATCTGTG); **GCLC** (FW:TGAGCTGGGAGGAAACCAAG; RV: AACATGTATTCCACCTCATCGC); **STEAP3** (FW:TTCAGCTTCGTTCAGTCCTC, RV:AGGCAGGTAGAACTTGTAGC); **SLC7A11** (FW:CTTTCAAGGTGCCACTGTTC, RV: GATAATACGCAGGGACTCCA); **Mitoferrin2** (FW: CCATCGACTGCGTCAAGACC; RV: CAAAATAAAGGGCGTGGGCA).

Autophagy and mitophagy induction

Autophagic flux was induced in mature hDANs using Valinomycin (Val, 1µM, 24h) or NH_4CL (20mM, 4h) and Leupeptin (Leu, 200µM, 4h) nDiff=3. Mitophagy was induced in hDANs using; 10µM CCCP for 2h, 4h, 6h, (6h+ 10µM MG132) and 24h or 1µM Valinomycin for 24h nDiff=3.

SDS-PAGE and Western blotting

All cell lysates were prepared in RIPA buffer (Sodium chloride 150mM, Tris-HCL 50mM, Sodium dodecyl sulfate 0.10% (w/v), Sodium deoxycholate 0.50% (w/v), Triton-X-100 1% (v/v)) containing 1X concentration of phosphatase inhibitor cocktail (Complete, Roche) and phosphatase inhibitor cocktail (PhosSTOP, Roche). Briefly, the lysis buffer was added directly to washed cells in dishes or washed cell pellets and kept at 4 °C. Needles were used to further homogenize the lysates (9 passes 20G, 9 passes 27G) and incubated 30 minutes on ice. Insoluble nuclear material was removed after centrifugation at 14,000 rpm for 10 minutes. Proteins were electrophoresed on self-made acrylamide gels or pre-cast Bis-Tris gels (Thermo Scientific) and transferred to nitrocellulose membranes using the iBlot device (Thermo Scientific), with the exception of very large target proteins or heavily lipidated proteins, in which case wet blotting with PVDF membranes was used. Total protein stain Ponceau (Applichem) was used to assess transfer and loading and the PageRuler plus pre-stained protein ladder (Thermo Scientific) for kDa range. Antibodies against PINK1 (Novus), Mitofusin1 (MFN1, AbCam), TOM70 (Santa Cruz), OPA1 (BD Biosciences), Parkin (Cell Signalling Technology), *m*Aconitase (BD Biosciences), β-Actin (Sigma Aldrich), GAPDH (Invitrogen, Thermo Scientific) Tom20 (Santa Cruz Biotechnology), LC3I/II (Novus), PGC1α (AbCam), MIRO-1 (Sigma Aldrich), OPA1 (Novus Biologicals), TH (Millipore), Vinculin (Sigma-Aldrich), MAO-A (In-house produced monoclonal antibody from Ellen Billett, Nottingham Trent University, UK), NECAB2 (a kind gift from Axel Methner, Johannes Gutenberg University Mainz / Germany) and Mitobiogenesis antibody (containing SDHA, GAPDH and MTCO1, AbCam) were used. Secondary antibodies were purchased

from GE Healthcare (HRP-conjugated) and from LiCOR (α-rabbit and mouse Alexa Fluophor™680, α-rabbit and mouse Alexa Fluophor™800). Fluorescence detection and analysis were performed using a LI-CORE blot scanner and Image Studio™ Lite software. Densitometry from Western blot was performed using the Image J 1.41o software (Wayne Rasband; National Institutes of Health, USA). Representative Western blots are shown. For calculating mitochondrial turnover statistics Figure S2D/E. Densitometry data was normalized and no outliers removed. Assuming normal distribution, the student's t test was assigned and ns=not significant, *=p<0.05. nDiff=3. Levenes test of variance was also performed in Microsoft Excel followed by single ANOVA (Untreated mitobiogenesis, p>0.050, valinomycine treated mitobiogenesis p0.030).

Complex I Dipstick Assay

Active Complex I was pulled down from mature hDAN homogenates using the Complex I Dipstick Assay from AbCam (ab109720) according to the manufacturer's instructions. The dipsticks were immediately scanned and the band densitometry quantified using the Image J 1.41o software (Wayne Rasband; National Institutes of Health, USA). Statistics Figure 1F and G: All densitometries derived from scanning the dipstick (nDiff=3) were listed in Graphpad Prism in columns. There were three values for each data set and therefore the test for Gaussian distribution could not be performed. Assuming non-normality, the Mann Whitney U-test was performed (Figure 1G, *=p0.023, Figure 1F, ns =not significant). Assuming normality, the t test was performed (Figure 1F, *=<0.05). 1-way ANOVA with the Kruskal Wallis test was

performed assuming a possible mixture of distributions (Figure 1F, p0.036 and Figure 1G, p0.0003).

Transmission Electron Microscopy

Mature hDANs were seeded on Matrigel (Corning) coated glass coverslips and cultivated for three days prior to treatment with N2 medium with and without 1 µM Valinomycin for 24 hours. After washing and fixation with 2.5% glutaraldehyde (Science Services, Munich, Germany) in cacodylate buffer (pH7.4; Merck-Millipore, Darmstadt, Germany) overnight at 4°C, cells were washed with cacodylate buffer, post fixed in 1% osmiumtetroxide, dehydrated and embedded in epoxide resin (Araldite, Serva, Heidelberg, Germany) as described previously (Wolburg-Buchholz et al., 2009). Ultrathin sections were performed using a Reichert Ultracut ultramicrotome (Leica, Bensheim, Germany) and were analyzed in an EM 10 electron microscope (Zeiss, Oberkochen, Germany). Images were taken by a digital camera (Tröndle, Germany). Qualitative data, representative images are shown, nDiff=3. The high quality images are available on request.

Mitochondrial Morphology (BacMam Mitogreen)

NPCs and mature hDANs were plated on Matrigel covered glass coverslips, treated with CellLight™ Mitochondria-GFP, BacMam 2.0 (Invitrogen) according to manufacturer's instructions for 24 hours in N2 medium. Mitochondria of transfected neurons were imaged using an LSM-510 confocal microscope (Zeiss). Z-stack images were analysed with ImageJ (Fiji, Rasband, W.S., ImageJ, U. S. National

Institutes of Health, Bethesda, Maryland, USA). Statistics Figure 2B: Blinded Z stack IF images were analyzed using ImageJ software (Rasband, W.S., ImageJ, U. S. National Institutes of Health, Bethesda, Maryland, USA, https://imagej.nih.gov/ij/). All values for mitochondrial area were listed in Excel per cell for each field of view (nDiff=4). The data was normalised to the isogenic control for hDANs and for NPCs. No outliers were removed and distribution analysis (D'Agostino & Pearson test) was not possible because nDiff=4. Significance test; Non-normal distribution was assumed and the non-parametric Mann Whitney U-test was used. Ns = not significant, *=$p<0.05$, **=$p<0.005$. Statistics Figure S2A: Blinded IF images were analyzed using particle analysis with IMARIS software and ImageJ (Fiji) across z stacks.

Mathematical calculations for mitochondrial circularity, aspect ratio (length) and form factor (degree of branching) was performed using ImageJ (Fiji), as follows; briefly, images were converted to 8-bit greyscale, → 'despeckle', → 'convolve', → 'subtract background', → 'create binary' and 'adjust threshold' (the threshold must remain the same for all images). 'Set measurements', check Area, Perimeter and Fit ellipse. 'Analyze particles'; Smallest particle set to 1 pixel, → 'Show outlines'. Data for each mitochondria is listed and raw data copied in Excel. Mean values for each measurement per image is used. Form factor (or degree of branching is the perimeter squared, divided by (4π x area). The data was set in columns in Graphpad Prism in columns (nDiff=4). No outliers were removed and distribution analysis (D'Agostino & Pearson test) was not possible because n=Diff4. Significance test; Non-normal distribution was assumed and the non-parametric Mann Whitney U-test was used. ns = not significant.

Calcium imaging

Mature hDANs were seeded on Matrigel-coated glass coverslips. Fluo-4 Direct Calcium Reagent (Invitrogen) was added to the cells and incubated for one hour at 37°C and 5% CO2. After washing the cells with growth medium, the 24mm coverslips were transferred into self-made imaging chambers and Fluo-4 reagent diluted in growth medium was added. 3 mM EGTA was added per well 10 minutes prior to imaging. Neurons were imaged on a LSM 510 Confocal microscope (Zeiss) taking a picture every 0.5 sec for 25 minutes. A baseline was recorded for two minutes and then 2 µM Thapsigargin was added. The data analysis was performed using ImageJ (Rasband, W.S., ImageJ, U. S. National Institutes of Health, Bethesda, Maryland, USA, https://imagej.nih.gov/ij/). The corrected total cell fluorescence per cell was determined for 10 neurons per experiment and plotted over time to evaluate the calcium signal. To account for variability in Fluo4 signal between imaging sessions we always normalized the Fluo4 signal to the baseline (average Fluo4 signal before the addition of Thapsigargin). Only PINK1 KO clone 1 passed the D'Agostino & Pearson normality test. Therefore, ordinary two-way ANOVA was used for statistical analysis. The data was statically significant comparing genotype across time (****=p<0.0001*).*

Flow cytometry experiments

Mature hDANs were carefully washed in PBS and then treated with Accumax (PAN Biotech) to remove them from the monolayer, quenched in PBS and centrifuged at

300 g for 5 minutes and then incubated in dye, buffer only or dye plus a control. For mitochondrial membrane potential, 200 nM Tetramethylrhodamine, Ethyl Ester, Perchlorate (TMRE, from Thermo Scientific) in PBS or TMRE plus Carbonyl cyanide-p-trifluoromethoxyphenylhydrazone (CCCP, Sigma Aldrich) 10 µM was used. Cells were measured using a MACSQuant® automated flow cytometer (Mitenyi Biotechnology) according to their mean average fluorescence signal. All mean average fluorescence values were divided by the background fluorescence in the same channel in the same unstained cells to account for auto-fluorescence. Statistics Figure 2D (left panel): Assuming normal distribution, the t test was performed. **= p<0.0026. ns=not significant. nDiff=3.

Live Cell Kinetic Measurement of Mitochondrial Membrane Potential

Cells were seeded in Ibidi® dishes and the media exchanged for HBSS containing 200 nM TMRE stain (Thermo Scientific) for 15 minutes at 37°C with CO_2. The TMRE was removed and replaced with 360 µl Hanks buffer. The cells were imaged using a Zeiss Inverted Confocal microscope at Excitation HeNe1, 543 nm and Emission LP 560 nm and brightfield for 20 × 4s cycles. Followed by the addition of 360 µL (0.25 mg/ml Oligomycin), measured for 20 × 4s cycles, 180 µL (10 µM Rotenone), measured for 20 × 4s cycles and 100 µL (10 µM FCCP) and measured for 20-40 × 4s cycles. Using ImageJ (Rasband, W.S., ImageJ, U. S. National Institutes of Health, Bethesda, Maryland, USA, https://imagej.nih.gov/ij/), each frame was analysed for TMRE fluorescence intensity, mean fluorescence and total area. The corrected total cell fluorescence (CTCF) over time was calculated using the formula: *CTCF = fluorescence intensity - (cell area × mean background fluorescence).* Statistics:

Figure 2D (right panel): $p<0.0001$, 2-way ANOVA (CTCF across genotype and time) for corrected total cell fluorescence from live imaging mean CTRL v PINK1 KO1 and KO2 hDANs. nDiff=3.

ATP Assay

ATP was measured using the ViaLight™ Cell Proliferation BioAssay Kit according to the manufacturer's instructions (Lonza) and normalized to the total protein content in each well. Luminescence was detected using SpectraMax L plate reader (Molecular Devices). Technical replicates =3 in each assay and *n*Diff=4. The mean data from each independent experiment comparing PINK1 KO1 and PINK1 KO2 to control was tested using the Mann Whitney U Test and the differences were not significant.

Mitochondrial turnover using MitoTimer™plasmid

Mitotimer is a fluorescent reporter suitable for the investigation of mitochondrial turnover. Based on oxidation state, the fluorescent protein (dsRed mutant) targeted to the mitochondria shifts its emission spectra from green to red as the protein matures (Hernandez et al., 2013). Approximately 100,000 hDANs were seeded per 24-well well on coated coverslips in maturation medium. Mature hDANs were transfected with pMitoTimer from Zhen Yan (Addgene plasmid # 52659;http://n2t.net/addgene:52659 ; RRID:Addgene_52659) using Fugene HD transfection reagent (Promega) according to manufacturer's instructions. Transfection efficiency ranged from 5-10% of total hDANs in the field of view. The hDANs were fixed 48 h post-transfection with 4% (v/v) PFA in PBS for 10 min RT.

Transfected hDANs were imaged for both green (Ex/Em, 488nm/518nm) and red channels (Ex/Em, 543nm/572nm) using a LSM 510 confocal (Zeiss). Z-Stack pictures were analyzed using IMARIS 8.3.1 (Bitplane). Statistics Figure S2B: Data were normalized to the isogenic control in each case and one outlier was removed. The student's t test was performed. **=*p*0.0043 and *=*p*0.0222. nDiff=3.

Tom22 flow cytometry

The Tom22 content in hDANs was measured using the Inside Stain Kit (Miltenyi Biotec). hDANs cultured on Matrigel (Corning) were pre-treated with N2 buffer 24 h prior to the experiment. Cells were harvested, suspended in PBS containing 0.5% BSA and 2mM EDTA and fixed using the same amount of Inside Fix solution (Miltenyi Biotec). After 20 min of incubation at RT neurons were centrifuged for 5 min at 300 g. The supernatant was removed and after a washing step the cell pellets were suspended in Inside Perm with Tom22-GFP antibody (diluted 1:10) or a mouse IgG control. The samples were incubated for 10 min at RT in darkness. To stop the staining samples were diluted with Inside Perm and centrifuged for 5 min at 300g. The supernatant was discarded, and the pellets were suspended in PBS containing 0.5% BSA and 2mM EDTA. Tom22-GFP fluorescence was measured using a MACSQuant Analyzer flow cytometer. IgG background control fluorescence was subtracted from the obtained Tom22-GFP fluorescence for analysis. Statistics Figure S2C: Data was normalised and no outliers removed. Assuming normal distribution, the t test was assigned and ns=not significant, *=p<0.05. nDiff=3.

Respiratory analyses

For the basic mitochondrial stress test, oxygen consumption rates (OCR) and extracellular acidification rates (ECAR) were measured in mature hDANs using a Seahorse™ XF96 Extracellular Flux Analyzer. Cells were seeded in Matrigel coated Seahorse cell plates 24-48h prior to the experiment. During the experiment, OCR/ECAR is measured before any injection of mitochondrial toxins. This is referred to as the basal state (The base media contains glucose, pyruvate and glutamine). The wells were then injected sequentially with 1µM Oligomycin (Santa Cruz Biotechnology) 'minimal respiration', 5µM FCCP (Santa Cruz Biotechnology) 'maximal respiration', and 1µM Antimycin A (Santa Cruz Biotechnology)/ 1µM Rotenone (Sigma Aldrich) 'mitochondrial inhibition'. Following the respiratory analysis, the media is removed and the cells are fixed with 4% (w/v) PFA containing Hoechst stain (1:10,000) for 5 minutes before washing and imaging for automated cell counting (BD Pathway 855, BD Bioscience). Normalisation was performed by counting the number of cells per well of the plate using a high content imager from BD Biosciences (BD Pathway 855). The cell counting was performed by the Pathway 855 using an in house written macro and the dimensions of the wells (0.358 cm^2). Statistics Figure 3A: For each condition per experiment at least 6 wells are used for technical reproducibility. The mean average OCR/ECAR values for each independent experiment are plotted and the error bars show standard deviation (nDiff=4). The t test was used. ns=not significant. ***=*p*0.0004, *=*p*0.0158.

Crude mitochondrial enrichment

Crude mitochondrial enrichment: Fresh cell pellets on ice were suspended in mitochondrial isolation buffer (10 mM HEPES pH 7.4, 50 mM sucrose, 0.4 M

mannitol, 10 mM KCl, 1 mM EGTA, phosphatase and protease inhibitors (Roche)) and passed through 20G, 27G and 30G needles 8 times to disrupt cells. Note: because of the size of hDANs and large amounts of axonal material, we found needle homogenization in the absence of detergents to yield the best mitochondrial enrichments. Fractionation was then achieved by several centrifugation steps. First, samples were centrifuged for 5 min at 1000 xg at 4°C and the supernatant was saved. The pellet was suspended in 500 µL mitochondrial isolation buffer and passed through a 30G needle 8 times before centrifuging 5 min at 900 g at 4°C. The second supernatant was pooled with the first and centrifuged for 15 min at 9000 g at 4°C. The obtained pellet comprises the mitochondrial fraction.

Complex I and citrate synthase activity

Complex I activity was measured in crude mitochondrial enrichments from hDANs previously described in (Fitzgerald et al., 2017) and based on the method of (Hargreaves et al., 2007). Following isolation of crude mitochondria, a total protein content >0.7mg/mL is required to have enough active mitochondria for each sample replicate in each independent assay which needs to be duplicated for the addition of rotenone as a negative control. Citrate synthase activity was measured on the same sample sets and independent differentiations according to (Hargreaves et al., 2007). The citrate synthase activity is used to normalise complex I activity (to account for mitochondrial mass). To later measure the whether citrate synthase activity alone was significantly altered between the groups citrate synthase activity was measured again, this time measuring the exact input protein per well. Citrate synthase is then expressed as a change in absorbance per min per µg protein. The SpectraMax® M

microplate reader (Molecular Devices) was used. Statistics Figure 3B/C. Outlier tests were performed in Graphpad Prism and no outliers were removed. Distribution analysis (D'Agostino & Pearson test) was not possible. The student's t test was used. ns=not significant. nDiff=6 (CI) and nDiff=3 (CS).

NAD^+ and NADH measurement

Mature hDANs were cultivated in N2 medium 24 h before the experiment. Whole cell NAD^+ and NADH-levels were determined using the NAD/NADH Assay Kit (Fluorometric) from Abcam according to manufacturer's instructions. NADH reaction mixture was incubated for 1 hour and fluorescence (Ex/ Em = 540/ 590 nm) was measured using a SpectraMax® M microplate reader (Molecular Devices). Statistics Figure 3D. Outlier tests were performed in Graphpad Prism and no outliers were removed. Distribution analysis (D'Agostino & Pearson test) was not possible. The student's t test was used. *=*p*0.0222, ***=*p*0.0004. nDiff=5. NADH levels were slightly increased in PINK1 KO hDANs but not significantly (data not shown).

αKetoglutarate dehydrogenase activity assay

Mature hDANs were pretreated with N2 medium for 24 hours prior to the experiment. Mitochondria were extracted using the protocol for crude mitochondrial enrichment. Measurement of alpha-ketoglutarate dehydrogenase activity in mitochondria was performed using the alpha-Ketoglutarate Dehydrogenase Activity Colormetric Assay Kit (Sigma-Aldrich) according to manufacturer's instructions. Absorbance (A_{450}) of the samples was measured in kinetic mode every minute for 1h at 37°C on a

SpectraMax®M microplate reader (Molecular Devices). Statistics Figure 3E. Outlier tests were performed in Graphpad Prism and no outliers were removed. The student's t test was used. ns=not significant. nDiff=3.

Mitochondrial Aconitase activity

*m*Aconitase activity was measured in mature hDANs using a protocol from (Pierik et al., 2009). Briefly, hDANs were washed with PBS and the cell pellet suspended in 200µl TNEGT buffer + protease inhibitors. Then dounced on ice using a loose then a tight fitting glass pestle. The homogenates were centrifuge at high and low speeds with rigorous vortexing inbetween (Pierik et al., 2009). The resulting supernatant is then centrifuged for 10 minutes at 13,000g at 4°C. The resulting supernatant is then protein estimated before being used in the assay. Set up of the assay plate: Per well: 95µl trietholamine buffer, 10µl cis aconititic acid (20mM), 20µl Isocitrate dehydrogenase (4U/ml), 10µl NADP (0.1M) and 40µg hDAN supernatant containing the enzyme. Blank = no cis aconitic acid, no isocitrate dehydrogenase. Read absorbance at 340nm, every 30s for 10 mins. We used a SpectraMax® M microplate reader (Molecular Devices). Statistics Figure 3F: Activity rates are normalised to the healthy control. No outliers were removed. The t test was used. *=p<0.05. ns= not significant. nDiff=3, Hela n=3.

Nuclear magnetic resonance (NMR) based metabolomics

hDAN metabolite extraction: hDAN pellets were collected, washed with PBS buffer and quenched in 400 µL ice-cooled ultrapure methanol. The cell suspensions were

then transferred to 2 mL glass tubes (Covaris Adaptive Focused Acoustics AFA^{TM}) and added to 1000 µL of *tert*-butyl methyl ether (MTBE), well mixed and submitted to AFA ultrasound metabolite extraction protocol (*Covaris* E220 Evolution Woburn, USA). Ultrasonication programme setup: two treatment cycles, 1st: 30s, Peak Power 125.0, Duty Factor 32.0, Cycles/Burst 400, Avg. Power 40.0. 2nd: 30s, Peak Power 100.0, Duty Factor 30.0, Cycles/Burst 800, Avg. Power 30.0. The ultrasonication was carried out in cooled water bath, temperature range 5.0 to 15.0 °C. Each cycle was repeated 5 times per sample, total run time per sample was 5 min. Following extraction, 400 µL of ultrapure water were added to the extraction mixture, thoroughly vortexed and centrifuged at 12'000 g for 10 min for optimum phase separation. After centrifugation, the two phases were manually separated: the top lipid (MTBE) layer was transferred to 2 mL HPLC (High-Performance Liquid Chromatography) glass vials; the bottom aqueous phase was moved to 1.5 mL *Eppendorf* cups. Those were then submitted to another centrifugation step at 30'000 g for 10 min to separate any undissolved cell culture residue. Following centrifugation, the aqueous supernatant was transferred to fresh *Eppendorf* cups and evaporated to dryness by a vacuum concentrator (Thermo Fisher Speedvac XYA). **NMR sample preparation**: Dried metabolite pellets were re-suspended in 45 µL 1M K_2HPO_4 (phosphate) buffer (pH = 7.4, containing NaN_3 and 1mM internal NMR standard TSP), thoroughly mixed and then centrifuged for 5 min with 30'000 g. 40 µL of the supernatant was filled into 1.7mm NMR tubes that are compatible to Bruker auto-sampler. **NMR spectra acquisition**: Metabolomics data were acquired on a 14.10 Tesla (600 MHz) ultra-shielded NMR spectrometer (Avance III HD, Bruker BioSpin, Karlsruhe, Germany) equipped with a 1.7 mm room temperature triple resonance probe (^{1}H, ^{13}C, ^{31}P). Spectra were recorded at 298 K. A quick

simple ZG experiment was performed followed by a 1D NOESY (Nuclear Overhauser Effect Spectroscopy) aiming to optimise offset and shim parameters. A CPMG (Carr-Purcell-Meiboom-Gill) experiment was used to suppress residual background signals from remaining macromolecules in the solution and water (time domain = 64k points, sweep width = 20 ppm, 2024 scans, 4 hours per sample). **NMR data analysis and statistics:** The recorded free induction decays (FIDs) were Fourier-transformed (FT) and NMR spectra were processed by Bruker TopSpin 3.6.1 software (automated baseline correction, phase correction and spectra offset adjustment). Metabolite annotation and quantification was done with ChenomX NMR Suite 8.5 software containing the additional HMDB (Human Metabolome Data Base) library. The MetaboAnalyst 4.0 web server (R-based online analysis tool, www.metaboanalyst.ca) was used for statistics. To make samples and features comparable, all data was normalised by a reference sample (probabilistic quotient normalisation (PQN) to account for dilution effects and scaled by the Pareto scaling method (mean-centred and divided by the square root of the standard deviation of each variable). Statistics Figure 3H, initially one-way ANOVA (analysis of variance) with $p < 0.05$. Then the student's t test was applied to compare metabolite concentrations between the control and each PINK1 KO clone. We used Principal component analysis (PCA), sparse partial least squares discriminant analysis (sPLS-DA), pattern hunter and heatmap tools for data visualisation. Independent biological experiments n=4 and nDiff=2.

Mitochondrial import Assay

Radiolabelled proteins were synthesized in rabbit reticulocyte lysate in the presence of ^{35}S-methionine after in vitro transcription by SP6 polymerase from pGEM4 vector (Promega). Radiolabelled precursor proteins were incubated at either 30°C (pSu9-DHFR) or 4°C (Fis1) in import buffer (250 mM sucrose, 0.25 mg/ml BSA, 80 mM KC1, 5 mM $MgCl_2$, 10 mM MOPS-KOH, 2 mM NADH, 4 mM ATP, pH 7.2) with crude mitochondria isolated from mature hDANs. Non-imported pSu9-DHFR molecules were removed by treatment with proteinase K (PK, 50 µg/ml) for 30 min on ice and then PK was inhibited with 5 mM Phenylmethanesulfonyl fluoride. Membrane integration of Fis1 molecules was confirmed by resistance to alkaline extraction (incubation on ice for 30 min with 0.1 M Na_2CO_3 followed by centrifugation to obtain membrane-embedded proteins in the pellet). Finally, samples were heated at 95°C for 5 min before their analysis by SDS-PAGE and autoradiography. Representative images of four independent experiments are shown. Quantification of band densitometry was performed with the AIDA software (Raytest). No outliers were removed. Error bars show standard deviation between independent experiments. Test for normality were not possible. The student's t test was performed comparing control to PINK1 KO hDANs at multiple time points. ns=not significant. nDiff=4.

Cytosolic ROS

Medium was changed to N2 medium 24 h prior to the experiment. On the following day mature hDANs were incubated with N2 medium or N2 medium containing 10µM Rotenone, 1mM Buthionine sulphoximine (BSO) or 50µM Mn-Tbap (a mitochondrial superoxide dismutase 2 mimic) (for 4h before measurement. 100µM dihydroethidium (DiHET) (Santa Cruz Biotechnology) was added to all wells and emission was

measured at 610nm emission (535nm excitation) (chromatin-bound, oxidized DiHET) was measured every 30 secs for 30 min on a SpectraMax® M microplate reader (Molecular Devices). No outliers were removed. Error bars show standard deviation between independent experiments. Tests for normality were not possible. The student's t test was performed and the data showed no statistically significant differences between control and PINK1 KO hDANs. nDiff=3.

Glutathione assay

Neurons on a 96-well plate were treated with different treatment conditions (untreated N2 medium only, 10µM Rotenone, 1mM BSO, and 10µM Rotenone plus 1mM BSO) in N2 medium 24 h prior to the experiment. Cells were briefly washed with HBSS (Gibco) and incubated with 100µL HBSS containing 50µM Monochlorobimane (Sigma) for 40 minutes @37°C, 5% CO2. Blanks were treated the same way but did not contain cells. After washing with HBSS, cells were imaged with a SpectraMax® M microplate reader (Molecular Devices) (Ex 390nm/Em 478nm) to detect the fluorescent adduct of Monochlorobimane and reduced Glutathione (GSH). Background fluorescence obtained from blanks was subtracted for analysis. No outliers were removed. Error bars show standard deviation between independent experiments. Tests for normality were not possible. The t test was performed and the data showed no statistically significant differences between control and PINK1 KO hDANs. nDiff=3.

RNA sequencing

Approximately 5 million hDANs were lysed in 350ml RTL buffer and homogenized using QIAshredder® homogenizer (Qiagen). RNA isolation was performed using RNeasy Mini Kit (Qiagen). RNA was eluted in 30µl RNase-free water. RNA quality was assessed with an Agilent 2100 Bioanalyzer and the Agilent RNA 6000 Nano kit (Agilent). Samples with very high RNA integrity number (RIN > 9) were selected for library construction. For polyA enrichment, a total of 200ng of total RNA was subjected to polyA enrichment and cDNA libraries were constructed using the resulting mRNA and the Illumina TruSeq Stranded mRNA kit (Illumina). Libraries were sequenced as single reads (65 bp read length) on a HighSeq 2500 (Illumina) with a depth of >22 million reads each. Library preparation and sequencing procedures were performed by the same individual and a design aimed to minimize technical batch effects was chosen. Read quality of raw RNA-seq data in FASTQ files was assessed using QoRTs (v1.2.37) to identify sequencing cycles with low average quality, adaptor contamination, or repetitive sequences from PCR amplification. Reads were aligned using STAR (v2.5.3a) allowing gapped alignments to account for splicing to the Ensembl Homo sapiens GRCh37 reference genome. Alignment quality was analyzed using ngs-bits (v0.1) and visually inspected with the Integrative Genome Viewer (v2.4.19). Normalized read counts for all genes were obtained using subread (v1.5.1) and edgeR (v3.24.3). Transcripts covered with less than 1 count-per-million in at least 5 out of 6 samples were excluded from the analysis leaving >13,000 genes for determining differential expression in each of the pair-wise comparisons between experimental groups. For statistics, we used the ederR statistical framework for the calculations (https://bioconductor.org/packages/release/bioc/html/edgeR.html). In short, the methods models read counts per gene using the negative binomial distribution

(capturing the abundance and variability between replicates). Variability is estimated for each gene and on a global scale. After establishing these models, using a generalized linear model (GLM) coefficients are fitted and each gene is tested individually using quasi-likelihood F-test to yield a significance value (*p* value). **Statistics**: For sample size *n*, we used minimum 3 replicates per group. This experiment is following a 2x2 design with 2 samples (nDiff=2) in Valinomycin treatment groups and nDiff=1 sample in control groups for each genotype. **Pathway Analysis**: The heatmap shows the top significant genes (<0.03 *p*-value) in contrast to untreated PINK1 KO vs. untreated isogenic control. Colored squares show the gene expression as per-row normalized (scaled and centered, i.e. mean=0, standard deviation=1) cpm (counts per million as a measure for gene expression strength) values - not log FC values. CPM data were refined by log2 fold change values (logFC) of PINK1 KO hDANs compared to control hDANs for Ingenuity Pathways Analysis (IPA, QIAGEN). First, twenty genes with the highest and lowest log2 fold change were listed. The gene ontology pathway analysis GOrilla was used to generate *p* values and maps of affected processes according to GO terms.

RNA extraction from PINK1 KO mice brain and PINK1 Q456X PD patient hDANs for *PNPO* expression analysis

RNA was prepared from the striatum of three healthy control mice and three PINK1 knockout mice (homogenized using QIAshredder® homogenizer (Qiagen). RNA isolation was performed using RNeasy Mini Kit (Qiagen)) and kindly provided through collaboration with Daniela Vogt-Weisenhorn and Wolfgang Wurst (Helmholtz

Zentrum München, German Research Center for Environmental Health, Institute of Developmental Genetics, Munich-Neuherberg, Germany).

Human iPSC-derived hDANs from three distinct PD patients carrying the PINK1 Q456X mutation and their corresponding gene-corrected isogenic controls were collected at day 30 of differentiation and subjected to RNA extraction by using the RNeasy mini kit (QIAGEN). Briefly, cells were washed twice in PBS and immediately lysed in RTL buffer supplemented with beta-mercaptoethanol. Lysate homogenization was obtained by using the QIAshredder system (QIAGEN), followed by on-column DNase digestion to remove DNA contamination. RNA was finally eluted in nuclease-free water and purity assessed by Nanodrop (A260/A280 and A260/A230 ratios). The cell models were kindly provided by Christine Klein and Philipp Seibler (University of Lubeck, Germany). Their corresponding gene-corrected controls were generated by Jens Schwamborn and Javier Jarazo (University of Luxembourg, Luxembourg).

Proteomics: Quantitative Hyper Reaction Monitoring (HRM)-based mass spectrometry

For lysis, mitochondrial pellets were suspended in 100 µl 6M urea, 100 mM Ammonium bicarbonate pH 8.0 and incubated for 30 min at 4°C. After clearance, the concertation of each lysate was determined by Bradford and 50µg protein per biological replicate were precipitated by methanol chloroform precipitation and processed as described previously (Gloeckner et al., 2009). Briefly, dried protein precipitates were re-dissolved in 30mM Ammonium bicarbonate pH8.0 supplemented with 0.2% RapiGestTM (Waters) surfactant and reduced/ alkylated by

DTT/ Idoacetamide prior to over-night proteolysis with trypsin (Promega). Proteolysis was followed by hydrolysis of the surfactant by TFA according to the manufacturer's protocol. Prior to MS analysis, samples were pre-cleaned with StageTips. For the final dataset two biological replicates (individual differentiations) have been analyzed in three technical replicates. For the generation of the assay library, three DDA runs per condition and biological replicate were acquired. Vacuum-dried samples were re-dissolved in 0.5% TFA and mixed with 2 µl iRT standard peptide mix (Biognosis). Extracted peptides were subsequently subjected to LC-MS/MS-analysis by a 180 min standard method: Tryptic peptide mixtures were injected automatically and loaded at a flow rate of 30 µl/min in 0.1% trifluoroacetic acid in high performance liquid chromatography (HPLC)-grade water onto a nano trap column (300 µm inner diameter × 5 mm precolumn, packed with Acclaim PepMap100 C18, 5 µm, 100 Å; Thermo Scientific). After 3 min, peptides were eluted and separated on the analytical column (75 µm inner diameter × 25 cm, Acclaim PepMap RSLC C18, 2 µm, 100 Å; Thermo Scientific) by a linear gradient from 2% to 30% of buffer B (80% acetonitrile and 0.08% formic acid in HPLC-grade water) in buffer A (2% acetonitrile and 0.1% formic acid in HPLC-grade water) at a flow rate of 300 nl/min over 147 min. Remaining peptides were eluted by a short gradient from 33% or 30% to 95% buffer B in 5 or 10 min. Eluting peptides were analysed on an Q-Exactive Plus mass spectrometer (Thermo Fisher). The HRM acquisition method was adapted from (Bruderer et al., 2015). To improve the quantification performance, 15 instead of the 19 variable windows have been used covering an MS rage from M/Z 457 to M/Z 914 (457-483, 481-506, 504-531, 529-554, 552-576, 574-600, 598-624, 622-650, 648-676, 674-704, 702-735, 733-771, 769-810, 808-856, 854-914). Each HRM sequence was preceded by a full-scan. MS1 and MS2 spectra were acquired in the profile

mode. MS2 spectra were acquired with a stepped collision energy (10% at 25%). DDA MS2 spectra for the assay library creation were acquired with a TOP10 method and in the centroided mode with a fixed collision energy of 25%.

HRM-workflow and statistical analysis

Assay library. The assay library was created with the trans-proteomic-pipeline (TPP v5.1) following published protocols (Schubert et al., 2015). The Thermo RAW files were converted into the mzXML format using MSConvert (Proteowizard v3.0.10765) with the TPP compatibility switch set. The files were filtered for the 150 most intense peaks to reduce the size of the datasets. Briefly, results from four search engines (Mascot [v.2.5.1], Comet [v.2017.01 rev. 1], Myrimatch [v.2.2.10165] and X!Tandem [v.2013.06.15.1]) with trypsin as enzyme, a peptide tolerance of 20 ppm and 3-Methoxythyramine as fixed modification. Individual searches were performed against the human subset of the Swissprot database (release 2016_05, 20201 entries). The masses of the iRT standard (Escher et al., 2012) and decoys (reversed sequences) were added. The assay library was generated by the published TPP workflow. Remaining decoy sequences were manually removed and protein names were replaced by the Uniprot identifiers and the final library was processed and converted into the PQP format by OpenMS (v. 2.4.0). The final assay library contained shuffled decoy sequences in the same amount as the targets. **OpenSWATH workflow.** The openSWATH analysis was performed as previously described (Rost et al., 2017). Briefly, prior to quantification the HRM RAW files were converted into the mzML format at 64bit precision. The files were processed by the OpenSWATHWorkflow (OpenMS v. 2.4.0; Revision: 103a38b) and subsequently analyzed by pyProphet

(v2.01) performing local, experiment-wide and global-statistics for filtering. Files exported to the legacy tsv format were re-aligned by TRIC (Rost et al., 2017). **MSStats.** The TRIC output was processed with SWATH2stats R package (v.1.12.0) (Blattmann et al., 2016) to generate the MSstats format. The final analysis and group comparison was performed using MSStats R package (v.3.12.3) (Choi et al., 2014). Final tables were generated by Perseus (v.1.6.1.3) (Tyanova et al., 2016) to extend the annotation by gene and protein names. **Data analysis**. Statistical significance for each gene Log2FC for control versus PINK1 KO clone 1 and control versus PINK1 KO clone 2 was assigned by an asterisk *p=<0.05 (*n*Diff=3). Filtering to minimize the top hits list for the figure was achieved by removing all significant proteins in the CTRL v PINK1 comparison that did not appear significant in both PINK1 KO lines. Then a cutoff point of +/- Log2FC 1 to limit only relevant fold changes and then an arbitrary +/-1.7 Log2FC cut off (-1.7 to +1.7 Log2FC was removed) to limit the number of hits shown because of space. Qiagen Ingenuity and GOrilla was used to generate a pathway analysis using the LogFC as metrics. The pathway analysis files are available as supplementary Excel files. For the comparison of the mitoproteome with gene expression, RNASeq data were merged on the SWATH proteomic dataset using the 'matching rows by name' function of Perseus.

Measurement of biogenic amines by HPLC-ED

Mature hDANs were expanded during differentiation into 175cm^2 Matrigel coated flasks. For each HPLC experiment, approximately 2-3 175cm^2 flasks were required. Although endogenous dopamine levels could be detected in hDANs derived from much larger cell volumes, we employed 50µM L-DOPA treatment overnight (16h) to

enhance dopamine metabolism without risk of dopamine toxicity (Allen et al., 2013, Burbulla et al., 2017). Following detachment of hDANs with Accumax, the cell suspensions were washed in PBS and cells counted. PBS was used to normalize the number of cells in the suspension. An aliquot of the normalized suspension was taken for preparation of protein lysate and RNA to determine the relative amount of TH positive cells in each experiment and differentiation for each cell line. Fresh (unfrozen) cell pellets kept on ice were suspended in 350µl of a standard HPLC elution buffer that does not contain detergents (Thermo Scientific). The suspensions were homogenized using 5mm stainless steel beads and the tissue lyser LT (Qiagen) for 4 minutes with 50Hz. The cell homogenate was centrifuged at 14000 g for 10 min and the supernatant was filtered through a 0.2µm nylon membrane. Samples were analyzed for catecholamine and indolamine content by ion-pair reverse phase HPLC with colorimetric detection (Ultimate 3000 LC with electrochemical detection ECD3000RS, Thermo Fischer Scientific, California, USA). A hypersil C18 column was used (150x3 mm, 3 µm) and the system was run with a Test mobile phase containing 10% acetonitrile and 1% phosphate buffer (Thermo Fischer Scientific, California, USA) at a flow rate of 0.4 ml/min at 30 °C. The potential of the first channel was set to +350 mV, the second channel to -250 mV. Epinephrine, Norepinephrine, Dopamine, 3,4-dihydroxyphenylacetic acid (DOPAC), homovanillic acid (HVA), 5-hydroxyindol-acetic acid (HIAA), 3-Methoxytyramine (3-MT) and 5-hydroxytryptamine/serotonin (5-HT), concentration was determined by comparing peak areas of the samples with those of standards using Chromeleon 7 chromatography data system software. The neurochemicals in standards were determined with a high correlation linearity ($r^2 = 0.98$) and good reproducibility in retention time (0.03%). The limit of detection was <1 pg on column for all the

metabolites analyzed. Statistics Figure 6A: The data was not normalized. One outlier for dopamine was removed from the control hDAN dataset. The data was normally distributed. The Student's t test was performed, **=*p*0.0045 (DOPAC), *p*0.0023 (DA), ns=not significant. nDiff=8. Figure 6B: The data was not normalized. One outlier for dopamine was removed from the control hDAN dataset. The data was normally distributed. The Student's t test was performed, *=*p*0.0130 (DOPAC/DA), *p*0.0144 (DOPAC+HVA/DA), ns=not significant. nDiff=8. Figure 6C: The Student's t test was performed, ns=not significant. nDiff=3. Figure 6D: The data was not normalized. No outliers were removed. Data distribution analysis was not possible. The Student's t test was performed, **=*p*0.0036 (L-DOPA, CTRL v KO), *p*0.046 (DOPAC+MAOi, CTRL v KO), ns=not significant. nDiff=4.

Neurotransmitter Uptake Assay

Neurotransmitter transporter activity in hDANs was measured using the Neurotransmitter Transporter Uptake Assay Kit (Molecular Devices) according to the manufacturer's instructions. Mature hDANs were seeded in Matrigel coated black, clear bottom 96-well plates prior to the assay at a density of 60,000/well in triplicates. Wells containing no cells were used as an internal control. hDANs were treated with a specific VMAT2 inhibitor (Tetrabenazine, 10µM), a TH inhibitor (3-Iondol-L-Tyrosine, 300µM), or a combination of MAO and COMT inhibitors (Tranylcypromine 10µM and Tolcapone 100nM respectively). These compounds were added in media containing L-DOPA (50µM) or without L-DOPA. A subset of hDANs triplicates were treated with media alone or media containing L-DOPA (50µM). All treatments were incubated on the cells at 37°C for 20 minutes prior to the addition of the substrates.

For the NT uptake in Figure 6G; hDANs were plated in the same way and either untreated or treated with 1mM BH4 for 2h prior to addition of substrates. Uptake fluorescence was measured using the SpectraMax M_2^e microplate reader in kinetic mode (Molecular Devices) measuring every 30s or as an endpoint after 30 minutes incubation with the substrates). After the assay, the hDANs were washed and fixed in 4% (v/v) PFA containing Hoechst to account for cell number in each well and then counterstained for TH to account for any large differences in TH positive hDANs in the culture wells. No outliers were removed. Statistics Figure 6E: Linear regression plotted, 2-way ANOVA was performed. Genotype across times was statistically significant ***=p<0.0001 nDiff=3. Figure 6F: In the presence of L-DOPA, THi and MAO/COMTi statistically significantly different to PINK1 KO hDANs using 2-way ANOVA (multiple comparisons). **=*p*0.0071 (*L-DOPA+THi, KO1), **=*p*0.0048 (*L-DOPA+THi, KO2), *=*p*0.049 (*L-DOPA+COMTi/MAOi, v KO1), **=*p*0.010 (*L-DOPA+COMTi/MAOi, v KO2) nDiff=3. Figure 6G: No outliers were removed. Neurotransmitter uptake was measured as a FL endpoint and normalized to the untreated control hDANs in each experiment, Welch's t test was performed. **=*p*0.0024 (untreated CTRL v PINK1 KO), *=*p*0.023 (untreated GC CTRL v PINK1 Q126P), ns=not significant. nDiff=3.

Monoamine oxidase (MAO) Activity Assay

MAO activity was monitored using a radiometric assay with ^{14}C-tyramine hydrochloride as substrate as previously described (Ugun-Klusek et al., 2019). Data were normalized for protein content and rates expressed as disintegrations of

14C/min/µg protein. The student's t test identified no significant differences. ns=not significant, nDiff=3.

Dopamine (Catecholamine) oxidation assay

The catecholamine oxidation assay was performed according to (Burbulla et al., 2017) using Biodyne® B 0.45µm membranes (Pall corporation) and detection using a LiCOR fluorescent scanning device. The quantification performed using Image Studio from LiCOR. Representative blots and standard curve are shown. Mean FL units were plotted for each genotype, fraction and treatment. No outliers were removed. The student's t tests were not significant (CTRL v PINK1 KO in each condition). 2-way ANOVA found significance across the genotypes (*=p0.144) including all the conditions. nDiff=3.

Supplementary Figures and Legends

Bus et al. Supplementary Figure 1

a

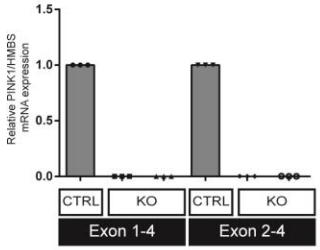

b

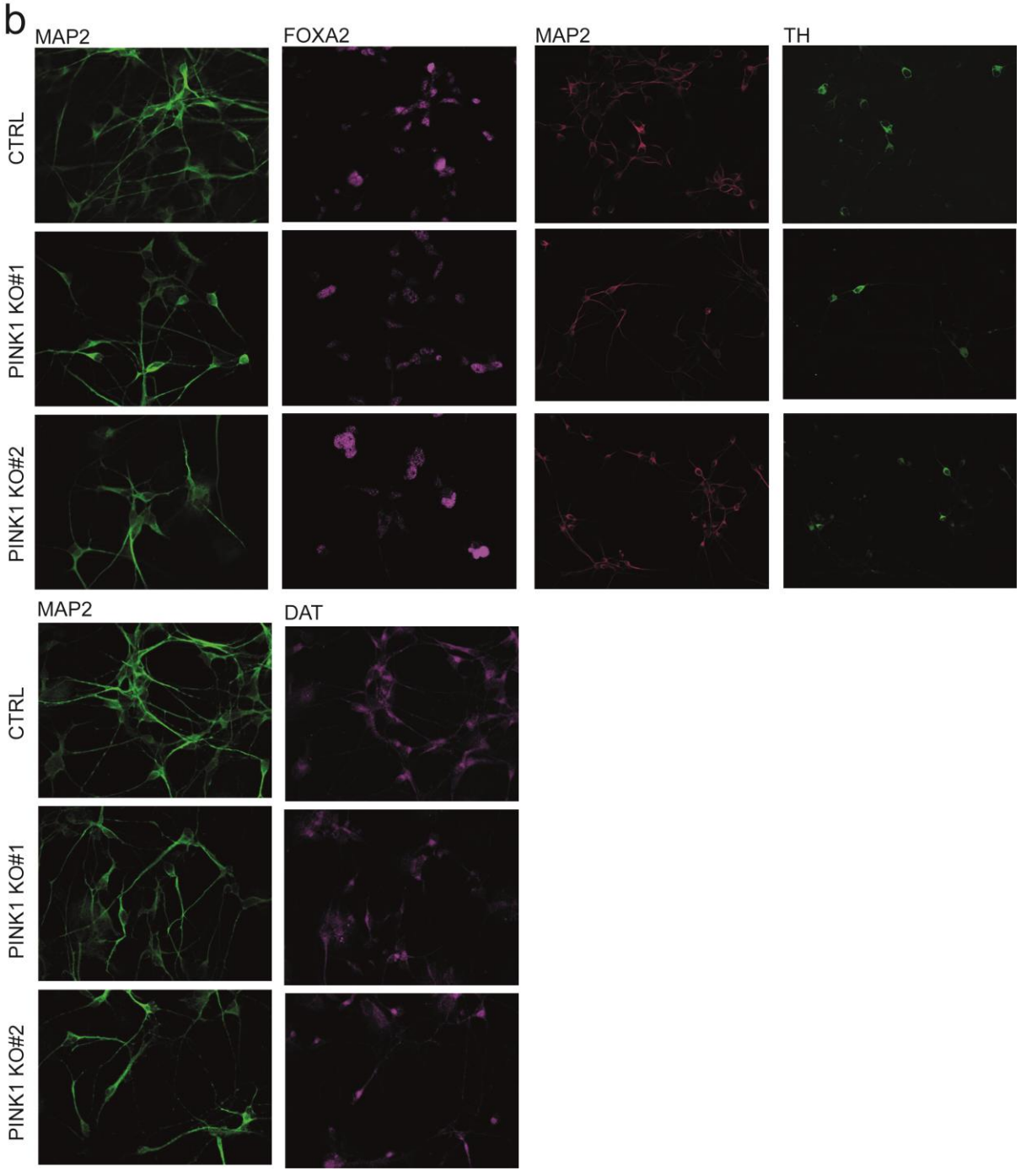

Supplementary Figure S1, related to Figure 1: S1A) Example immunocytochemistry staining of MAP2, TH and FOXA2 in fixed hDANs. Representative images are shown (nDiff=4). **S1B)** Relative PINK1 gene expression in control and PINK1 KO hDAN clones using primers directed to exon1-4 and exon 2-4 (nDiff=3).

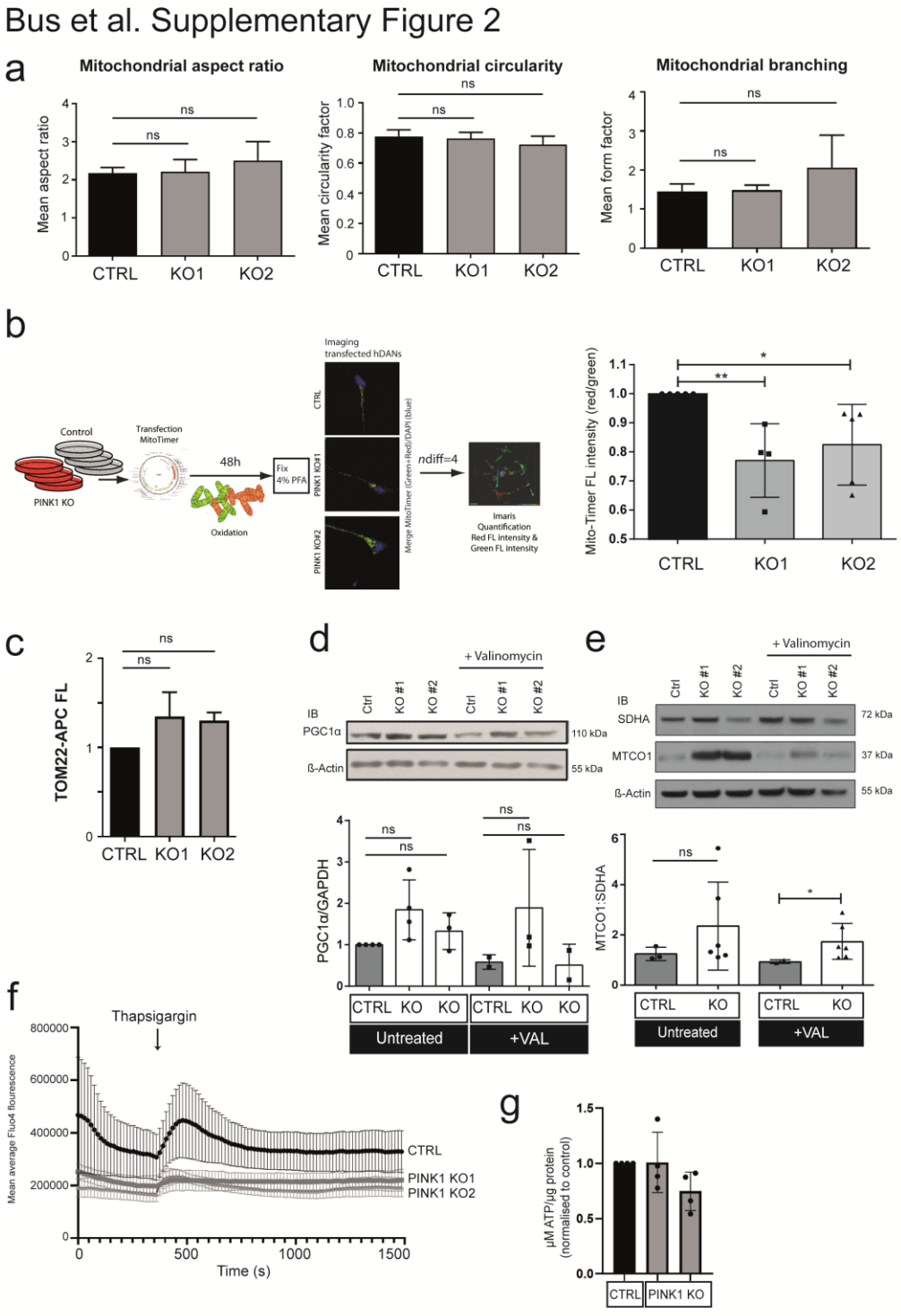

Supplementary Figure S2, related to Figure 2: S2A) Readouts of mitochondrial morphology in hDANs from live cell imaging (nDiff=3, ns=not significant). **S2B)** Diagram showing work flow for MitoTimer experiments in hDANs. Right panel: MitoTimer live cell imaging red/green fluorescence intensity ratio of PINK1 KO hDANs normalised to the isogenic control **=p0.0043 and *=p0.0222 (nDiff=3, error bars=SD). **S2C)** Tom22 fluorescence (APC-FL) detected by inside staining and flow cytometry in hDANs. ns=not significant (nDiff=3, error bars=SD). **S2D)** Upper panel respective Western blot of PGC1alpha in PINK1 KO hDANs and isogenic control under untreated conditions (UT) or valinomycin (VAL) 1µM, 24h (UT n=diff3-4; VAL n=2-3diff, error bars=SD). Lower panel densiometric quanitification of PGC1alpha signal normalised to GAPD and isogenic control. ns=not significant. **S2E)** Upper panel respective Western blot of SDHA and MTCO1 in PINK1 KO hDANs and healthy control under untreated conditions or valinomycin (VAL) 1µM, 24h (nDiff=3-5). Lower panel densiometric signal ratio of MTCO1/SDHA of PINK1 KO hDANs and healthy control (ns= not significant, *=p<0.05, error bars=SD). **S2F)** Total corrected cell Fluo4 fluorescence (cytosolic calcium) calculated for every live image frame across 1500 seconds (nDiff=4, error bars=SD) for CTRL and PINK1 KO hDANs. **S2G)** Normalised ATP levels in CTRL and PINK1 KO hDANs (nDiff=4, error bars =SD, T-test).

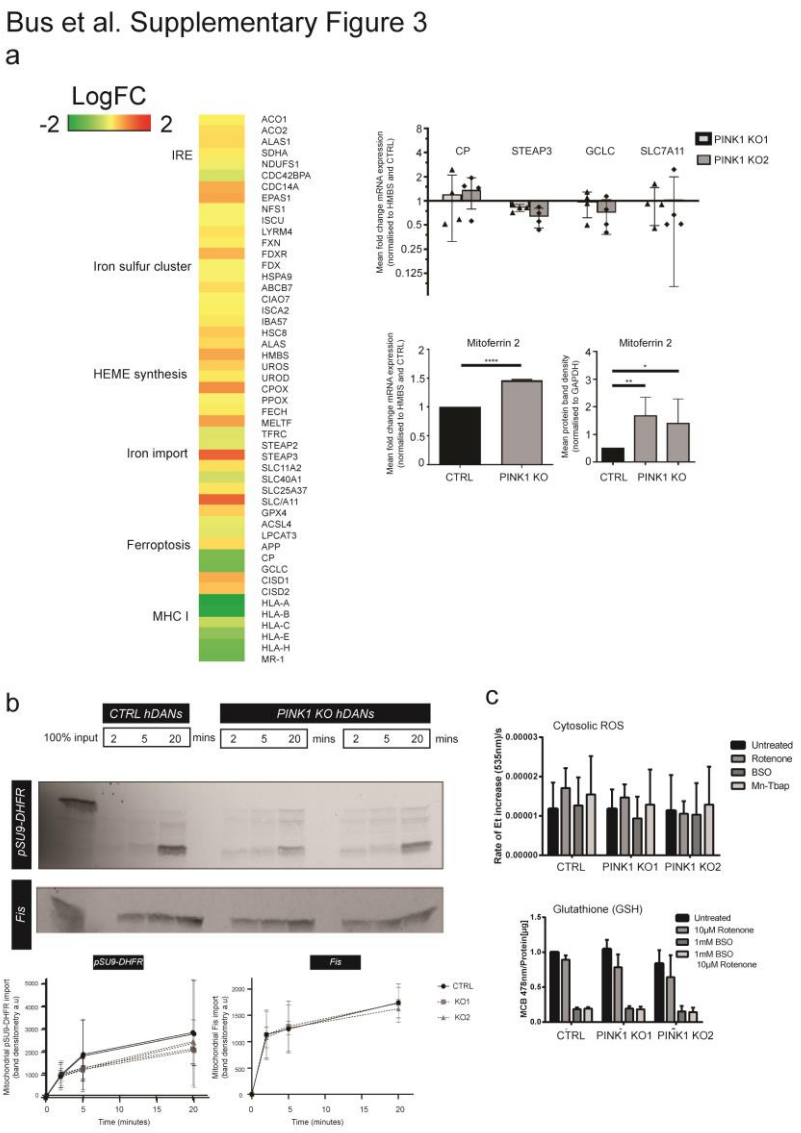

Supplementary Figure S3, related to Figure 3 A-F: S3A) Left panel: Genes identified from RNA sequencing related to iron metabolism. Log2FC values are shown for PINK1 KO hDAN clonal lines versus isogenic control (n=3, nDiff=1). Right panel: Mean fold change of mRNA expression of iron related genes; *CP*, *STEAP3*, *GCLC*, *SLC7A11* in PINK1 KO hDANs normalised to healthy control and HMBS (nDiff=4, error bars=SD). Lower panel: Expression of Mitoferrin-2. mRNA in PINK1 KO hDANs and isogenic control determined by qRT-PCR, results in mean fold change normalised to HMBS and control (nDiff=3; ****=p<0.0001). Western blot of Mitoferrin-2 in PINK1 KO hDANs compared to healthy control, mean protein band density normalised to GAPDH (nDiff=3-5, *=p<0.0179 **=p<0.0079). **S3B)** SDS–PAGE/ autoradiography analysis showing import of radiolabelled proteins 5S-pSU9-DHFR and ^{35}S-

Fis1 in PINK1 KO and healthy control hDANs after different time points (2, 5 and 20 min), arrows indicate precursor and mature pSU9-DHFR protein (nDiff=4, error bars=SD). **S3C)** Top panel: Mean rates of oxidised DiHET (Et) fluorescence signal increase (Ex 535nm/Em 610) per sec in PINK1 KO and isogenic control hDANs untreated or treated with 10µM Rotenone/ 1mM BSO/ 50µM Mn-Tbap indicating cytosolic ROS (nDiff=3, error bars=SD). Bottom panel: Fluorescence signal increase of MCB-GSH adduct in PINK1 KO hDANs and isogenic control untreated or treated with 10µM Rotenone/ 1mM BSO/ 1mM BOS + 10µM Rotenone (nDiff=3). Values normalised per µg protein of cell lysates and to untreated healthy control.

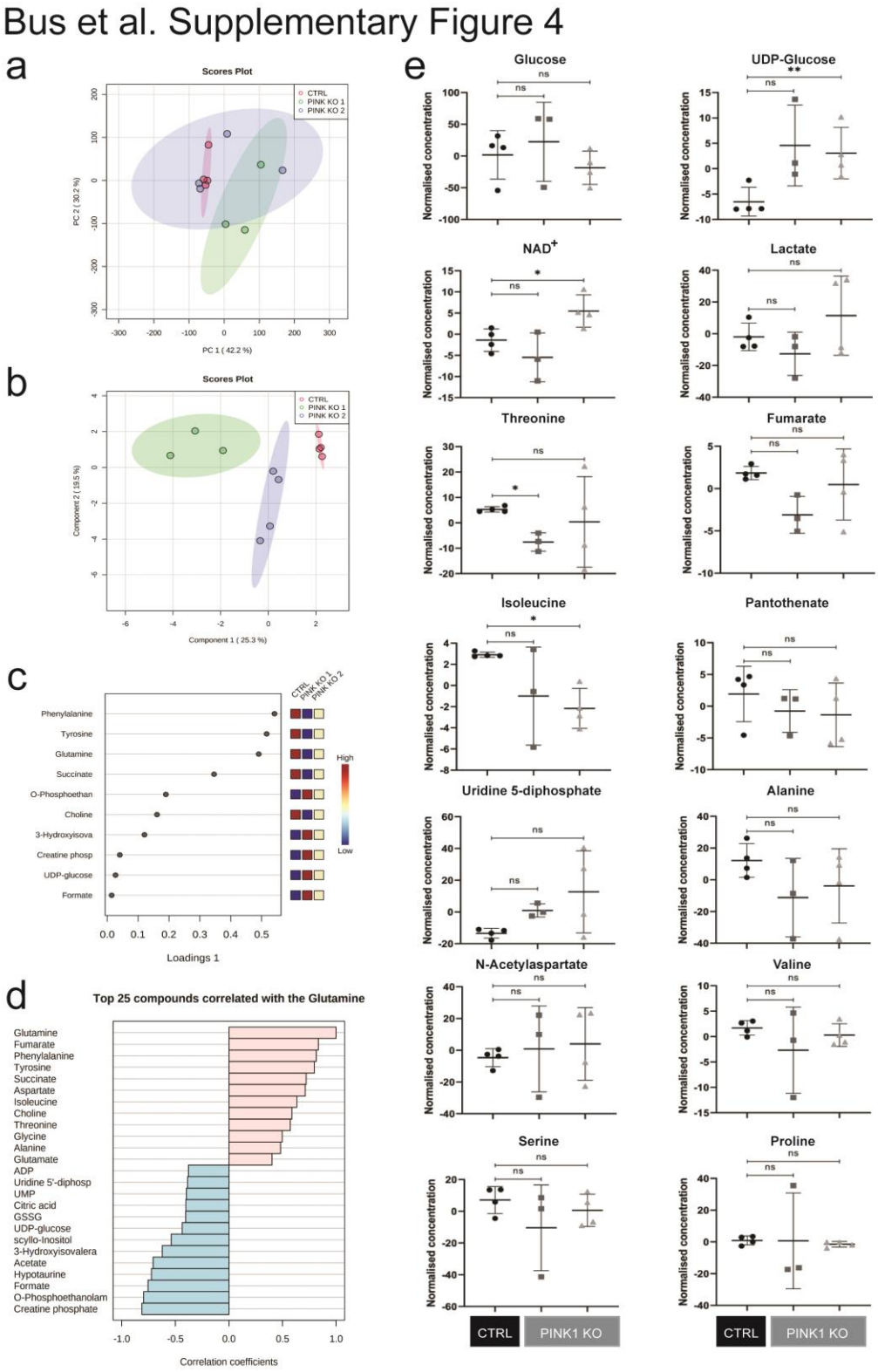

Supplementary Figure S4, related to Figure 3G-I: S4A) Principal Component Analysis (PCA) was generated for the control, KO 1 and 2 metabolomics data comparison. Generally, all three groups have strong similarities between the first two principal components since the

overlap is almost complete. **S4B)** Sparse partial least squares discriminant analysis (sPLS-DA) algorithm allowed reducing the dimensional complexity and illustrated the changes driven by most significant features of the groups. Here, the group separation is significantly improved which correlates to multiple metabolites having significant p-values. **S4C)** sPLS-DA loadings plot illustrates the metabolites which drive the group differences. Here, as top scoring metabolites are phenylalanine, tyrosine, glutamine and succinate, which we identify as main statistical significant metabolite changes. **S4D)** Pattern hunter was generated for glutamine and illustrated the top 25 metabolites which correlate the most strongly with this compound in the dataset (Pearson r distance measure). Glutamine concentration changes in this metabolic setup have the strongest correlation with fumarate, phenylalanine, tyrosine, succinate, aspartate, isoleucine, choline, threonine, glycine, alanine and glutamate, most of which are the amino acids supplying TCA cycle. **S4E)** Scatter plots were generated for all the metabolites of interest based on their changes between the control and KO groups. ns=not significant, *=p<0.05, **=p<0.005 (n=4, nDiff=2, error bars=SD).

Bus et al. Supplementary Figure 5

a

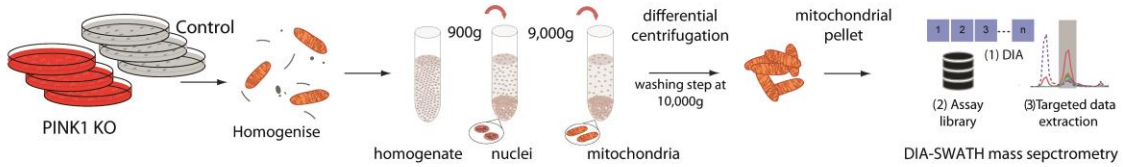

b

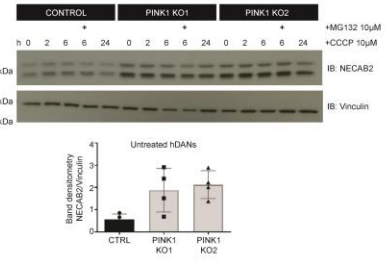

c

Diseases or Functions Annotation	p-value
Migration of cells	1,26E-07
Severe psychological disorder	3,26E-07
Mood Disorders	5,97E-07
Infarction	7,43E-07
Polyneuropathy	9,46E-07
Primary colorectal adenocarcinoma	9,66E-07
Primary colon carcinoma	9,66E-07
Autosomal dominant myopathy	1,08E-06
Peripheral neuropathy	1,76E-06
Healing of wound	2,40E-06
Hereditary motor neuropathy	2,78E-06

d

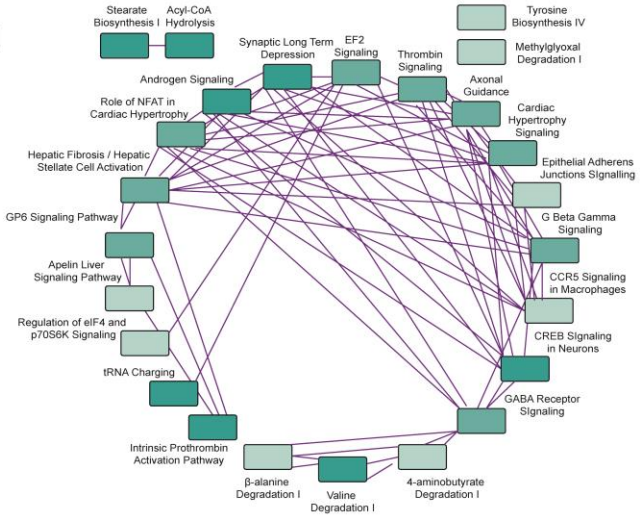

Supplementary Figure S5, related to Figure 5: S5A) Diagram of workflow and mitochondrial preparations from hDANs for quantitative mass spectrometry. **S5B)** Representative Western blot of NECAB2 (MitoNEET) and vinculin (loading control) in PINK1 KO hDANs and healthy control untreated or treated with 10µM CCCP for 0, 2, 6 (+/- 10µM MG132) for 24 hours. Densiometric quantification of NECAB2 Protein in untreated PINK1 KO hDANs and isogenic control normalized to Vinculin. Not significant. (nDiff=4, error bars=SD). **S5C)** Top annotate hits according to disease or function using Qiagen Ingenuity software. listed with respective *p* values. **S5D)** Plot of interactions between annotated biological pathways determined by Qiagen Ingenuity.

Supplementary References

ALLEN, G. F., ULLAH, Y., HARGREAVES, I. P., LAND, J. M. & HEALES, S. J. 2013. Dopamine but not l-dopa stimulates neural glutathione metabolism. Potential implications for Parkinson's and other dopamine deficiency states. *Neurochem Int,* 62**,** 684-94.

BLATTMANN, P., HEUSEL, M. & AEBERSOLD, R. 2016. SWATH2stats: An R/Bioconductor Package to Process and Convert Quantitative SWATH-MS Proteomics Data for Downstream Analysis Tools. *PLoS One,* 11**,** e0153160.

BRUDERER, R., BERNHARDT, O. M., GANDHI, T., MILADINOVIC, S. M., CHENG, L. Y., MESSNER, S., EHRENBERGER, T., ZANOTELLI, V., BUTSCHEID, Y., ESCHER, C., VITEK, O., RINNER, O. & REITER, L. 2015. Extending the limits of quantitative proteome profiling with data-independent acquisition and application to acetaminophen-treated three-dimensional liver microtissues. *Mol Cell Proteomics,* 14**,** 1400-10.

BURBULLA, L. F., SONG, P., MAZZULLI, J. R., ZAMPESE, E., WONG, Y. C., JEON, S., SANTOS, D. P., BLANZ, J., OBERMAIER, C. D., STROJNY, C., SAVAS, J. N., KISKINIS, E., ZHUANG, X., KRUGER, R., SURMEIER, D. J. & KRAINC, D. 2017. Dopamine oxidation mediates mitochondrial and lysosomal dysfunction in Parkinson's disease. *Science,* 357**,** 1255-1261.

CERMAK, T., DOYLE, E. L., CHRISTIAN, M., WANG, L., ZHANG, Y., SCHMIDT, C., BALLER, J. A., SOMIA, N. V., BOGDANOVE, A. J. & VOYTAS, D. F. 2011. Efficient design and assembly of custom TALEN and other TAL effector-based constructs for DNA targeting. *Nucleic Acids Res,* 39**,** e82.

CHOI, M., CHANG, C. Y., CLOUGH, T., BROUDY, D., KILLEEN, T., MACLEAN, B. & VITEK, O. 2014. MSstats: an R package for statistical analysis of quantitative mass spectrometry-based proteomic experiments. *Bioinformatics,* 30**,** 2524-6.

ESCHER, C., REITER, L., MACLEAN, B., OSSOLA, R., HERZOG, F., CHILTON, J., MACCOSS, M. J. & RINNER, O. 2012. Using iRT, a normalized retention time for more targeted measurement of peptides. *Proteomics,* 12**,** 1111-21.

FITZGERALD, J. C., ZIMPRICH, A., BERRIO, D. A. C., SCHINDLER, K. M., MAURER, B., SCHULTE, C., BUS, C., HAUSER, A. K., KUBLER, M., LEWIN, R., BOBBILI, D. R., SCHWARZ, L. M., VARTHOLOMAIOU, E., BROCKMANN, K., WUST, R., MADLUNG, J., NORDHEIM, A., RIESS, O., MARTINS, L. M., GLAAB, E., MAY, P., SCHENKE-LAYLAND, K., PICARD, D., SHARMA, M., GASSER, T. & KRUGER, R. 2017. Metformin reverses TRAP1 mutation-associated alterations in mitochondrial function in Parkinson's disease. *Brain,* 140**,** 2444-2459.

GLOECKNER, C. J., SCHUMACHER, A., BOLDT, K. & UEFFING, M. 2009. The Parkinson disease-associated protein kinase LRRK2 exhibits MAPKKK activity and phosphorylates MKK3/6 and MKK4/7, in vitro. *J Neurochem,* 109**,** 959-68.

HARGREAVES, I. P., DUNCAN, A. J., WU, L., AGRAWAL, A., LAND, J. M. & HEALES, S. J. 2007. Inhibition of mitochondrial complex IV leads to secondary loss complex II-III activity: implications for the pathogenesis and treatment of mitochondrial encephalomyopathies. *Mitochondrion,* 7**,** 284-7.

HERNANDEZ, G., THORNTON, C., STOTLAND, A., LUI, D., SIN, J., RAMIL, J., MAGEE, N., ANDRES, A., QUARATO, G., CARREIRA, R. S., SAYEN, M. R., WOLKOWICZ, R. & GOTTLIEB, R. A. 2013. MitoTimer: a novel tool for monitoring mitochondrial turnover. *Autophagy,* 9**,** 1852-61.

PIERIK, A. J., NETZ, D. J. & LILL, R. 2009. Analysis of iron-sulfur protein maturation in eukaryotes. *Nat Protoc,* 4**,** 753-66.

PRESTEL, J., GEMPEL, K., HAUSER, T. K., SCHWEITZER, K., PROKISCH, H., AHTING, U., FREUDENSTEIN, D., BUELTMANN, E., NAEGELE, T., BERG, D., KLOPSTOCK, T. & GASSER, T. 2008. Clinical and molecular characterisation of a Parkinson family with a novel PINK1 mutation. *J Neurol,* 255**,** 643-8.

REINHARDT, P., GLATZA, M., HEMMER, K., TSYTSYURA, Y., THIEL, C. S., HOING, S., MORITZ, S., PARGA, J. A., WAGNER, L., BRUDER, J. M., WU, G., SCHMID, B., ROPKE, A., KLINGAUF, J., SCHWAMBORN, J. C., GASSER, T., SCHOLER, H. R. & STERNECKERT, J. 2013. Derivation and expansion using only small molecules of human neural progenitors for neurodegenerative disease modeling. *PLoS One,* 8**,** e59252.

ROST, H. L., AEBERSOLD, R. & SCHUBERT, O. T. 2017. Automated SWATH Data Analysis Using Targeted Extraction of Ion Chromatograms. *Methods Mol Biol,* 1550**,** 289-307.

SCHUBERT, O. T., GILLET, L. C., COLLINS, B. C., NAVARRO, P., ROSENBERGER, G., WOLSKI, W. E., LAM, H., AMODEI, D., MALLICK, P., MACLEAN, B. & AEBERSOLD, R. 2015. Building high-quality assay libraries for targeted analysis of SWATH MS data. *Nat Protoc,* 10**,** 426-41.

TYANOVA, S., TEMU, T. & COX, J. 2016. The MaxQuant computational platform for mass spectrometry-based shotgun proteomics. *Nat Protoc,* 11**,** 2301-2319.

UGUN-KLUSEK, A., THEODOSI, T. S., FITZGERALD, J. C., BURTE, F., UFER, C., BOOCOCK, D. J., YU-WAI-MAN, P., BEDFORD, L. & BILLETT, E. E. 2019. Monoamine oxidase-A promotes protective autophagy in human SH-SY5Y neuroblastoma cells through Bcl-2 phosphorylation. *Redox Biol,* 20**,** 167-181.

WOLBURG-BUCHHOLZ, K., MACK, A. F., STEINER, E., PFEIFFER, F., ENGELHARDT, B. & WOLBURG, H. 2009. Loss of astrocyte polarity marks blood-brain barrier impairment during experimental autoimmune encephalomyelitis. *Acta Neuropathol,* 118**,** 219-33.

Journal of Molecular Medicine (2022) 100:747–762
https://doi.org/10.1007/s00109-022-02191-6

JMolMed

ORIGINAL ARTICLE

The role of the individual TOM subunits in the association of PINK1 with depolarized mitochondria

Klaudia K. Maruszczak[1] · Martin Jung[2] · Shafqat Rasool[3] · Jean-François Trempe[3] · Doron Rapaport[1]

Received: 25 January 2022 / Revised: 8 March 2022 / Accepted: 17 March 2022 / Published online: 7 April 2022

Abstract

Mitochondria dysfunction is involved in the pathomechanism of many illnesses including Parkinson's disease. PINK1, which is mutated in some cases of familial Parkinsonism, is a key component in the degradation of damaged mitochondria by mitophagy. The accumulation of PINK1 on the mitochondrial outer membrane (MOM) of compromised organelles is crucial for the induction of mitophagy, but the molecular mechanism of this process is still unresolved. Here, we investigate the association of PINK1 with the TOM complex. We demonstrate that PINK1 heavily relies on the import receptor TOM70 for its association with mitochondria and directly interacts with this receptor. The structural protein TOM7 appears to play only a moderate role in PINK1 association with the TOM complex, probably due to its role in stabilizing this complex. PINK1 requires the TOM40 pore lumen for its stable interaction with the TOM complex and apparently remains there during its further association with the MOM. Overall, this study provides new insights on the role of the individual TOM subunits in the association of PINK1 with the MOM of depolarized mitochondria.

Key messages

- TOM70 is the main receptor for the import of PINK1 into mitochondria.
- TOM20 plays only a minor role in PINK1 recognition at the organellar outer membrane.
- PINK1 association with the TOM complex is reduced upon knock-down of TOM7.
- The lumen of the TOM pore is crucial for PINK1 association with the outer membrane. TcPINK1 blocks the TOM pore in depolarized mitochondria.

Keywords Mitochondria · Outer membrane · Parkinson's disease · PINK1 · TOM complex

Introduction

Mitochondria are versatile organelles that form tubular networks within eukaryotic cells. They are highly dynamic structures undergoing fission and fusion processes to adjust to existing conditions and to maintain cells in a healthy state [1]. Mitochondria also harbor many metabolic pathways and have a crucial role in supplying cells with energy in the form of ATP [2]. Being critical for cellular homeostasis, mitochondria have to be continuously monitored by different quality control proteins and mechanisms. One of these mechanisms relies on mitochondrial autophagy (mitophagy) that is mediated by the proteins PINK1 and Parkin [3]. In fully functional mitochondria, PINK1 is imported into the organelle where the inner membrane protease, PARL, cleaves it within the transmembrane domain [4]. Such processed PINK1 is subsequently retro-translocated into the cytosol and degraded by the proteasome [5]. In contrast, upon mitochondrial depolarization, PINK1 is accumulated at the mitochondrial outer membrane (MOM), where it phosphorylates itself and ubiquitin moieties conjugated to MOM proteins. Additionally, it phosphorylates also Parkin (E3 Ub ligase), which in turn ligates additional ubiquitin molecule

✉ Doron Rapaport
doron.rapaport@uni-tuebingen.de

[1] Interfaculty Institute of Biochemistry, University of Tübingen, Auf der Morgenstelle 34, 72076 Tübingen, Germany

[2] Medical Biochemistry and Molecular Biology, Saarland University, UKS, 66421 Homburg, Germany

[3] Department of Pharmacology & Therapeutics and Centre de Recherche en Biologie Structurale, McGill University, Montréal, Québec, Canada

to the previously phosphorylated ubiquitin [6, 7]. This process leads to the formation of poly-ubiquitin chains and generation of positive feedback loop that eventually result in the specific elimination of compromised mitochondria by mitophagy. Hence, the association of PINK1 with the MOM is crucial for the whole mitophagy process. Dysfunctional mitophagy, and specifically, mutations in PINK1 and/or Parkin, can lead to the development of neurodegenerative diseases with Parkinson's disease as the main example [8].

So far, the import of PINK1 into polarized mitochondria has been elucidated in some detail [5, 9, 10]. In contrast, much less is known about its recognition and the subsequent integration into the MOM in depolarized organelles. Previous studies reported on the importance of the translocase of the mitochondrial outer membrane (TOM complex) for the integration of PINK1 into the MOM. For example, Lazarou et al. [11] showed that PINK1 accumulates in the MOM in the form of high molecular weight complexes with the TOM complex. Later, Okatsu et al. [12] discovered that PINK1 forms dimers in such complexes and is found there in its phosphorylated form. Considering these findings, a model was suggested in which the TOM complex facilitates the accurate orientation of the dimeric PINK1 so that intermolecular phosphorylation and subsequent activation can occur [12]. The structure of the *Tribolium castaneum* (Tc) PINK1 cytosolic domain revealed how dimerization enables *trans* autophosphorylation at Ser228 and suggests that anchoring on the TOM complex via an N-terminal helix is critical for PINK1 activation [13].

Additional studies investigate the specific contribution of individual components of the TOM complex. For example, two studies proposed the relevance of the structural subunit TOM7, as being a "side gate" for PINK1 membrane insertion [9, 14]. Accordingly, addition of an uncoupler to HeLa cells lacking TOM7 failed to induce PINK1 accumulation at the MOM [14]. In addition, both receptors of the TOM complex, TOM20 and TOM70, were suggested by two different studies to play an important role in PINK1 recognition at the MOM. Zhang et al. [15] reported a drastic effect of TOM20 inhibition by celastrol on PINK1 association with mitochondria, and Kato et al. [16] showed that PINK1 relies on the TOM70 receptor for its import into healthy mitochondria. Collectively, it seems that various subunits of the TOM complex contribute by an undefined way to the association of PINK1 with the MOM.

In addition to such trans elements, cis sequences within PINK1 itself were found to be important for its integration into the MOM. The outer mitochondrial membrane localization signal (OMS), which comprises a weak hydrophobic segment localized N-terminally to the transmembrane domain of PINK1 and encompasses amino acids residues 70–95, was reported to mediate association with the MOM [17]. Along this line, Sekine et al. [14] have proposed that both TOM7 and OMS are crucial for PINK1 retention, with TOM7 mediating the lateral release of the protein from the TOM40 channel. Despite this progress, the location of PINK1 at the MOM of depolarized mitochondria and the factors that contribute to this positioning are only partially resolved.

Here, we investigated the initial import steps of PINK1 into depolarized mitochondria. We demonstrate that PINK1 heavily relies on TOM70 for its assembly into depolarized organelles and directly interacts with this receptor. Our findings further suggest that the accessory protein, TOM7, plays only a moderate role in PINK1 association with the TOM complex, probably due to its contribution to the stability of this complex. Importantly, PINK1 requires the TOM40 pore lumen for its association with the TOM complex and apparently remains there during its association with the MOM. Overall, this study provides new insights on the role of the TOM complex in the association of PINK1 with the MOM of depolarized mitochondria.

Results

PINK1 associates with the TOM complex upon depolarization of mitochondria

PINK1 accumulates at the MOM upon deprivation of mitochondrial inner membrane potential ($\Delta\Psi m$). As part of our effort to dissect this process, we aimed to use a specific assay to monitor the association of PINK1 with the MOM. It was previously reported that PINK1 associates with the TOM complex upon CCCP treatment and forms a stable 700 kDa species that can be analyzed by blue native (BN)-PAGE [11]. Hence, we decided to use this association as a readout for the productive association of PINK1 with the TOM complex. To validate that the detected 700 kDa band represents indeed an adduct of PINK1 and the TOM complex, we performed in organello import assay with radiolabelled PINK1 and mitochondria isolated from HeLa cells. As anticipated, when the import reactions were solubilized with digitonin and analyzed by BN-PAGE, we observed a band at ca. 700 kDa only if mitochondria were depolarized before (Fig. 1a). To verify the identity of this band, we aimed to immunodeplete the TOM complex from the digitonin suspension by addition of an antibody against TOM22 conjugated to protein A beads. This procedure allowed us to deplete the TOM complex, as analyzed by BN-PAGE, from the organelle's lysate (Fig. 1b). In agreement with previous studies [9, 11], this treatment removed also the 700 kDa PINK1-TOM complex from the lysate and in parallel resulted in binding of the PINK1-TOM adduct to the anti-TOM22 beads (Fig. 1a). Accordingly, we detected TOM40 and TOM22 in the eluate as well as radiolabeled PINK1. Interestingly, we could also observe a faint band of

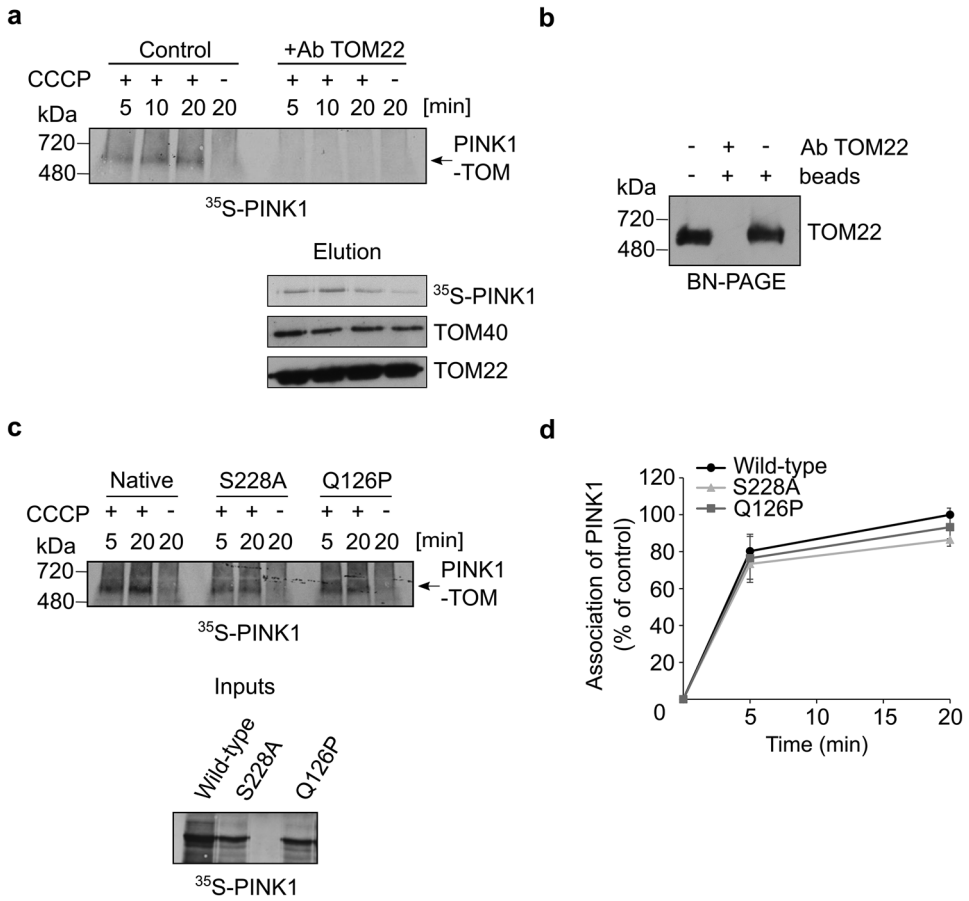

Fig. 1 PINK1 associates with the TOM complex upon depolarization of mitochondria. **a** Radiolabeled PINK1 was imported into mitochondria for indicated time periods. In some cases, the isolated organelles were pretreated with CCCP. At the end of the import reactions, organelles were solubilized with digitonin-containing buffer and the indicated samples were subjected to pull-down with anti-TOM22 antibodies. Samples were then centrifuged, and the supernatant was analyzed by BN-PAGE followed by autoradiography (upper panel). The PINK1-TOM complex species is indicated with an arrow. The immunodepleted proteins were analyzed by SDS-PAGE followed by autoradiography and western blotting using antibodies against TOM40 and TOM22 (lower panel). **b** Solubilized mitochondria were left untreated or were incubated with protein A beads in the presence or absence of TOM22 antibody. Samples were then analyzed by BN-PAGE followed by western blotting using TOM22 antibody. **c** Radiolabeled native PINK1 and the indicated mutants were incubated with isolated mitochondria. Further analysis was as described in panel (a). Lower panel: Radiolabeled samples that were used for the in organello import reactions were analyzed by SDS-PAGE and autoradiography. **d** The bands corresponding to PINK1 association with TOM complex in three independent experiments were quantified. The amount of assembled native PINK1 after 20 min was set to 100%

PINK1 in the eluate when polarized organelles were used (Fig. 1a, lower panel). This finding demonstrates that the interactions of PINK1 with the TOM complex of healthy mitochondria are too weak to withstand the conditions of the BN-PAGE analysis.

To demonstrate the specificity of the TOM depletion, we confirmed that PINK1 could not be depleted from the 700 kDa species by antibodies against non-TOM components like Cytochrome C or VDAC1 (Fig. S1a). We further verified the identity of the 700 kDa band as an adduct of PINK1 and the TOM complex by performing an antibody shift assay. In this experiment, we performed an in vitro import assay of radiolabeled PINK1 to unpolarized organelles. In the end of the import reaction, the organelles were solubilized by digitonin and antibodies against either TOM22 or ATP5A (as a control for unrelated protein) were added to the suspension before the analysis by BN-PAGE (Fig. S1b). The results clearly indicate that the presence of the antibody against TOM22 resulted in a shift in the migration of the 700 kDa band supporting the notion that TOM22 is part of this complex. We conclude that the formation of the 700 kDa species is a robust readout for stable association of PINK1 with the TOM complex. Next, we checked whether mutating an autophosphorylation site of PINK1 (S228A) or N-terminally localized glutamine residue, Q126P, a mutation reported in Parkinsonism, affect its association with the TOM complex. However, we did not observe any differences as compared to native PINK1 (Fig. 1c, d). Our findings regarding the S228A variant are in line with previous

findings and support the validity of our assay [12, 13]. Thus, it appears that the defects related to these mutations do not arise from compromised interaction with the TOM complex.

Identification of TOM70 as a potential receptor for PINK1 import into mitochondria

PINK1 is synthesized on cytosolic ribosomes and therefore, has to be targeted to mitochondria. Our first aim was to identify which receptors of the TOM complex could recognize PINK1 upon its translocation to the MOM. First, since we previously found TOM70 to play a role in PINK1 recognition [16], we performed a peptide scan, in which peptides encompassing the N-terminal 140 amino acids of PINK1, a region that is sufficient for PINK1 targeting to mitochondria [17, 18], were synthesized onto a membrane. Next, the membrane was incubated with purified recombinant cytosolic domain of yeast Tom70. In line with our previous observations, we detected interactions of the cytosolic domain of Tom70 with PINK1 peptides (Fig. S2a). We could observe Tom70 binding to PINK1 N-terminal region, with the highest intensities at MTS, OMS, and TMD (Fig. S2b). Hence, it appears that TOM70 can directly bind to all three structural elements: PINK1 MTS, the signal that mediates interactions with the outer membrane (OMS), as well as to the putative TMD. These findings agree with current knowledge about the capacity of TOM70 to recognize not only hydrophobic internal segments of mitochondrial proteins but rather also internal MTSs [19, 20].

To test the contribution of TOM70 in more detail, we used in vitro pull-down assay to study whether the cytosolic

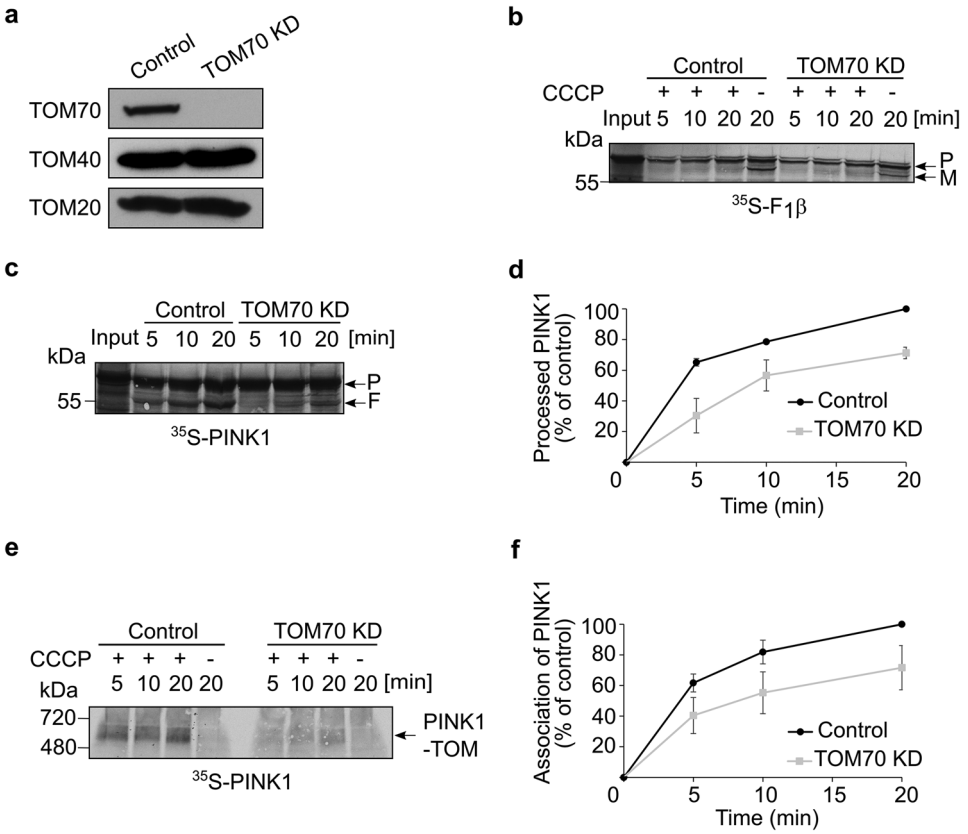

Fig. 2 TOM70 plays an important role in PINK1 import into mitochondria. **a** Mitochondria were isolated from either control or cells knocked down for TOM70. Isolated organelles (50 µg) were analyzed by SDS-PAGE and western blotting with the indicated antibodies. **b** Radiolabeled $F_1\beta$ was incubated for the indicated time periods with mitochondria isolated from either control or TOM70 KD cells in the absence or presence of CCCP. Subsequently, samples were analyzed by SDS-PAGE and autoradiography. The precursor (P) and mature (M) forms of the protein are indicated. **c** Radiolabeled PINK1 was incubated with mitochondria isolated from either control or TOM70 KD cells. Next, samples were analyzed by SDS-PAGE and autoradiography. The bands corresponding to the precursor form of PINK1 (P) or the PARL-processed form (F) are indicated. **d** The bands corresponding to processed PINK1 (F) were quantified and the intensity of the band corresponding to import for 20 min into control organelles was set to 100%. The results present the average of three independent experiments (±SD). **e** Import into the indicated isolated organelles was performed and analyzed as described in the legend to Fig. 1a. **f** The bands corresponding to PINK1 association with TOM complex were quantified. The intensity of the band corresponding to assembled PINK1 in control mitochondria after 20 min was set up to 100%. The results represent the average of three independent experiments (±SD)

domains of Tom70 or Tom20 (for comparison) can bind radiolabeled PINK1. Our results revealed that whereas Tom20 has only a weak binding capacity to PINK1, Tom70 can do so with a much higher efficiency (Fig. S2c). Next, we were interested to find out whether the MTS in residues 1–35 of PINK1 is crucial to the recognition by TOM70. Of note, we could observe that both fragments of PINK1: 1–120 as well as 35–120 were bound by the Tom70 receptor suggesting that PINK1 recognition by Tom70 does not solely depend on its MTS (Fig. S2d). These results agree with previous reports [17, 21], which showed that PINK1 without its MTS could still be imported into depolarized mitochondria. Thus, we concluded that TOM70 could be the primary receptor for PINK1 import into mitochondria by recognizing the OMS and the TMD elements of the protein.

TOM70 is important for PINK1 import into mitochondria

To further validate the importance of TOM70 receptor, we knocked it down in HeLa cells and isolated mitochondria from either control or these manipulated cells. Figure 2a shows the validation by Western blotting of the TOM70 depletion in the isolated organelles. To exclude general problem in the import capacity of mitochondria isolated from the TOM70 KD cells, we imported into these organelles radiolabelled F1β (subunit of ATP synthase), which requires the presence of ΔΨm for its translocation to the matrix where it is processed from the precursor (P) form to the mature (M) one by removal of the MTS (Fig. 2b, lanes with no CCCP addition). As expected for an MTS-containing matrix substrate [20], the import of this precursor protein into mitochondria depleted for TOM70 was comparable to its import into control organelles (Fig. 2b). In contrast, when radiolabeled PINK1 was imported into control and TOM70 KD mitochondria that were either polarized (Fig. 2c) or depolarized by addition of CCCP (Fig. 2e), the absence of TOM70 resulted in a significant retardation of the import capacity of the organelles. Import into healthy organelles was measured by the appearance of 52 kDa-processed version of PINK1 (F, Fig. 2c, d) and association of PINK1 with the TOM complex in depolarized mitochondria was quantified based on the built-up of the 700 kDa species upon BN-PAGE analysis (Fig. 2e, f). In both cases, PINK1 import was reduced to about 70% of the control. Hence, we propose that TOM70 plays a central role in PINK1 recognition at the MOM and subsequent import into both healthy and depolarized mitochondria.

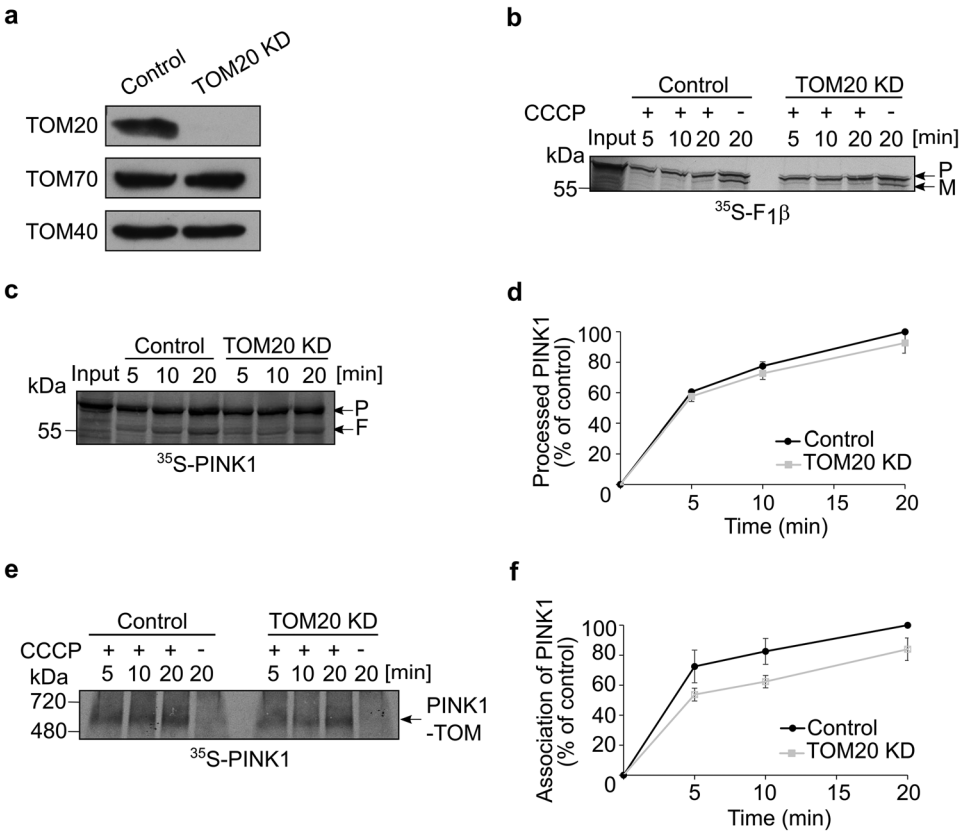

Fig. 3 TOM20 plays only a minor part in PINK1 recognition at the MOM. **a** Mitochondria were isolated from either control or cells knocked down for TOM20. Isolated organelles (50 µg) were analyzed by SDS-PAGE and western blotting with the indicated antibodies. **b** Radiolabeled $F_1\beta$ was imported and analyzed as described in the legend to Fig. 2b. **c**, **d** Radiolabeled PINK1 was incubated with mitochondria isolated from either control or TOM20 KD cells. Further analysis and quantification were as described in the legends to Fig. 2c, d. **e**, **f** Import into the indicated isolated organelles was performed and analyzed as described in the legend to Fig. 1a. Quantification of bands was as described in the legend to Fig. 2f

TOM20 plays only a minor role in PINK1 recognition at the MOM

Our in vitro binding experiments described in Suppl. Figure 2c suggested that TOM20 has only a weak binding capacity to PINK1. To check whether TOM20 could play a role in PINK1 recognition in vivo, we depleted U2OS cells of the TOM20 receptor and isolated mitochondria from these cells (Fig. 3a). Initially, we controlled whether MTS containing precursor protein like F1β is affected by the absence of TOM20. As expected, we observed a reduction in the import capacity of this protein into organelles lacking TOM20 and in both types of organelles the import was eliminated by adding CCCP (Fig. 3b). Next, we imported radiolabeled PINK1 into polarized mitochondria isolated from either control or TOM20 KD cells and found that PINK1 processing by PARL was hardly affected, if at all, by the absence of TOM20 (Fig. 3c, d). Along the same line, association of PINK1 with the TOM complex in depolarized mitochondria was decreased in the TOM20 depleted organelles by only 20% (Fig. 3e, f). Thus, we concluded that TOM20 does play, however rather marginal, a role in PINK1 recognition.

Double knockdown of TOM70 and TOM20 has a synthetic effect on PINK1 import

Since we observed that PINK1 is imported into mitochondria even upon the individual knock down of the import receptors, we wondered whether in the absence of one receptor, the other one can take over its function. To address this possibility, we knocked down both proteins in HeLa cells and then isolated mitochondria. While TOM70 was not detected at all in the organelles from the double KD cells, we detected faint band of TOM20 in these cells (Fig. 4a). Of note, the levels of the central TOM subunit, TOM40 was not affected by the practical absence of both receptors. As previously, we used $F_1\beta$ import as a control substrate and as an indication for successful CCCP-treatment (Fig. 4b). Indeed, while certain levels of the protein were imported into organelles lacking either TOM70 (Fig. 2b) or TOM20 (Fig. 3b), the removal of both receptors eliminated completely the import of $F_1\beta$ (Fig. 4b). In sharp contrast, when radiolabeled PINK1 was imported into control and double KD polarized mitochondria, the processing of PINK1 by PARL remained at approximately 80% (Fig. 4c, d). The dependency on the receptors was different when depolarized organelles were

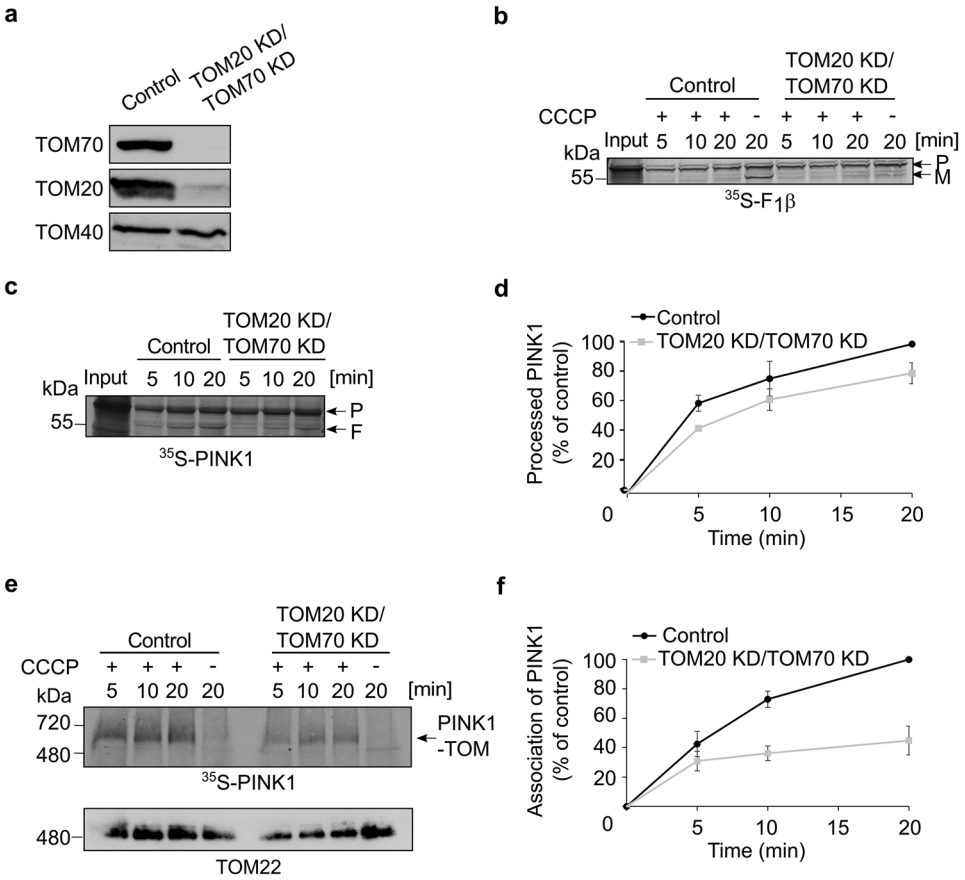

Fig. 4 Double knockdown of both receptors TOM70 and TOM20 compromises the import of PINK1 into depolarized mitochondria. **a** Mitochondria were isolated from either control or cells knocked down for both TOM70 and TOM20. Isolated organelles (50 µg) were analyzed by SDS-PAGE and western blotting with the indicated antibodies. **b** Radiolabeled $F_1\beta$ was imported and analyzed as described in the legend to Fig. 2b. **c**, **d** Radiolabeled PINK1 was incubated with mitochondria isolated from either control or TOM20 KD/TOM70 KD cells. Further analysis and quantification were as described in the legends to Fig. 2c, d. **e**, **f** Import into the indicated isolated organelles was performed and analyzed as described in the legend to Fig. 1a. Quantification of bands was as described in the legend to Fig. 2f. The lower panel of (**e**) is an immunodecoration of the same membrane with antibodies against TOM22

used. Under these conditions, association of PINK1 with the TOM complex lacking both receptors dropped to approximately 40% (Fig. 4e, f). These findings support our assumption that basically, both receptors can recognize PINK1 and in the absence of a single receptor, the other can perform most of the recognition. Next, we investigated the possibility that secondary effects of the double depletions on the fitness of the TOM complex caused the dramatic reduction in the import of PINK1. Monitoring the assembly of the TOM complex by BN-PAGE revealed that the migration of the translocase from the double depleted cells remained unchanged (Fig. 4e, lower panel). This observation agrees with previous findings that the peripheral receptors TOM20 and TOM70 are not part of the TOM core complex, which is detected by BN-PAGE under these conditions. Collectively, we suggest that the strong effect of the double depletion of TOM70 and TOM20 indicates the potential exchangeable roles of both receptors in protein recognition. The fact that double knockdown only moderately affected PINK1 import and PARL-processing in polarized mitochondria and on the other hand, had a drastic effect on association with the TOM complex of depolarized mitochondria, might suggest that both receptors have a stabilizing role in the association of PINK1 with the TOM complex.

PINK1 association with the TOM complex is reduced upon KD of TOM7 and TOM7/TOM70

TOM7 was found to play a role in the integration of PINK1 into the MOM [9, 14]. However, it is still unclear how TOM7 facilitates this process. To test for potential involvement of TOM7 in the association with the TOM complex, we isolated mitochondria from TOM7 KD U2OS cells. Since we could not find a functional antibody against TOM7, we verified the KD by performing a RT-qPCR and detecting dramatically lower levels of the encoding mRNA (not shown). To substantiate the assumption that the levels of TOM7 are indeed profoundly reduced, we followed the behavior of the TOM complex on BN-PAGE. It was previously reported that upon TOM7 depletion, the levels of the TOM complex are decreased, and the complex migrates at apparently lower molecular mass [22]. In agreement with this previous report, the TOM complex in the samples from the TOM7 KD cells was detected as a weaker band, which migrated faster than the control complex (Fig. 5a). Moreover, when radiolabeled TOM40 was imported in organello into mitochondria isolated from the KD cells, it integrated into a smaller species of the TOM complex as compared to the species observed with organelles isolated from untreated cells or those that obtained scrambled siRNA (Fig. 5b). Immunodecoration of the same membrane with antibodies against TOM40 confirmed this observation (Fig. 5b, lower panel). Taken together, we concluded that TOM7 was indeed depleted in these KD cells.

Subsequently, we wanted to check how the absence of TOM7 would affect import of matrix residing protein. The import of pSu9-DHFR, as monitored by its processing by MPP, was compromised by 20–30% upon the depletion of TOM7 (Fig. 5c, d), probably due to the reduced stability of the TOM complex. A similar degree of reduction was also observed upon studying the association of PINK1 with the TOM complex of depolarized organelles from the TOM7 KD cells (Fig. 5e, f). Thus, it seems that TOM7 depletion does not specifically affect PINK1 MOM integration, but also other proteins that depend on the correct conformation of the TOM complex for their import. To corroborate this suggestion, we imported a multi-span MOM protein, PBR (TPSO), that was previously reported to insert in the MOM independently of the TOM complex [23]. Indeed, TOM7 KD did not affect PBR integration into the MOM (Fig. 5g, h).

Next, we aimed to investigate whether double depletion of TOM7 and TOM70 would have a synthetic effect on PINK1 association with mitochondria. TOM70 KD was confirmed by immunodecoration (Fig. 6a), whereas the depletion of TOM7 via the altered migration behavior of the TOM complex in BN-PAGE (Fig. 6b, lower panel). When radiolabeled PINK1 was imported into TOM7/TOM70 double depleted depolarized mitochondria, we observed a dramatic reduction of more than 60% in the association of PINK1 to the TOM complex as compared to control organelle (Fig. 6b, c). This striking reduction is larger than what could be expected from the single deletions. This synergistic effect is probably the outcome of the combined effects of absence of the main receptor for PINK1 import, TOM70, as well as the destabilization of the TOM core complex in the absence of TOM7.

The lumen of the TOM pore is crucial for PINK1 association with the MOM

There are three main hypotheses in the literature regarding the precise location of PINK1 in the MOM of depolarized organelles: The first suggests that PINK1 is laterally released from the TOM complex into the bulk of the outer membrane [10], the second argues that PINK1 is arrested in the TOM40 lumen from where it can trigger the mitophagy cascade [9], whereas the third proposes that the N-terminal segment of PINK1 could undergo lateral release, but remains bound to the TOM complex and is not released into the bulk OM [13]. Since all alternatives emphasize the role of TOM40 in this process, we aimed to study the dependence of PINK1 on the TOM pore upon import into CCCP-treated mitochondria. TOM40 is the central essential component of the TOM complex and therefore its knockdown could lead to many secondary effects such as altered levels of many additional

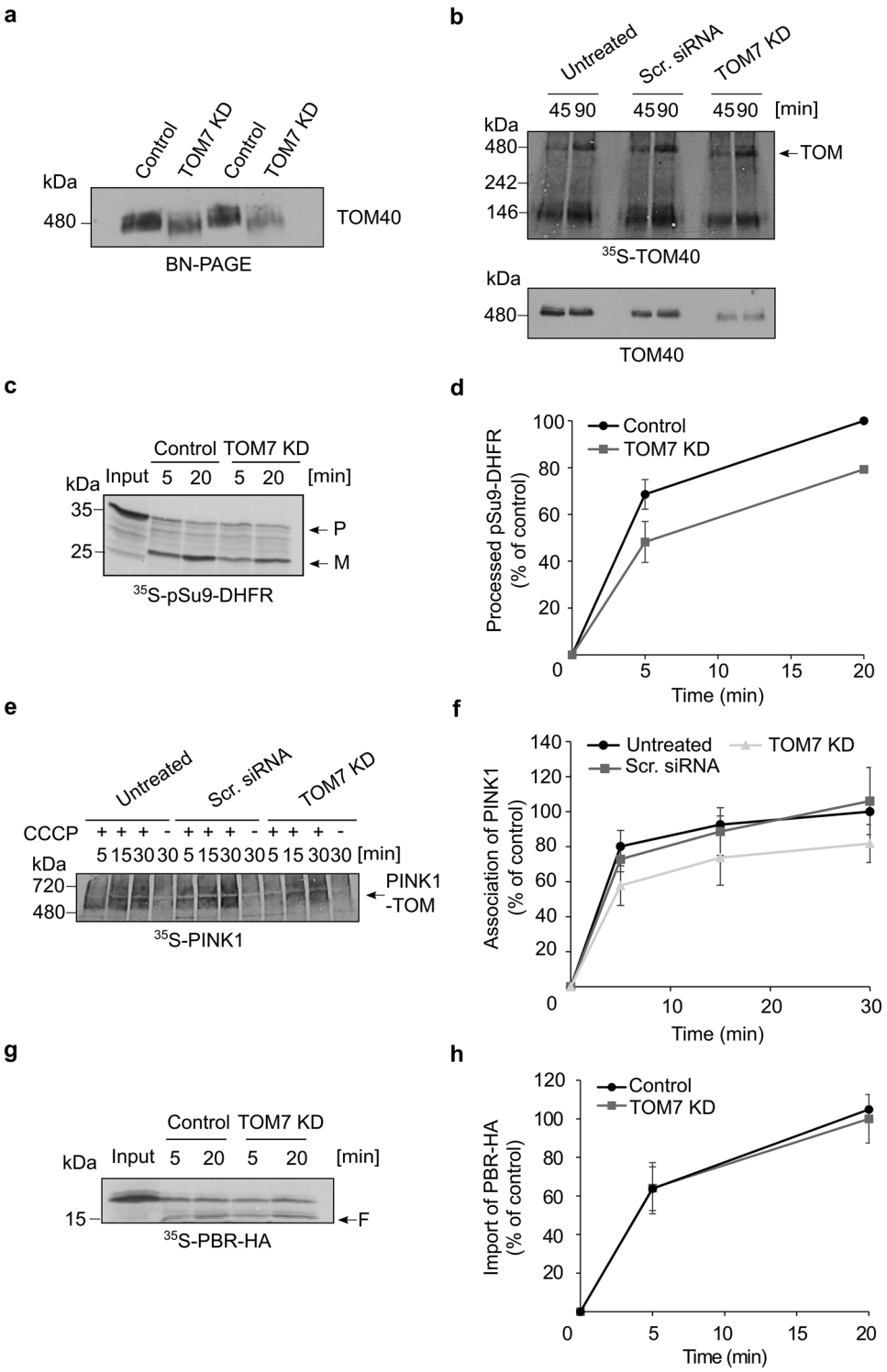

other mitochondrial proteins. Thus, we used an alternative method namely, the addition of excess amounts of purified recombinant pSu9-DHFR to clog the TOM complex. Ideally, the MTS of Su9 would drive the protein into the matrix; however, by addition of the DHFR ligand, methotrexate, DHFR domain becomes tightly folded and disables the translocation of the protein across the TOM complex. The latter results in the blockage of the TOM entry gate, making it almost impossible for other proteins to pass through it. As expected, import of PINK1 and $F_1\beta$ into polarized mitochondria that were blocked by pSu9-DHFR was acutely affected (Fig. 7a and b, respectively). Both proteins are translocated

◂**Fig. 5** PINK1 association with the TOM complex is reduced upon depletion of TOM7. **a** Mitochondria isolated from control or TOM7 KD cells were analyzed by BN-PAGE followed by immunodecoration with an antibody against TOM40. Duplicates of each sample were loaded in an alternating manner to emphasize the different levels and migration behavior of the TOM complex. **b** Mitochondria were isolated from untreated U2OS cells or from cells treated with either scrambled (Scr.) siRNA or TOM7 siRNA. Radiolabeled TOM40 was imported into the isolated organelles for either 45 or 90 min and samples were analyzed via BN-PAGE and autoradiography (upper panel). After exposing to autoradiography, the same membrane was immunodecorated with TOM40 antibody to visualize the TOM endogenous complex (lower panel). The assembled TOM complex is indicated with an arrow. **c** Radiolabeled pSu9-DHFR was imported into control and TOM7 KD mitochondria for the indicated time periods. Unimported proteins were removed with PK and samples were analyzed via SDS-PAGE and autoradiography. The precursor (P) and mature (M) forms are indicated. **d** The bands corresponding to processed pSu9-DHFR were quantified and the intensity of the band corresponding to import into control mitochondria for 20 min was set to 100%. The results represent the average of three independent experiments (±SD). **e**, **f** Import into the indicated isolated organelles was performed and analyzed as described in the legend to Fig. 1a. Quantification of bands was as described in the legend to Fig. 2f. **g** Radiolabeled PBR was incubated with either control or TOM7 KD mitochondria for the indicated time periods. PK was added at the end of the import reaction and samples were then analyzed by SDS-PAGE and detected via autoradiography. A typical proteolytic fragment of membrane integrated PBR is indicated (F). **h** Bands representing the proteolytic fragment of PBR were quantified. The intensity of the band corresponding to import into control mitochondria for 20 min was set to 100%. The results represent the average of three independent experiments (±SD)

into the matrix via the presequence pathway; therefore, they rely on TOM40 as their initial entry gate.

Along the same line, and in agreement with previous results with fungal organelles [24], when radiolabeled TOM40 was imported, its integration into the MOM was reduced to around 60% when the entry channel was clogged with pSu9-DHFR (Fig. 7c, d). This reduction was more moderate than the one observed for the matrix proteins because the biogenesis of TOM40 does not require TIM23 and depends on the TOM and SAM complexes that are more abundant than the TOM/TIM23 supra-complexes. As expected, when PBR, which is not dependent on the TOM complex for its membrane assembly, was imported into mitochondria preincubated with pSu9-DHFR, we could not observe any difference as compared to control conditions (Fig. 7e, f). This observation suggests that there is no general defect in the import capacity of mitochondria upon the addition of the clogger. Finally, we imported radiolabelled PINK1 into depolarized mitochondria in which TOM40 was blocked by pSu9-DHFR. We observed a dramatic decrease in the PINK1 association with the TOM complex to less than 40% as compared to control reactions (Fig. 7g, h). Thus, these experiments strongly suggest that PINK1 uses the lumen of TOM40 for its stable association with the TOM complex.

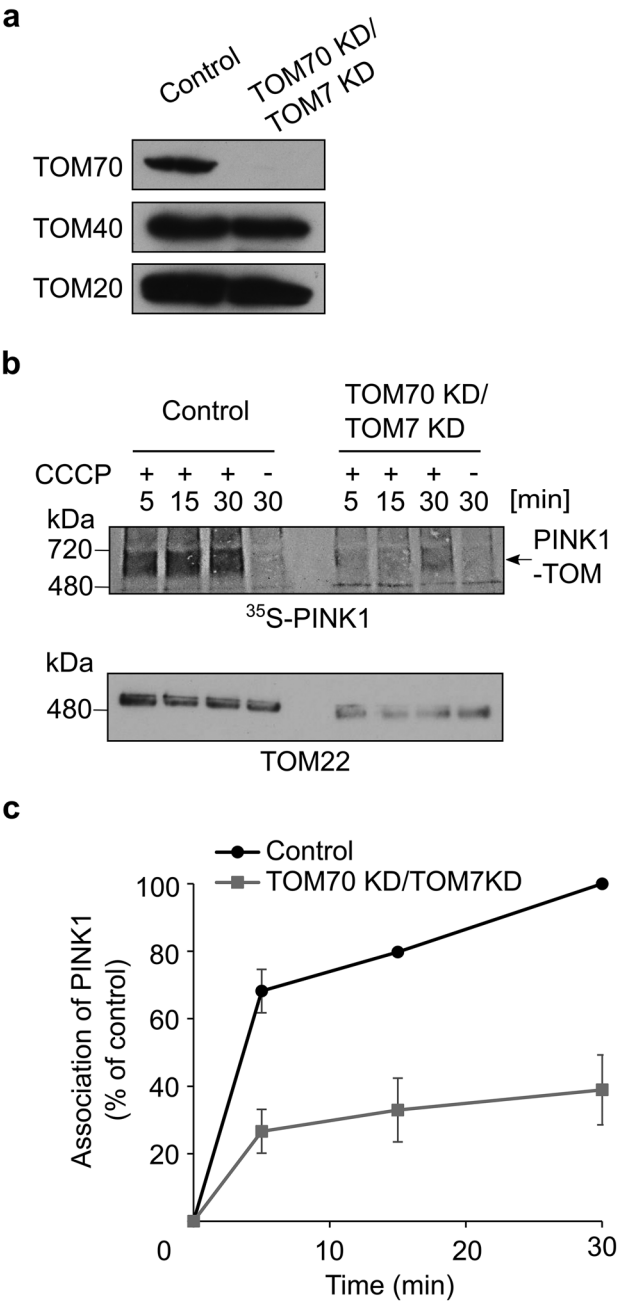

Fig. 6 Double knockdown of TOM70 and TOM7 has a dramatic effect on PINK1 import into depolarized mitochondria. **a** Mitochondria were isolated from either control or cells knocked down for both TOM70 and TOM7. Isolated organelles (50 µg) were analyzed by SDS-PAGE and western blotting with the indicated antibodies. **b** Radiolabeled PINK1 was imported into either control or TOM7/TOM70 KD depolarized mitochondria for the indicated time periods. Samples were subsequently analyzed by BN-PAGE and autoradiography (upper panel). After autoradiography exposures, the same membrane was incubated with TOM22 antibody to show the appearance of the TOM complex (lower panel). **c** The bands corresponding to PINK1 association with the TOM complex were quantified. The band corresponding to assembled PINK1 after 30 min import into control mitochondria was set to 100%. The results represent the average of three independent experiments (±SD)

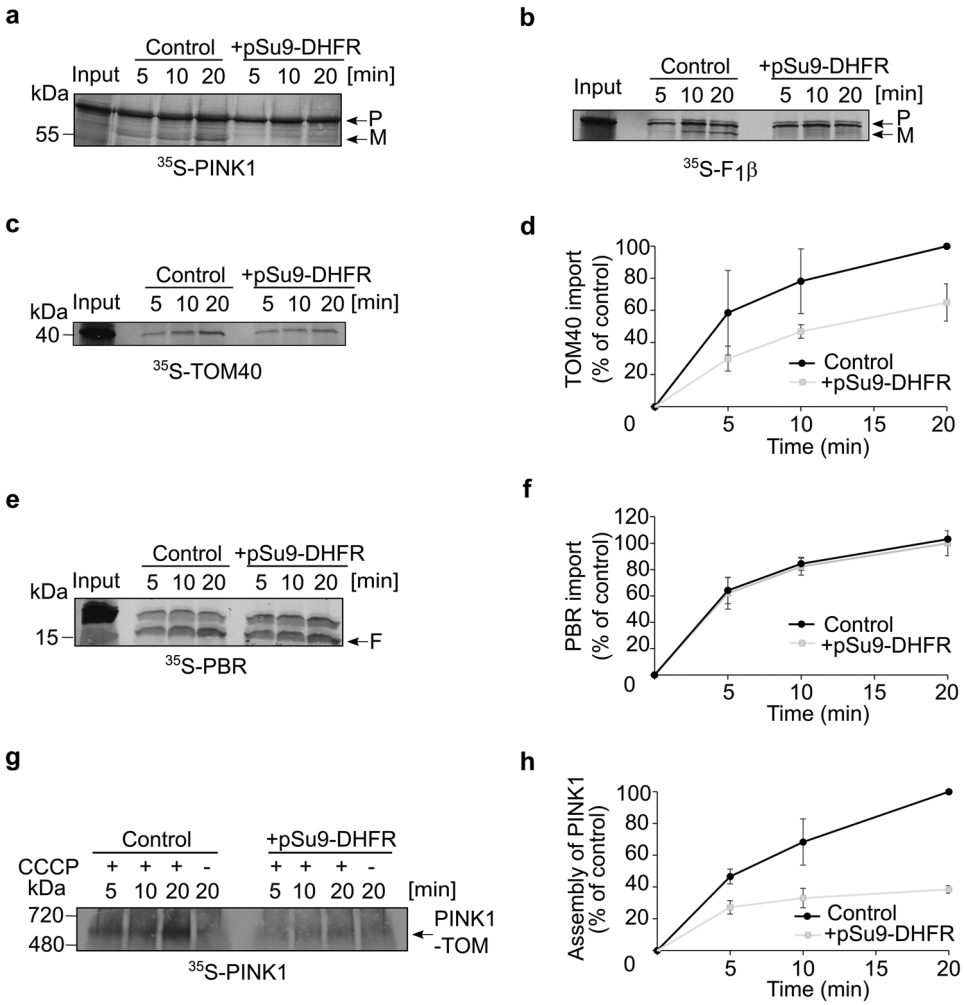

Fig. 7 TOM40 lumen is crucial for PINK1 association with the TOM complex. Isolated polarized mitochondria were preincubated in the absence or presence of purified pSu9-DHFR for 10 min on ice prior to the import of the radiolabeled proteins. Radiolabeled PINK1 (**a**), F1β (**b**), or TOM40 (**c**) were imported into the isolated organelles. Samples were then analyzed by SDS-PAGE followed by autoradiography. **d** The bands corresponding to membrane integrated TOM40 were quantified. The band corresponding to integrated TOM40 after 20 min import into untreated mitochondria was set to 100%. The results represent the average of three independent experiments (±SD). **e** Radiolabeled PBR was incubated with either treated or untreated mitochondria for the indicated time periods. PK was added at the end of the import reaction and samples were then analyzed by SDS-PAGE and detected via autoradiography. A typical proteolytic fragment of membrane integrated PBR is indicated (F). **f** Bands representing the proteolytic fragment of PBR were quantified. The intensity of the band corresponding to import into control mitochondria for 20 min was set to 100%. The results represent the average of three independent experiments (±SD). **g** Radiolabeled PINK1 was imported into either control or pSu9-DHFR treated mitochondria for the indicated time periods. Samples were subsequently analyzed by BN-PAGE and autoradiography. **h** The bands corresponding to PINK1 association with the TOM complex were quantified. The band corresponding to assembled PINK1 after 20 min import into control mitochondria was set to 100%. The results represent the average of three independent experiments (±SD)

TcPINK1 apparently blocks the TOM pore in depolarized mitochondria

Lastly, we aimed to determine which scenario is more probable upon mitochondrial depolarization: PINK1 is laterally released into the bulk of the MOM, gets stalled in the TOM40 pore, or remains bound to TOM, but outside the TOM40 barrel. To address this question, we purified recombinant TcPINK1, which was previously used in studies on structure–function relationships of PINK1 [13, 25–27]. We opted for TcPINK1 rather that human PINK1 since the former is more stable and can be easier purified as a recombinant protein. Initially, we confirmed that TcPINK1 can associate in depolarized mitochondria with human TOM complex to the same oligomeric species as human PINK1 (hPINK1) (Fig. 8a). Next, we performed reciprocal experiments to the ones described above by testing whether TcPINK1 can clog the TOM complex and thereby inhibit

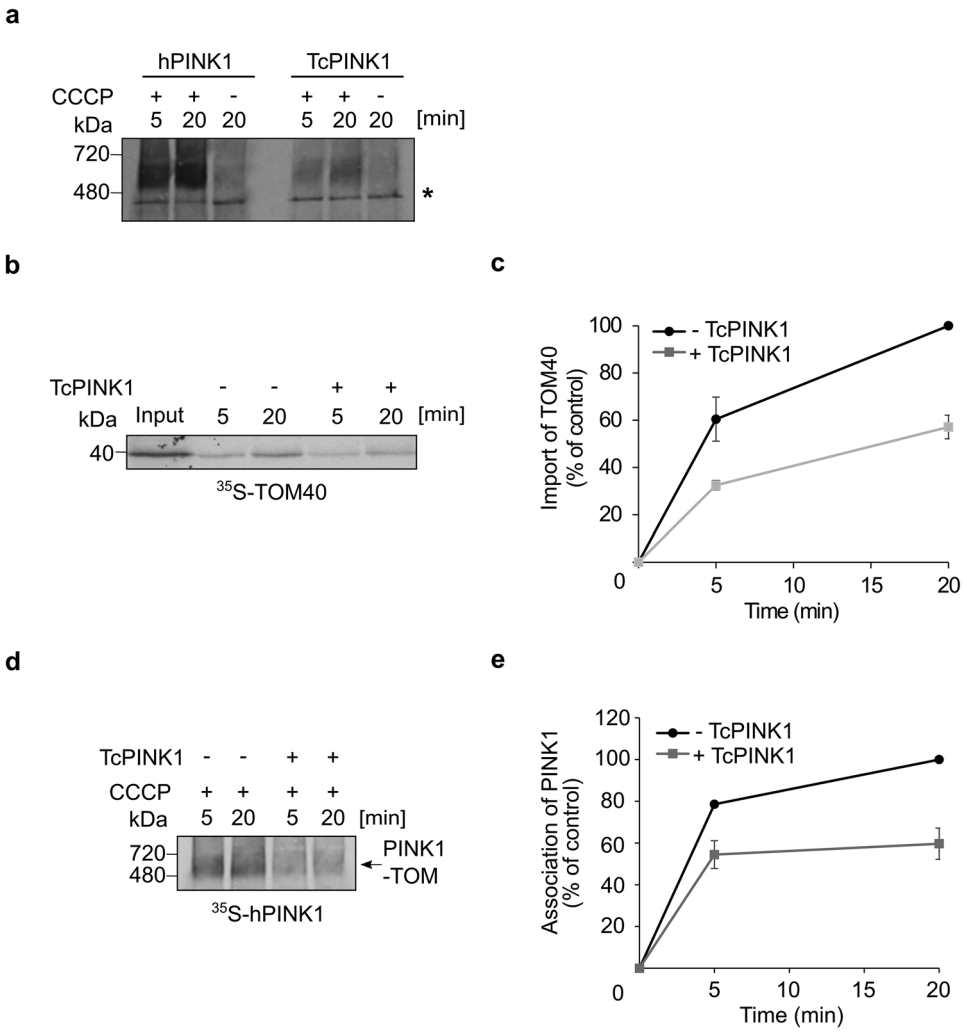

Fig. 8 TcPINK1 apparently blocks the TOM pore in depolarized mitochondria. **a** Radiolabeled hPINK1 and TcPINK1 were imported into mitochondria isolated from U2OS cells. The organelles were depolarized prior to the import in the indicated samples. Samples were then analyzed by BN-PAGE and autoradiography. *, indicates an unspecific band. **b** Radiolabeled TOM40 was incubated for indicated time periods with depolarized mitochondria that were preincubated in the presence or absence of recombinant TcPINK1. At the end of the import reactions, samples were subjected to alkaline extraction and the pellet fractions were analyzed by SDS-PAGE and autoradiography. **c** The bands corresponding to membrane-embedded TOM40 were quantified. The band corresponding to membrane embedded TOM40 after 20 min import into control mitochondria was set to 100%. The results present the average of two independent experiments (±SD). **d** Radiolabeled hPINK1 was incubated for indicated time periods with depolarized mitochondria that were preincubated in the presence or absence of recombinant TcPINK1. At the end of the import reactions, samples were analyzed by BN-PAGE and autoradiography. **e** The bands corresponding to PINK1 association with the TOM complex were quantified. The intensity of the band corresponding to assembled PINK1 in control mitochondria after 20 min was set up to 100%. The results represent the average of three independent experiments (±SD)

the import of other TOM-dependent substrates. Hence, we performed in organello import assays in which mitochondria were first depolarized and incubated with TcPINK1. Subsequently, radiolabeled TOM40 or hPINK1 was imported into these treated organelles. We observed that both proteins were compromised in their integration into the MOM under these conditions (Fig. 8b–e). Of note, import of TOM40 into mitochondria in which the TOM pore was blocked with either pSu9-DHFR (Fig. 7c, d) or TcPINK1 (Fig. 8b, c) resulted in a similar import reduction to approximately 60%. Although, we cannot exclude the possibility that the kinase domain of PINK1 contributes to the import inhibition by hindering access of other substrates to the TOM pore, we assume that most of the competition is because PINK1, similarly to pSu9-DHFR, occupies the lumen of the TOM pore in depolarized mitochondria.

Discussion

PINK1 import into healthy mitochondria is relatively well described; however, its fate in depolarized organelle remained unclear. In the current study, TOM70 was found to be the main receptor for PINK1 import into either healthy or compromised mitochondria. Our results are in line with previous report [16] and demonstrate in addition direct interaction between both proteins. Although the single depletion of TOM20 did not result in a major reduction of PINK1 interactions with the TOM complex, the double KD of both receptors TOM20 and TOM70, caused a dramatic decrease in this interaction, which was more than expected according to the additive effects of the single KDs. Thus, we conclude that, although TOM70 plays the primary role, both receptors can contribute to the import of PINK1 and if one of them is missing, the other can compensate (at least partially) for this absence. The fact that PINK1 contains a classical MTS and yet does not primarily depend on TOM20 shows that either, as reported before for other substrates [20], TOM70 can also recognize this MTS, or that the internal signals like the OMS or the TMD, which can be recognized by TOM70, are playing a superior role in recognition at the surface of the organelle under these conditions. Of note, our peptides scan assay showed that TOM70 can bind all the three elements (MTS, OMS, and TMD) of PINK1 and thus the two aforementioned options are not mutually exclusive.

Regardless of the identity of the primary receptor, after the initial recognition, PINK1 molecules are relayed to further locations within the MOM of depolarized organelles. A previous report on that topic suggested that TOM7 mediates the lateral translocation of the PINK1 from the TOM40 pore [14]. However, the recently published atomic structure of the human TOM complex, where the β-barrels formed by TOM40 appear to be tightly closed [28, 29], raised the question if such a lateral release can be anticipated. As was already published before [22], our findings suggest that the TOM complex in the absence of TOM7 is less stable. If TOM7 is indeed a gate for a lateral release, we would assume that initial PINK1 association with the TOM complex should not be affected, but rather further downstream steps. However, we observe that the absence of TOM7 causes a reduction in the initial association of PINK1with the TOM complex. Therefore, and considering the observation that also other substrates are affected by depletion of TOM7, we propose that the contribution of TOM7 to the association of PINK1 with the MOM is probably rather indirect and occurs through the stabilization effect of TOM7 on the overall structure of the TOM complex. Although we do not favor this option, we cannot exclude the possibility that PINK1 binds both TOM7 and TOM70 at two different places, which would explain why the double KD TOM7/TOM70 has such a dramatic effect on formation of PINK1-TOM.

In an additional set of experiments, we demonstrate that PINK1 association with the TOM complex is compromised by clogging the lumen of this complex and reciprocally, PINK1 itself can block the import pore of the translocase. Hence, although previous reports suggested a PINK1 lateral release from the TOM complex [11, 14], we favor the possibility that PINK1 remains at the lumen of the TOM40 in depolarized organelles. The following arguments support this proposal: (i) PINK1 co-migrates with the core TOM complex on BN-PAGE that consists of TOM40, TOM22, and accessory small TOMs: TOM5, TOM6, TOM7. This means that the interactions of PINK1 with the TOM complex are stable enough to sustain the analysis conditions. (ii) Blocking of the TOM channel by PINK1 would also prevent an import of all other TOM-dependent substrate proteins. Such a blockage would be prudent as the malfunctional compromised organelles are destined for degradation upon induction of mitophagy. (iii) PINK1 was reported to be reimported and cleaved by PARL rather fast upon re-polarization of mitochondria [11]. Location of PINK1 at the pore of the TOM complex can readily explain such a fast re-import. In contrast, re-translocation from the lipid core of the MOM would require initially an extraction from the membrane and then, a putative re-entering route into the TOM complex. Nevertheless, despite these supportive arguments, only future structural studies of the PINK1-TOM adduct would be able to resolve this issue. In summary, our current study provides new insights into the crucial initial stage of PINK1-dependent mitophagy namely, the anchoring of PINK1 to the MOM of compromised mitochondria.

Materials and methods

Cell culture and induction of knockdown of selected proteins

HeLa and U2OS cells were used in the current study, and both were cultured at 37 °C under 5% CO_2 in Dulbecco's modified Eagles medium (DMEM, Gibco) supplemented with 10% (vol/vol) fetal bovine serum (FBS). To knock down TOM70, HeLa cells expressing shRNA against TOM70 under the control of doxycycline promoter were used [30]. To deplete TOM70, 1 μg/ml doxycycline was added every second day for 7 days.

TOM20 and TOM7 KDs were induced with Flex-iTube siRNA purchased from QIAGEN (SI00301959 and SI04364955, respectively). The target sequences were 5′-AAAGTTACCTGACCTTAAAGA-3′ in the case of TOM20 and 5′-CACGGCCGTCGCCATGGTGAA-3′ for TOM7. U2OS cells were transfected twice with these siRNAs with a

24 h interval. After 72 h, the cells were harvested, and mitochondria isolated. To create TOM70/TOM20 or TOM70/TOM7 double KD lines, HeLa cells were first induced with 1 µg/ml doxycycline for 24 h and then transfected with siRNA against either TOM20 or TOM7 twice within 24 h interval. Each time, the cells were recovered with DMEM containing 20% FBS and 2 µg/ml doxycycline. Cells were harvested 72 h after the second transfection with TOM20 or TOM7 siRNA, and isolation of mitochondria was performed. According to the required amount of isolated mitochondria, cells were seeded in different numbers of TC Dish 150 Standard plates and grown until 80% confluent.

Isolation of mitochondria

Cells were washed once with PBS buffer and scraped from the plate using a spatula before transferring the cell suspension to a small Eppendorf tube. Subsequently, the cells were centrifuged(300×*g*, 5 min, 4 °C) and resuspended in HMS-A buffer (0.22 M mannitol, 0.07 M sucrose, 0.02 M HEPES–KOH, pH 7.6, 1 mM EDTA, 0.1% BSA, 1 mM phenylmethylsulfonyl fluoride (PMSF)). The used buffers were described previously [18]. Afterwards, the samples were passed nine times through needles of different sizes (20G, 23G, and 27G, Sterican). The homogenized lysates were centrifuged (900×*g*, 5 min, 4 °C) and the supernatants were collected whereas the pellets were discarded. The latter supernatants were centrifuged (9000×*g*, 15 min, 4 °C) to obtain crude mitochondria in pellets. The pellets were then washed with HMS-B buffer (HMS-A buffer lacking BSA) and centrifuged again (10,000×*g*, 10 min, 4 °C). The pellets representing the mitochondrial fraction were used for in vitro import assays.

Mitochondrial in vitro import followed by SDS-PAGE or BN-PAGE

Radiolabeled proteins were synthesized in the presence of ^{35}S-methionine and ^{35}S-cysteine using either coupled reticulocyte lysate system (TNT, Promega) or uncoupled reticulocyte lysate system (Promega). For the import reaction, 50–100 µg of isolated mitochondria were resuspended in HS buffer (20 mM HEPES–KOH, pH 7.6, 250 mM sucrose, 5 mM magnesium acetate, 80 mM potassium acetate, 7.5 mM glutamate, 5 mM malate, 1 mM DTT) and incubated at 30 °C for different time periods with radiolabeled proteins in the presence of 4 mM ATP and 2 mM NADH. Where indicated, mitochondria were pre-incubated for 5 min on ice with 20 µM of the uncoupler carbonyl cyanide chlorophenylhydrazone (CCCP) prior to the import reactions.

To clog the TOM pore, isolated organelles were pre-incubated on ice for 10 min with 20 µg of recombinantly expressed pSu9-DHFR-His, in the presence of 1 mM methotrexate and 1 mM NADPH prior to the import of the radiolabeled proteins. Alternatively, the TOM pore was blocked by addition of 10–20 µg of TcPINK1 for 10 min at 30 °C. At the end of the import reactions, samples were centrifuged (13,200×*g*, 10 min, 4 °C) and handled differently depending on the expected localization of the protein of interest within the organelle. Isolated mitochondria with imported outer membrane proteins such as PBR/TSPO and matrix localized proteins were treated on ice for 20 min with 50 µg/ml of proteinase K. To inactivate the protease, 5 mM of PMSF was added to each reaction and the reaction was kept on ice for 10 min. Subsequently, the samples were centrifuged (20,000×*g*, 10 min, 4 °C) and the pellets were mixed with 2×sample buffer and boiled for 5 min at 95 °C.

Import of TOM40 was monitored by resistance to alkaline extraction. To this aim, mitochondria were incubated for 30 min with 0.1 M Na_2CO_3 at 4 °C. Then, samples were centrifuged (76,000×g, 30 min, 2 °C), and the pellets were dissolved in 40 µl of 2×sample buffer and heated at 95 °C for 5 min before further analysis by SDS-PAGE. In some cases, the import of F1β and PINK1 was monitored by processing of the protein upon mitochondrial import. In these cases, at the end of the import reactions, the mitochondrial pellets were directly resuspended in 2×sample buffer.

Some import reactions were analyzed by blue native (BN)-PAGE. In such cases, at the end of the import reactions, the samples were centrifuged (13,200×*g*, 10 min, 4 °C) and the pellets resuspended in digitonin-containing HMS-B buffer (3:1 (w/w) ratio of detergent to protein). Organelles were solubilized for 30 min at 4 °C and non-solubilized material was removed via centrifugation (13,000×*g*, 10 min, 4 °C). The supernatant was mixed with BN-PAGE sample buffer (5% w/v Coomassie blue G, 500 mM ε-Amino-n-caproic acid, 100 mM Bis–Tris, pH 7.0) and samples were separated through a 4–16% polyacrylamide gradient gel. Radiolabeled proteins were detected by autoradiography.

Expression and purification of recombinant proteins

Recombinant pSu9-DHFR-His was purified using a previously described protocol [23]. In brief, overnight culture of *Escherichia coli* BL21 cells expressing pSu9-DHFR-His was diluted in the morning to OD_{600} of 0.1 and once the culture reached an OD of 0.5, it was induced with 1 mM IPTG. The culture was grown for 3 h at 37 °C and then cells were harvested by centrifugation. The pellet was resuspended in ice-cold buffer containing 50 mM Tris–HCl, pH 7.5, 150 mM NaCl as well as protease inhibitor cocktail (Sigma-Aldrich) and sonicated. The lysate was centrifuged to get rid of cell debris (15,000×*g*, 15 min, 4 °C) and the clarified supernatant was applied to a nickel affinity resin column (Cube Biotech). The column was first washed with the buffer mentioned above supplemented with 10 mM imidazole.

pSu9-DHFR-His was eluted in two steps using 40 mM and then 100 mM imidazole-containing buffer. To dilute out the imidazole and concentrate the sample, the eluted fractions were dialyzed against the same buffer lacking imidazole.

The purification of TcPINK1 was according to a protocol published by Rasool et al. [26]. The concentrated TcPINK1 was further purified by size exclusion chromatography (Superdex S200, GE Healthcare).

For purification of GST-fusion proteins, overnight cultures of *Escherichia coli* BL21 expressing GST alone, GST-Tom70, or GST-Tom20 were diluted in the morning to OD_{600} of 0.1 and, once the culture reached an OD of 0.5, it was induced with 1 mM IPTG. The cultures were grown for 4 h at 37 °C and then the cells were harvested by centrifugation. The cells at the pellets were resuspended in ice-cold GST lysis buffer (20 mM HEPES, pH 7.25, 100 mM NaCl, 1.5 mM $MgCl_2$, 2 mM PMSF, 1 mM DTT, 3 mM EDTA, protease inhibitor cocktail) and sonicated. Lysates were then centrifuged to remove cell debris (15,000 × *g*, 15 min, 4 °C). Glutathione Sepharose 4B beads (GE Healthcare) were washed with GST basic buffer (20 mM HEPES, pH 7.25, 100 mM NaCl, 1.5 mM $MgCl_2$) and incubated overnight at 4 °C with the resulting supernatants. The beads with bound proteins were then transferred to purification columns. The columns were washed with GST basic buffer and subsequently, proteins were eluted with GST basic buffer containing 15 mM reduced L-glutathione. The fractions with the eluted proteins were then dialyzed to clear out L-glutathione and to concentrate the samples. Such purified proteins were then used in pull-down experiments. Tom70 used for peptide scan was further incubated overnight at 4 °C with thrombin to cleave the GST tag. Afterwards, the GST moiety was rebound to the glutathione beads in the column and the flow-through containing Tom70 without the GST-tag was collected and used for further experiments.

Immunodepletion and antibody shift of TOM complex from solubilized mitochondria

After import of PINK1 into depolarized mitochondria, the reactions were centrifuged (13,200 × *g*, 10 min, 4 °C) and the pellets were solubilized with digitonin as described above. Non-solubilized material was removed via centrifugation (13,000 × *g*, 10 min, 4 °C) and the resulting supernatant was incubated for 30 min at 4 °C with antibodies against TOM22. Next, this mixture was incubated for another 30 min at 4 °C with Protein A beads that were pre-washed with HMS-B buffer. The reaction mixtures were centrifuged (500 × *g*, 1 min, 4 °C) and the supernatants were mixed with BN-PAGE sample buffer. Centrifuged protein A beads were washed three times with HMS-B buffer and proteins were eluted at 95 °C for 10 min with 2 × sample buffer. In case of the antibody shift, the supernatant containing solubilized mitochondria was incubated for 30 min at 4 °C in the absence or presence of antibodies raised against either TOM22 and ATP5A and then samples were analyzed by BN-PAGE and autoradiography.

Peptide scan

Cellulose membranes harboring 15-mer peptides covering the sequence of a.a. residues 1–140 of PINK1 were activated in methanol for 1 min and washed twice with sterile water for 1 min. Then, membranes were equilibrated at room temperature with binding buffer (50 mM Tris–HCl, 150 mM NaCl, 0.1% Triton X 100, pH 7.5) for 2 h. After blocking with 1 µM BSA for 1 h, membranes were incubated overnight with recombinant Tom70-cytosolic domain. Next, the membranes were washed three times with binding buffer and bound protein was visualized by immunodecoration using antibodies against Tom70.

Pull-down of radiolabelled proteins with GST-fusion proteins

Radiolabeled proteins were synthesized as described above. Glutathione Sepharose 4B beads (GE Healthcare) were washed with GST basic buffer and incubated with purified GST-fusion proteins for 1 h at 4 °C. Then, the reactions were centrifuged (500 × *g*, 1 min, 4 °C) and supernatants discarded. Subsequently, the beads with bound recombinant proteins were blocked for 1 h at 4 °C using reticulocyte lysate (Promega). Next, the beads were reisolated (500 × *g*, 1 min, 4 °C) and incubated for 1 h at 4 °C with radiolabeled proteins. ATP (0.2 mM) was added to the reactions every 30 min. At the end of the binding reactions, the samples were centrifuged again (500 × *g*, 1 min, 4 °C) and supernatants discarded. The beads were then washed twice with GST basic buffer and pelleted again. Bound proteins were eluted at 95 °C for 10 min with 2 × sample buffer and analyzed with SDS-PAGE followed by autoradiography.

Supplementary Information The online version contains supplementary material available at https://doi.org/10.1007/s00109-022-02191-6.

Acknowledgements We thank E. Kracker for excellent technical assistance, N. Bartlick and A. Stasiak for help with some experiments, A.N. Bayne for help with the purification of TcPINK1, and V. Kozjak-Pavlovic for kindly providing cells.

Author contribution Klaudia K. Maruszczak designed and conducted experiments and analyzed data, Martin Jung prepared the peptide scan membranes, Shafqat Rasool and Jean-François Trempe established a purification protocol for TcPINK1, Doron Rapaport designed experiments and analyzed data. The first draft of the manuscript was written by Klaudia K. Maruszczak and all authors commented on previous versions of the manuscript. All authors read and approved the final manuscript.

Funding Open Access funding enabled and organized by Projekt DEAL. This research was supported by the German Research Foundation (DFG) through Research Training Group 2364 to K.M. and D.R. and through CRC 894 to M.J.

Availability of data and materials The datasets and cell lines generated during the current study are not publicly available but are available from the corresponding author on reasonable request.

Declarations

Ethics approval and consent to participate Not applicable.

Consent for publication Not applicable.

Competing interests The authors declare no competing interests.

References

1. Ni HM, Williams JA, Ding WX (2015) Mitochondrial dynamics and mitochondrial quality control. Redox Biol 4:6–13. https://doi.org/10.1016/j.redox.2014.11.006
2. Bertram R, Gram Pedersen M, Luciani DS, Sherman A (2006) A simplified model for mitochondrial ATP production. J Theor Biol 243:575–586. https://doi.org/10.1016/j.jtbi.2006.07.019
3. Vincow ES, Merrihew G, Thomas RE, Shulman NJ, Beyer RP, MacCoss MJ, Pallanck LJ (2013) The PINK1-Parkin pathway promotes both mitophagy and selective respiratory chain turnover in vivo. Proc Natl Acad Sci 110:6400–6405. https://doi.org/10.1073/pnas.1221132110
4. Greene AW, Grenier K, Aguileta MA, Muise S, Farazifard R, Haque ME, McBride HM, Park DS, Fon EA (2012) Mitochondrial processing peptidase regulates PINK1 processing, import and Parkin recruitment. EMBO Rep 13:378–385. https://doi.org/10.1038/embor.2012.14
5. Yamano K, Youle RJ (2013) PINK1 is degraded through the N-end rule pathway. Autophagy 9:1758–1769. https://doi.org/10.4161/auto.24633
6. Narendra DP, Jin SM, Tanaka A, Suen DF, Gautier CA, Shen J, Cookson MR, Youle RJ (2010) PINK1 is selectively stabilized on impaired mitochondria to activate Parkin. PLoS Biol 8:e1000298. https://doi.org/10.1371/journal.pbio.1000298
7. Matsuda N, Sato S, Shiba K, Okatsu K, Saisho K, Gautier CA, Sou YS, Saiki S, Kawajiri S, Sato F (2010) PINK1 stabilized by mitochondrial depolarization recruits Parkin to damaged mitochondria and activates latent Parkin for mitophagy. J Cell Biol 189:211–221. https://doi.org/10.1083/jcb.200910140
8. Morais VA, Verstreken P, Roethig A, Smet J, Snellinx A, Vanbrabant M, Haddad D, Frezza C, Mandemakers W, Vogt-Weisenhorn D et al (2009) Parkinson's disease mutations in PINK1 result in decreased complex I activity and deficient synaptic function. EMBO Mol Med 1:99–111. https://doi.org/10.1002/emmm.200900006
9. Hasson SA, Kane LA, Yamano K, Huang CH, Sliter DA, Buehler E, Wang C, Heman-Ackah SM, Hessa T, Guha R et al (2013) High-content genome-wide RNAi screens identify regulators of Parkin upstream of mitophagy. Nature 504:291–295. https://doi.org/10.1038/nature12748
10. Nguyen TN, Padman BS, Lazarou M (2016) Deciphering the molecular signals of PINK1/Parkin mitophagy. Trends Cell Biol 26:733–744. https://doi.org/10.1016/j.tcb.2016.05.008
11. Lazarou M, Jin S, Kane L, Youle R (2012) Role of PINK1 binding to the TOM complex and alternate intracellular membranes in recruitment and activation of the E3 ligase Parkin. Dev Cell 22:320–333. https://doi.org/10.1016/j.devcel.2011.12.014
12. Okatsu K, Uno M, Koyano F, Go E, Kimura M, Oka T, Tanaka K, Matsuda N (2013) A dimeric PINK1-containing complex on depolarized mitochondria stimulates Parkin recruitment. J Biol Chem 288:36372–36384. https://doi.org/10.1074/jbc.m113.509653
13. Rasool S, Veyron S, Soya N, Eldeeb MA, Lukacs GL, Fon EA, Trempe JF (2021) Mechanism of PINK1 activation by autophosphorylation and insights into assembly on the TOM complex. Mol Cell. https://doi.org/10.1016/j.molcel.2021.11.012
14. Sekine S, Wang C, Sideris DP, Bunker E, Zhang Z, Youle RJ (2019) Reciprocal roles of Tom7 and OMA1 during mitochondrial import and activation of PINK1. Mol Cell 73:1028-1043.e5. https://doi.org/10.1016/j.molcel.2019.01.002
15. Zhang C, Wang R, Liu Z, Bunker E, Lee S, Giuntini M, Chapnick D, Liu X (2019) The plant triterpenoid celastrol blocks PINK1-dependent mitophagy by disrupting PINK1's association with the mitochondrial protein TOM20. J Biol Chem 294:7472–7487. https://doi.org/10.1074/jbc.ra118.006506
16. Kato H, Lu Q, Rapaport D, Kozjak-Pavlovic V (2013) Tom70 is essential for PINK1 import into mitochondria. PLoS ONE 8:e58435. https://doi.org/10.1371/journal.pone.0058435
17. Okatsu K, Kimura M, Oka T, Tanaka K, Matsuda N (2015) Unconventional PINK1 localization mechanism to the outer membrane of depolarized mitochondria drives Parkin recruitment J Cell Sci 128. https://doi.org/10.1242/jcs.161000
18. Becker D, Richter J, Tocilescu MA, Przedborski S, Voos W (2012) Pink1 kinase and its membrane potential (deltaψ)-dependent cleavage product both localize to outer mitochondrial membrane by unique targeting mode. J Biol Chem 287:22969–22987. https://doi.org/10.1074/jbc.M112.365700
19. Endo T, Yamano K, Kawano S (2011) Structural insight into the mitochondrial protein import system. Biochimica et Biophysica Acta (BBA) - Biomembranes 1808:955–970. https://doi.org/10.1016/j.bbamem.2010.07.018
20. Backes S, Hess S, Boos F, Woellhaf MW, Gödel S, Jung M, Mühlhaus T, Herrmann JM (2018) Tom70 enhances mitochondrial preprotein import efficiency by binding to internal targeting sequences. J Cell Biol 217:1369–1382. https://doi.org/10.1083/jcb.201708044
21. Zhou C, Huang Y, Shao Y, May J, Prou D, Perier C, Dauer W, Schon EA, Przedborski S (2008) The kinase domain of mitochondrial PINK1 faces the cytoplasm. Proc Natl Acad Sci 105:12022–12027. https://doi.org/10.1073/pnas.0802814105
22. Kato H, Mihara K (2008) Identification of Tom5 and Tom6 in the preprotein translocase complex of human mitochondrial outer membrane. Biochem Biophys Res Commun 369:958–963. https://doi.org/10.1016/j.bbrc.2008.02.150
23. Otera H, Taira Y, Horie C, Suzuki Y, Suzuki H, Setoguchi K, Kato H, Oka T, Mihara K (2007) A novel insertion pathway of

mitochondrial outer membrane proteins with multiple transmembrane segments. J Cell Biol 179:1355–1363. https://doi.org/10.1083/jcb.200702143
24. Rapaport D, Neupert W (1999) Biogenesis of Tom40, core component of the TOM complex of mitochondria. J Cell Biol 146:321–332. https://doi.org/10.1083/jcb.146.2.321
25. Kumar A, Tamjar J, Waddell AD, Woodroof HI, Raimi OG, Shaw AM, Peggie M, Muqit MM, van Aalten DM (2017) Structure of PINK1 and mechanisms of Parkinson's disease-associated mutations. ELife 6. https://doi.org/10.7554/elife.29985
26. Rasool S, Soya N, Truong L, Croteau N, Lukacs GL, Trempe J (2018) PINK 1 autophosphorylation is required for ubiquitin recognition. EMBO reports 19. https://doi.org/10.15252/embr.201744981
27. Okatsu K, Sato Y, Yamano K, Matsuda N, Negishi L, Takahashi A, Yamagata A, Goto-Ito S, Mishima M, Ito Y et al (2018) Structural insights into ubiquitin phosphorylation by PINK1. Scientific Reports 8 https://doi.org/10.1038/s41598-018-28656-8
28. Wang W, Chen X, Zhang L, Yi J, Ma Q, Yin J, Zhuo W, Gu J, Yang M (2020) Atomic structure of human TOM core complex. Cell Discovery 6. https://doi.org/10.1038/s41421-020-00198-2
29. Guan Z, Yan L, Wang Q, Qi L, Hong S, Gong Z, Yan C, Yin P (2021) Structural insights into assembly of human mitochondrial translocase TOM complex Cell Discovery 7. https://doi.org/10.1038/s41421-021-00252-7
30. Kozjak-Pavlovic V, Ross K, Benlasfer N, Kimmig S, Karlas A, Rudel T (2007) Conserved roles of Sam50 and metaxins in VDAC biogenesis. EMBO Rep 8:576–582. https://doi.org/10.1038/sj.embor.7400982

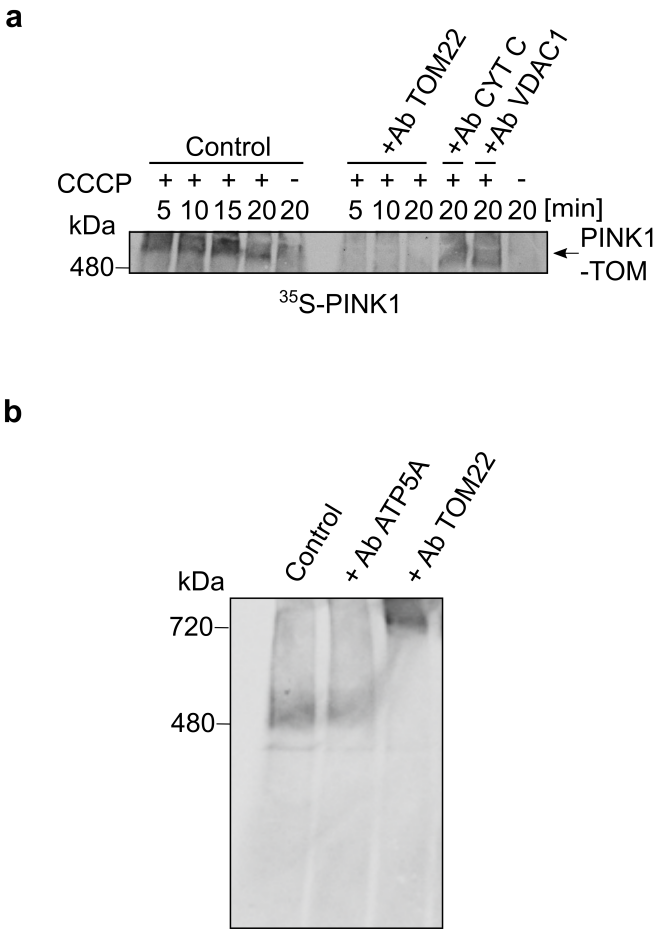

Supplementary Figure 1. **PINK1 associates specifically with the TOM complex upon depolarization of mitochondria. (a)** Radiolabeled PINK1 was incubated for the indicated time periods with isolated mitochondria, which in some cases were pretreated with CCCP. Organelles were then solubilized with digitonin and the lysate was incubated for 30 min at 4° C with antibodies against TOM22, Cytochrome C (CYT C), or VDAC1. Next, protein A beads were added for 30 min at 4°C and beads were pelleted. The supernatants were analyzed by BN- PAGE followed by autoradiography. **(b)** Radiolabeled PINK1 was incubated with CCCP-treated mitochondria for 20 min. Organelles were then solubilized with digitonin and the lysates were incubated for 30 min at 4°C in the absence or presence of antibodies against either ATP5A or TOM22. The samples were analyzed by BN-PAGE followed by autoradiography.

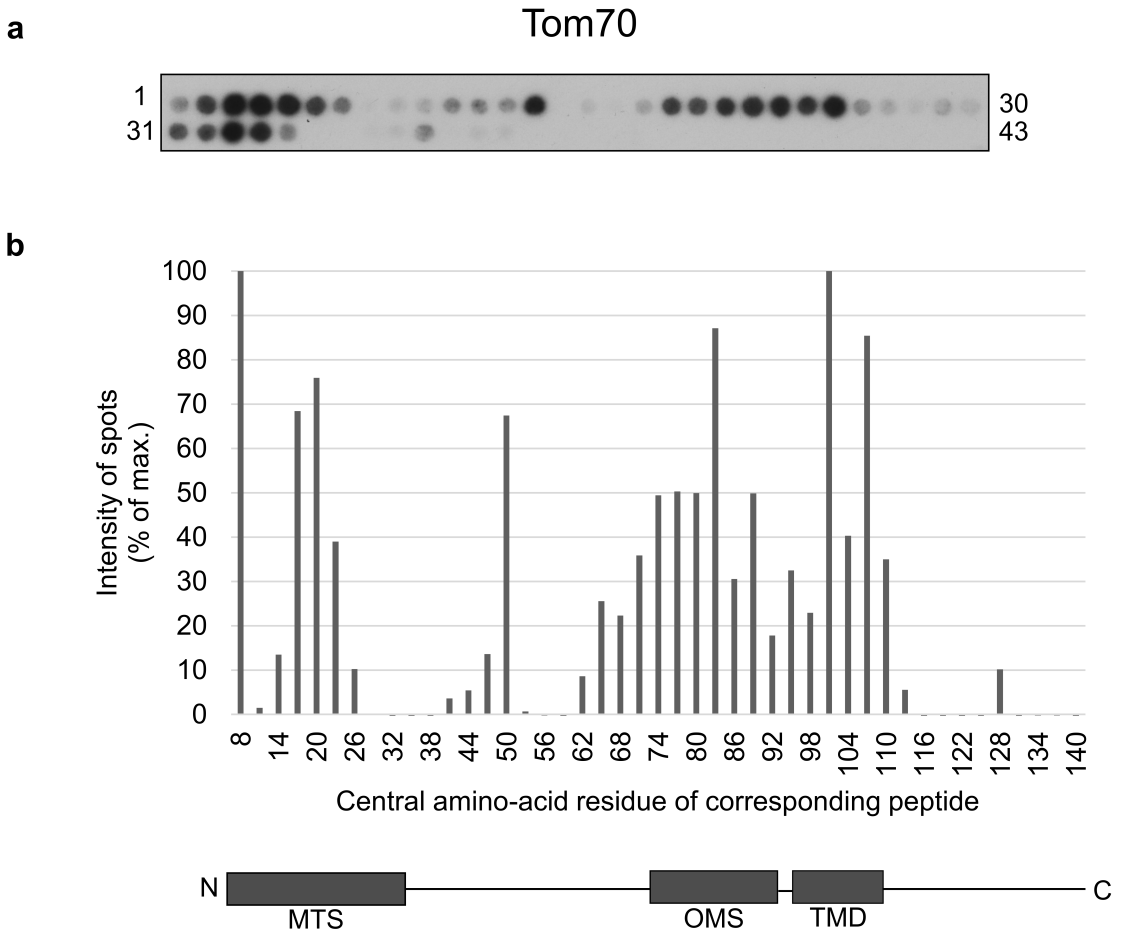

Maruszczak et al., Fig. S2

Supplementary Figure 2. **The cytosolic domain of Tom70 interacts directly with PINK1.** **(a)** Nitrocellulose membrane containing 15-mer peptides covering amino acid residues 1-140 of PINK1 was incubated with recombinantly expressed cytosolic domain of yeast Tom70. After incubation, the interaction was visualized by immunodecoration using antibody against Tom70. The numbers flanking the panel reflect the serial numbers of the peptides. **(b)** The intensity of each dot was quantified and the average quantification of three independent experiments were plotted. The dot with the strongest intensity was set as 100%. The numbers on the X-axis reflect the central amino acid residue of each peptide. Lower panel: A schematic representation of the N-terminal region of PINK1 is shown. MTS, mitochondrial targeting signal; OMS, outer mitochondrial membrane localization signal; TMD, transmembrane domain. **(c)** GST, GST-Tom20, and GST-Tom70 were bound to glutathione beads and incubated with radiolabeled PINK1 for 1 h. Afterwards, proteins bound to the beads were eluted with 2x Sample buffer and analyzed by SDS-PAGE followed by blotting onto a nitrocellulose membrane. Radiolabeled proteins were detected by autoradiography whereas the recombinant GST-fusion proteins were visualized by Ponceau staining. **(d)** GST-Tom70 was bound to glutathione beads and incubated for 1 h with radiolabeled eGFP (as a control), PINK1(1-120)-eGFP, or PINK1(35-120)-eGFP. Afterwards, bound proteins were eluted with 2x Sample buffer and analyzed with SDS-PAGE followed by blotting onto a nitrocellulose membrane. Radiolabeled proteins were detected by autoradiography whereas recombinant GST-Tom70 was visualized by Ponceau staining.

Table S1. List of cell lines used in this study.

Histology	Cell line	Growth medium*	Source	Note
Human cervical cancer	HeLa	DMEM*	Kindly provided by Vera Kozjak-Pavlovic, Würzburg, Germany	HeLa cells carrying a doxycycline-inducible shRNA directed against TOM70 (Kozjak-Pavlovic *et al.*, 2007). Uninduced cells were used as control in this study.
Human osteosarcoma	U2OS	DMEM*	Kindly provided by Ana J. Garcia-Saéz, Köln, Germany	

* DMEM (Dulbecco's Modified Eagle's Medium – low glucose with 1000 mg/L, L-glutamine, and sodium bicarbonate supplemented with fetal bovine serum (10% or 20%) and Penicillin-Streptomycin (10,000 units penicillin and 10 mg streptomycin/mL), all purchased from Sigma-Aldrich, Germany.

Table S2. List of plasmids used in this study.

Plasmid	Promoter	Coding Sequence	Markers	Source
pRS426-PINK1-eGFP	TPI	Human PINK1 (full-length)-GFP	Amp, URA3	Lab stock
pRS426-PINK1(35-120)-eGFP	TPI	Human PINK1(35-120)-GFP	Amp, URA3	Lab stock
pRS426-PINK1(1-120)-eGFP	TPI	Human PINK1(1-120)-GFP	Amp, URA3	Lab stock
pIVEX1.3-PINK1	T7	Human PINK1 full-length	Amp	This study
pGEM4-F1β	SP6	*S. cerevisiae* F1β	Amp	Lab stock
pGEM4-hTOM40	SP6	Human TOM40	Amp	Lab stock
pSP64-PBR-HA	SP6	*Mus musculus* PBR-HA	Amp	Lab stock
pGEM4-GFP	SP6	GFP	Amp	Lab stock

pGEX4TI-GST-Tom20cd	Tac	*S. cerevisiae* Tom20 cytosolic domain N-terminally tagged with GST	Amp	Lab stock
pGEX4TI-GST-Tom70cd	Tac	*S. cerevisiae* Tom70 cytosolic domain N-terminally tagged with GST	Amp	Lab stock
pGEX4TI-GST	Tac	GST	Amp	Lab stock
pQE60-pSu9-DHFR-His	T5	*Neurospora Crassa* pSu9 tagged with DHFR and His	Amp	Lab stock
pGEX6p1-TcPINK1(1-570)	Tac	*Tribolium castaneum* PINK1(1-570), N-terminally tagged with GST (HRV 3C protease cleavage site between the sequences)	Amp	Lab of Jean-Francois Trempe, Montreal, Canada
pGEM4-pSu9-DHFR	SP6	*Neurospora Crassa* pSu9 tagged with DHFR	Amp	Lab stock

Table S3. List of primers used in this study.

Primer name	**Sequence (5'-3')**	**Note**
TNT_hPINK1_For	ATTTAGGTGACACTATAGaagacacggaattcaagccaccatggcggtgcgacaggcgctg	Contains SP6 promoter and Kozak sequence upstream PINK1 (human) starting sequence; used to produce linear DNA for coupled transcription and translation
TNT_hPINK1_Rev	cgatccttacagggctgccctccatgagcagagg	Anneals to the 3' sequence of PINK1 (human), contains the stop codon; used to produce linear DNA for coupled transcription and translation
hPINK1_S228A_For	cggcaggtgcgtccagcgaagcc	Mutagenesis S228A
hPINK1_S228A_Rev	ggcttcgctggacgcacctgccg	Mutagenesis S228A

hPINK1_Q126P_For	ctcggcctgtccggagatccagg	Mutagenesis Q126P
hPINK1_Q126P_Rev	cctggatctccggacaggccgag	Mutagenesis Q126P
TNT_TcPINK1_For	ATTTAGGTGACACTATAGaagacacggaattcaagccaccATGAGCGTTCGTGCAGTTGG	Contains SP6 promoter and Kozak sequence upstream PINK1 (*Tribolium castaneum*) starting sequence; used to produce linear DNA for coupled transcription and translation
TNT_TcPINK1_Rev	cttggatcCttaATCCAGTTCCGGCAGG	Anneals to the 3' sequence of PINK1 (*Tribolium castaneum*), contains the stop codon; used to produce linear DNA for coupled transcription and translation
TNT_hPINK1(1-120)-eGFP_For	ATTTAGGTGACACTATAGaagacacggaattcaagccaccatggcggtgcgacaggcgctg	Contains SP6 promoter and Kozak sequence upstream PINK1 (human) starting sequence; used to produce linear DNA for coupled transcription and translation
TNT_hPINK1(1-120)-eGFP_Rev	Gcttcgagcgtcccaaaaccttctcaagcaagg	Reverse primer for hPINK1(1-120)-eGFP; used to produce linear DNA for coupled transcription and translation
TNT_hPINK1(35-120)-eGFP_For	ATTTAGGTGACACTATAGaagacacggaattcaagccaccatgggcccggcggcgggctg	Contains SP6 promoter and Kozak sequence upstream PINK1 (human) starting sequence; used to produce linear DNA for coupled transcription and translation
TNT_hPINK1(35-120)-eGFP_Rev	Gcttcgagcgtcccaaaaccttctcaagcaagg	Reverse primer for hPINK1(35-120)-eGFP; used to produce linear DNA for coupled transcription and translation

Table S4. List of antibodies used in this study.

Antibodies	**Dilution**	**Source**
Mouse monoclonal Anti-VDAC1	1:500	ab14734, abcam
Rabbit polyclonal Anti-TOMM22/TOM22	1:500	ab246862, abcam
Rabbit polyclonal anti-Human Cytochrome b-c1 complex subunit 8	1:500	MBS715150, MyBioSource
Mouse monoclonal anti-TOM70	1:500	sc-390545, Santa Cruz Biotechnology
Mouse monoclonal anti-TOM40	1:500	sc-365467, Santa Cruz Biotechnology
Rabbit polyclonal anti-TOM40	1:500	sc-11414, Santa Cruz Biotechnology
Mouse monoclonal anti-TOM20	1:500	sc-17764, Santa Cruz Biotechnology
Mouse monoclonal anti-ATP5A	1:500	ab14748, abcam